University of Alberta

A Methodology for Evaluating Rainfall-induced Railway Ground Hazards Encountered at Port Douglas, June 1998

by

Ruifeng Shi

A thesis
Submitted to the Faculty of Graduate Studies and Research
in partial fulfillment of the requirements for
the Degree of Master of Science
in Geotechnical Engineering

Department of Civil and Environmental Engineering

Edmonton, Alberta
Fall 2006

Library and Archives Canada

Published Heritage Branch

395 Wellington Street
Ottawa ON K1A 0N4
Canada

Bibliothèque et Archives Canada

Direction du Patrimoine de l'édition

395, rue Wellington
Ottawa ON K1A 0N4
Canada

Your file Votre référence
ISBN: 978-0-494-22368-0
Our file Notre référence
ISBN: 978-0-494-22368-0

NOTICE:
The author has granted a non-exclusive license allowing Library and Archives Canada to reproduce, publish, archive, preserve, conserve, communicate to the public by telecommunication or on the Internet, loan, distribute and sell theses worldwide, for commercial or non-commercial purposes, in microform, paper, electronic and/or any other formats.

The author retains copyright ownership and moral rights in this thesis. Neither the thesis nor substantial extracts from it may be printed or otherwise reproduced without the author's permission.

AVIS:
L'auteur a accordé une licence non exclusive permettant à la Bibliothèque et Archives Canada de reproduire, publier, archiver, sauvegarder, conserver, transmettre au public par télécommunication ou par l'Internet, prêter, distribuer et vendre des thèses partout dans le monde, à des fins commerciales ou autres, sur support microforme, papier, électronique et/ou autres formats.

L'auteur conserve la propriété du droit d'auteur et des droits moraux qui protège cette thèse. Ni la thèse ni des extraits substantiels de celle-ci ne doivent être imprimés ou autrement reproduits sans son autorisation.

In compliance with the Canadian Privacy Act some supporting forms may have been removed from this thesis.

While these forms may be included in the document page count, their removal does not represent any loss of content from the thesis.

Conformément à la loi canadienne sur la protection de la vie privée, quelques formulaires secondaires ont été enlevés de cette thèse.

Bien que ces formulaires aient inclus dans la pagination, il n'y aura aucun contenu manquant.

Canada

ABSTRACT

Over the course of a prolonged heavy rainfall in June and early July 1998, a section of the Canadian Pacific Railway near Port Douglas, New York, endured numerous embankment small and large earth slides, and overland flow erosion events.

The stability of two typical embankments during the prolonged rainfall was assessed using unsaturated soil theory. It was found that the stability of the embankments decreased as the rainfall continued and the critical slip surfaces moved gradually towards the ground surface. The surface region and the toes of the embankments were more vulnerable to failure than other regions during heavy rainfall.

The watershed boundaries within the study site were determined with a Geographic Information System program from a digital elevation model. Hydrology and hydraulic modeling were performed to check the flow capacities of the culverts under the base of the embankments. Possible culvert performance and their effect on the embankment stability were discussed.

ACKNOWLEDGEMENTS

The author wishes to thank Professors C.D. Martin and N.R. Morgenstern, who initially suggested the thesis topic and substantially guided and encouraged the work throughout the course of the study.

The author would also like to thank the Canadian Pacific Railway for providing valuable background information on this project. This work would not have been possible without the support of the Canadian Pacific Railway.

Thanks are also extended to Dr. Rajaratnam and Ms. E. Herd for their help in hydraulics and GIS application, respectively.

Last but not least, the helpful discussions with the author's colleagues in the Geotechnical Group and Water Resource Group in the Department of Civil and Environmental Engineering are sincerely appreciated.

Table of Contents

Chapter 1 Introduction 1

1.1 Problem Background 1

1.2 Scope of the Study 6

Chapter 2 Description of CPR Port Douglas Event in June 1998 7

2.1 Precipitation during June and early July, 1998 7

2.1.1 Radar Rainfall Data for June 1998 8

2.1.2 Potential Sources of Error for Radar-derived Rainfall Data 10

2.1.3 Rainfall Data for Early July 1998 11

2.2 Geological Setting 12

2.3 Watershed Delineation in the ArcGIS Program 12

2.3.1 Obtaining a Digital Elevation Model 12

2.3.2 Procedures to Derive Hydrologic Characteristics 13

2.3.3 Result of Stream Network and Watershed Boundaries 16

2.4 Classification of Rainfall-induced Railway Ground Hazards 17

2.4.1 Railway Ground Hazard Classification System by Keegan 17

2.4.2 Classification of Rainfall-induced Railway Ground Hazards 18

Chapter 3 Railway Embankment Stability Analysis 31

3.1 Components of Railway Track Structure 31

3.2 Method for Assessment of Embankment Stability 32

3.2.1 Seepage Analysis with SEEP/W 33

3.2.2 Slope Stability Analysis with SLOPE/W 36

3.3 Seepage and Stability Modeling Results 37

3.3.1 MP 154.47 Embankment Stability Analysis 38

3.3.2 MP 150.17 Embankment Stability Analysis 53

3.3.3 MP 150.10 Embankment Stability Analysis 67

3.4 Discussion 72

Chapter 4 Hydrology and Hydraulic Modeling 76

4.1 Hydrology and Hydraulic Modeling Method 76

4.1.1 Hydrology Modeling with HEC-HMS 76
4.1.2 Culvert Modeling in HEC-RAS 80
4.2 Hydrology and Hydraulic Modeling Results 82
4.3 Discussions 87
Chapter 5 Conclusions and Recommendations 89
5.1 Conclusions 89
5.2 Recommendations for Future Research 91
References 92
Appendix A Description of the Overland flow erosion Sites 95
Appendix B Borehole Log and Grain Size Curves 98
Appendix C Seepage Modeling Results 119
Appendix D Hydrology and Hydraulic Results 151

List of Tables

Table 2-1	Summary of all the Overland flow erosion sites	20
Table 2-2	Summary of the railway shallow earth slide Sites	27
Table 2-3	Upslope shallow earth slides	28
Table 3-1	Factors of safety of embankment at MP 154.47 by using strength parameters c'=3kPa, Φ'=27°, Φ^b=12°	48
Table 3-2	Factors of safety with different strength parameters for embankment at MP 154.47	51
Table 3-3	Factor of Safety for Embankment at MP 150.17 by using c'=0, Φ'=30°, Φ^b=15°	61
Table 3-4	Factors of safety of embankment at MP 150.17 by using different strength parameters	63
Table 3-5	Effect of trainload on the stability of embankment at MP 150.17	63
Table 3-6	Shear strength parameters for embankment materials at MP 150.10	69
Table 3-7	Change of factor of safety with time for embankment at MP 150.10	71
Table 4-1	Hydrology modeling parameters for watershed 154.47	82
Table 4-2	Input parameters for hydrology modeling	83
Table 4-3	Input parameters for culvert modeling	83
Table 4-4	Summary of peak flow and culvert capacity results	86

List of Figures

Figure 1-1	Location of study area	2
Figure 1-2	Damage sites along CPR between MP 147.33 and 155.50	3
Figure 1-3	View of derailment at MP 150.17	4
Figure 1-4	Erosion of railway embankment at MP 154.44	4
Figure 1-5	Components for evaluating rainfall-induced railway ground hazards	5
Figure 2-1	Rain gauge locations around the study site	7
Figure 2-2	Total precipitation in June 1998 from final adjusted radar data	9
Figure 2-3	Radar daily rainfall data for June 1998	10
Figure 2-4	Radar hourly rainfall data from June 25th to June 27th 1998	10
Figure 2-5	Rainfall data for early July 1998 used in this study	11
Figure 2-6	Digital elevation model for the study site from USGS	13
Figure 2-7	Outline of deriving surface characteristics from a DEM	14
Figure 2-8	Determining the flow direction from a DEM	14
Figure 2-9	Calculating flow accumulation	16
Figure 2-10	Result of stream network and watershed boundaries from DEM	17
Figure 2-11	Railway ground hazard classification system	18
Figure 2-12	Overland flow erosion at MP 154.47	19
Figure 2-13	Overland flow erosion at MP 154.44	20
Figure 2-14	View of failure scarp at MP 150.17	22
Figure 2-15	Earth slide at MP 150.10	24
Figure 2-16	Earth slide at MP 154.41	25
Figure 2-17	Embankment slides along railway	25

Figure 2-18 Upslope shallow earth slide at MP 151.30 26

Figure 2-19 Scarp due to settlement at MP 151.38 29

Figure 2-20 Classification of rainfall-induced railway ground hazards found at Port Douglas CPR Site 30

Figure 3-1 Components of the track structure 32

Figure 3-2 Factors affecting the stability of railway embankment 32

Figure 3-3 Volume water content function 35

Figure 3-4 Geometry and finite element mesh for embankment at MP 154.47 39

Figure 3-5 Volume water content and hydraulic conductivity functions of embankment material at MP 154.47 41

Figure 3-6 Rainfall data for seepage analysis of embankment at MP 154.47 42

Figure 3-7 Analysis scenarios for embankment at MP 154.47 42

Figure 3-8 Pore-water pressure head profiles after June 27 for initially dry embankment at MP 154.47 44

Figure 3-9 Pore-water pressure head profiles after June 27 for initially wet embankment at MP 154.47 45

Figure 3-10 Critical slip surface for embankment at MP 154.47 if matric suction not considered 47

Figure 3-11 Critical slip surfaces for initially dry and wet embankments at MP 154.47 using c'=3kPa, $\Phi'=27^o$, $\Phi^b=12^o$ 48

Figure 3-12 Change in the factor of safety with time for Initially Wet Embankment at MP 154.47 using Ksat = 1E-7m/s, c'=3kPa, $\Phi'=27^o$ and $\Phi^b=12^o$ 50

Figure 3-13 Evolution of critical slip surfaces for initially wet embankment at MP 154.47 using Ksat = 1E-7m/s, c'=3kPa, $\Phi'=27^o$, $\Phi^b=12^o$ 50

Figure 3-14 Seepage and stability results for embankment at MP 154.47 with an initial GWT at the base of the embankment 52

Figure 3-15 Geometry and finite element mesh for embankment at MP 150.17 54

Figure 3-16 Volume water content and hydraulic conductivity functions for embankment fill at MP 150. 17 55

Figure 3-17 Analysis scenarios for embankment at MP 150.17 56

Figure 3-18 Pore-water pressure head profiles after June 25 for Initially Dry Embankment at MP 150.17 58

Figure 3-19 Pore-water pressure head profiles after June 25 for Initially Wet Embankment at MP 150.17 59

Figure 3-20 Critical slip surfaces for initially dry and wet embankments at MP 150.17 by using Ksat = 1E-6m/s, c'=0, Φ'=30°, and Φ^b=15° 61

Figure 3-21 Change in factor of safety with time of initially wet embankment at MP 150.17 62

Figure 3-22 Critical slip surface for initially wet embankment at MP 150.17 with a train loading 60kPa 64

Figure 3-23 Pore-water pressure distributions and slope stability for embankment at MP 150.17 with an initial GWT at base of the embankment 65

Figure 3-24 Effect of upstream water level on the slope stability of downstream slope at MP 150.17 for initially wet embankment with an initial GWT at base of embankment 66

Figure 3-25 Critical slip surface for initially wet embankment at MP 150.17 with an initial GWT at the base of embankment when considering train loading 67

Figure 3-26 Finite element mesh for embankment at MP 150.10 68

Figure 3-27 Volume water content and hydraulic conductivity functions for embankment materials at MP 150.10 68

Figure 3-28 Final pore-water pressure head profiles after July 5 for initially dry and wet embankments at MP 150.10 70

Figure 3-29 Move of critical slip surface with time for initially dry and wet embankments at MP 150.10 72

Figure 4-1 Typical HEC-HMS representation of watershed runoff 77

Figure 4-2 Conceptual model of a watershed with kinematic wave method 78

Figure 4-3 Cross section layout for culvert 80

Figure 4-4 Culvert performance curve with roadway overtopping 81

Figure 4-5 Subbasin delineation and hydrologic model for Watershed 154.47 84

Figure 4-6 Modelled hydrograph at outlet of watershed 154.47 85

Figure 4-7 Modelled water surface profile at culvert 154.47 86

Chapter 1 Introduction

1.1 Problem Background

Over the course of June and July 1998, a section of the Canadian Main Line of the Canadian Pacific Railway (CPR) near Port Douglas, New York, between Mile Post 147.3 and 155.5 (Figures 1-1 and 1-2), endured a severe rainfall weather condition resulting in numerous railway embankment large and small earth slides and overland flow erosion events. Figure 1-2 shows the damage sites along this section of railway track. This eight-mile section of track is located on the west side of Lake Champlain and traversed bedrock outcrops, colluvial and dense till side slopes, alluvial and lacustrine sand and silt terraces, and lacustrine silt and clay deposits. The height of the embankments ranged from several meters to 20 meters. Streams and brooks running into Lake Champlain were conveyed through the embankments by masonry or metal culverts. The damage resulting from this unusually heavy rainfall was significant and threatened the railway operation. On the morning of June 26, 1998, a train derailed and the embankment's east slope failed at Mile Post (MP)150.17 near Port Douglas, resulting in one locomotive and 4 cars falling down to the toe of the embankment (see Figure 1-3). Figure 1-4 shows one of the major overland flow erosion sites, which was measured to be around 23 m long and 12 m deep. The railway line was out of service for six weeks.

Similar erosion and landslide events occur elsewhere. The records compiled over the past 122 years by Canadian Pacific Railway indicate that at least 30% of the large volume hazards occurred synchronously with severe weather events, which were usually prolonged periods of increased precipitation intensity (Bunce, 2003). Canadian National Railway also experienced similar problems. For example, the Canadian National rail line was severely impacted between Winnipeg and Thunder Bay during June 2002 by extreme rainfall, and one of the overland flow erosion events measured almost a kilometer in length (Keegan, pers. comm.).

The focus of this research was to examine the hazards resulting from an intense rainfall event that can affect railway operations. By using the Port Douglas event as a case study, a methodology was developed for assessing rainfall-induced damage utilizing Geographic Information System technology (GIS), Hydrology and hydraulic tools linked to GIS, and seepage and slope stability analysis (Figure 1-5). GIS is an information system used to store, manipulate and analyze geographically referenced data. It was used to derive the watershed and the stream network upstream of the railway line from a digital elevation model (DEM) and provide input parameters for hydrology modeling. Hydrology modeling was carried out with the HEC-HMS (Hydrology Modeling System) to obtain the water flow hydrograph. Then the flow capacity of the culvert under the embankment was checked by using the HEC-RAS (River Analysis System). Considering the effects of rainfall infiltration, upstream impoundment and the train loading, the stability of the railway embankment was analyzed using seepage analysis software SEEP/W coupled with slope stability analysis using the software SLOPE/W.

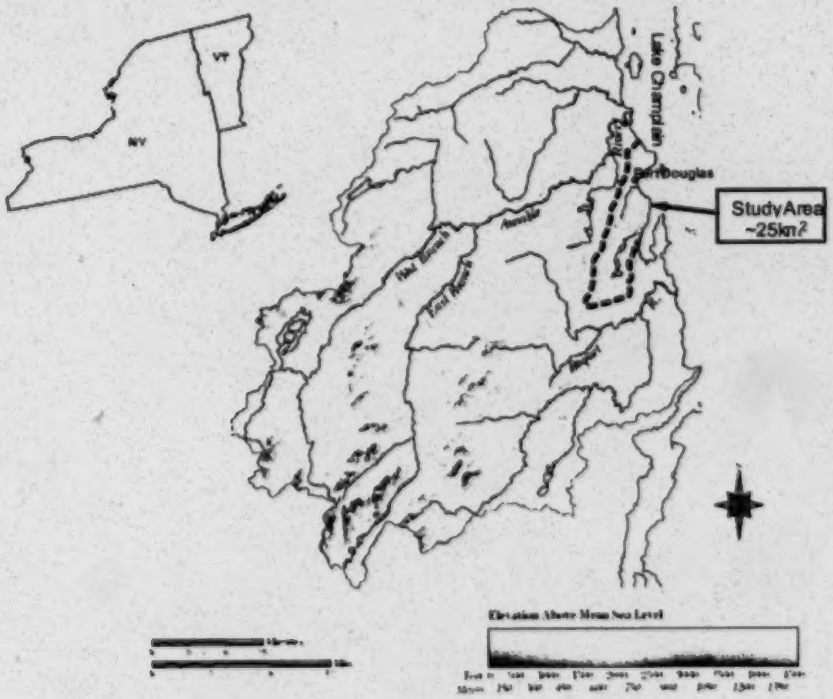

Figure 1-1 Location of study area

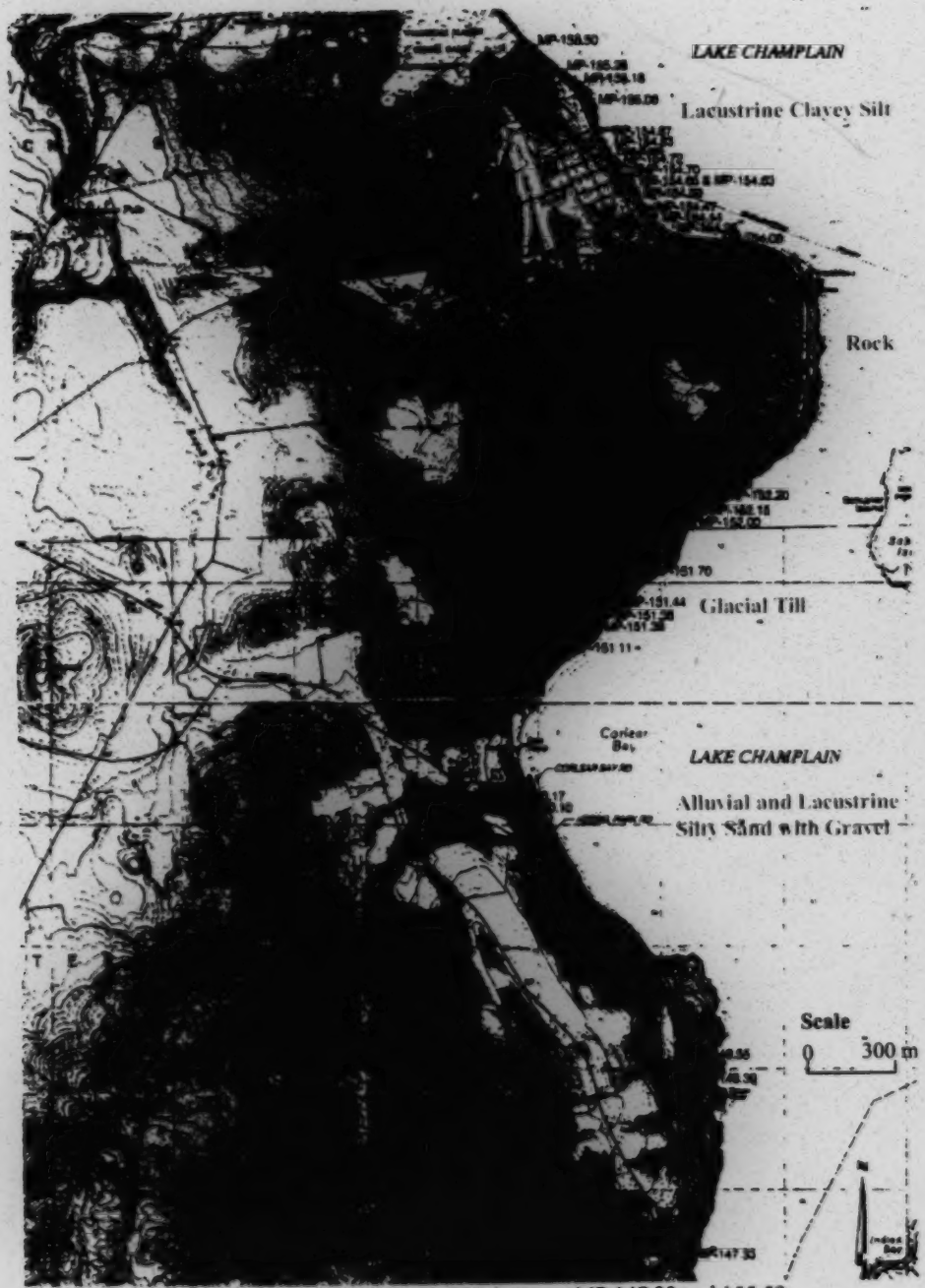

Figure 1-2 Damage sites along CPR between MP 147.33 and 155.50
(from Canadian Pacific Railway, 1998)

Figure 1-3 View of derailment at MP 150.17 , looking south along tracks
(from Canadian Pacific Railway, photograph taken on June 27, 1998)

Figure 1-4 Complete overland flow erosion of railway embankment at MP 154.44
(from Canadian Pacific Railway, photograph taken in July 1998)

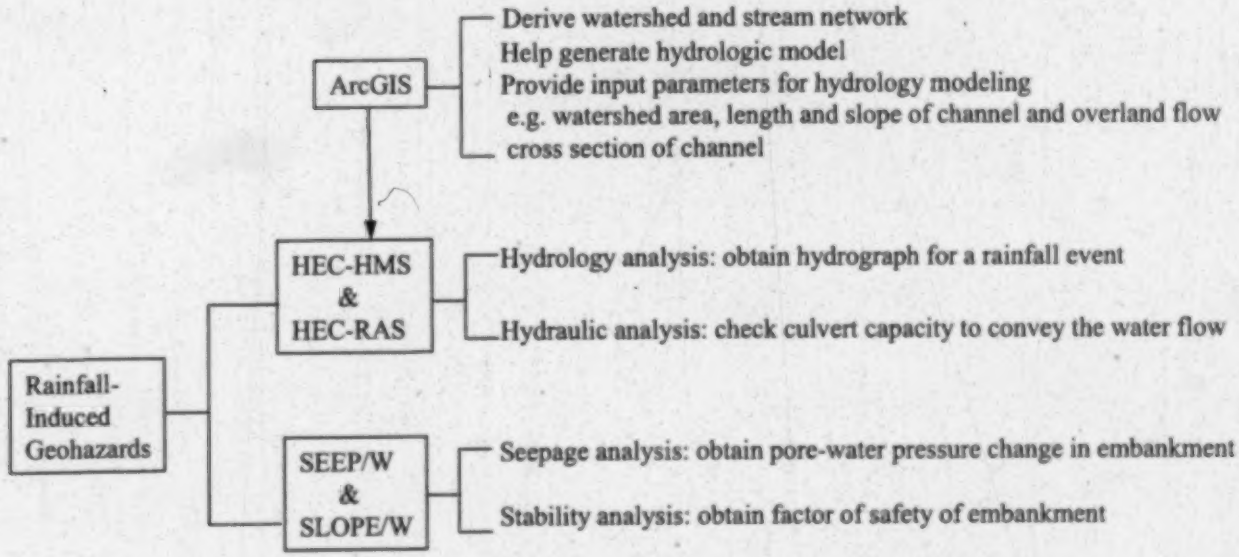

Figure 1-5 Components for Evaluating Rainfall-induced Railway Ground Hazards

1.2 Scope of the Study

The overall goal of this research was to investigate the failure mechanisms of railway embankment landslides and overland flow erosion during periods of heavy rainfall and to improve the basic understanding of rainfall-induced railway ground hazards.
Three potential failure mechanisms were investigated for the embankment overland flow erosions:

1) The initial failure of the slope is caused by the infiltration of rainwater, resulting in the overall instability of the embankment and damage to the culvert. The reduced capacity of the culvert causes water flow in the stream to overtop the embankment and erode the remaining embankment soils.
2) Local surface failure of the embankment resulted in a blocked culvert, which caused the stream flow to overtop the embankment and to erode the embankment.
3) The failure of the embankment and culvert was due to the high flows generated by the heavy rainfall overtopping the embankment and eroding the embankment soil gradually.

Which was the most likely failure mechanism? How should railway personnel prepare before a heavy rainfall event?

The following specific objectives are required to achieve the ultimate goal:

1) classification of the variety of railway ground hazards triggered by the unusual rainfall in the Port Douglas area during June and early July 1998
2) seepage and stability analyses of several typical embankments by using SEEP/W and SLOPE/W programs and unsaturated soil theory
3) evaluation of the effects of the soil hydraulic conductivity, the embankments' initial pore-water pressure condition, the antecedent rainfall before the main event, and the effect of the train loading on the stability of the embankments' slopes
4) assessment of the capacities of the existing culverts to convey the peak water flow, through hydrology and hydraulic analysis using the HEC-HMS and the HEC-RAS
5) investigation of the factors inducing railway embankment overland flow erosions

Chapter 2 Description of CPR Port Douglas Event in June 1998

2.1 Precipitation during June and early July, 1998

Figure 2-1 shows the location of Port Douglas and the locations of the key rain gauges within the vicinity of the study area. The geographic coordinates are indicated on the left and bottom axis and represent respectively, the latitude and longitudes in decimal degrees. The nearest rain gauges were located several miles from the railway line.

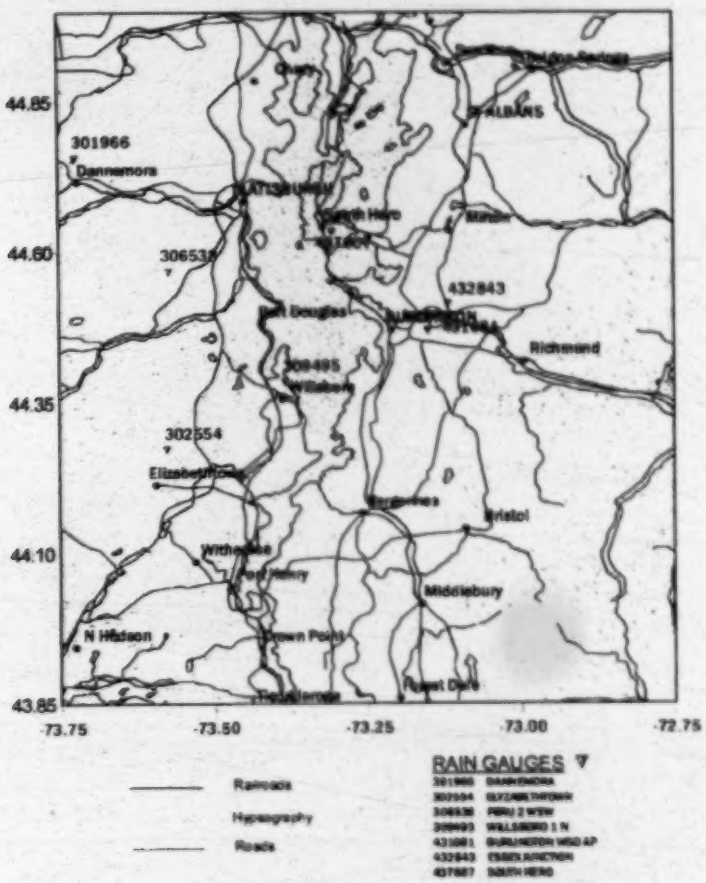

Figure 2-1 Rain gauge locations around the study site

Because of the inherently high variability of precipitation events located at any appreciable distance away from a rain gauge, especially highly localized summer thunderstorms, weather radar technology was used to analyze the rainfall event near Port Douglas, NY in June 1998. A previously completed analysis of radar-derived rainfall data was prepared for CPR. The results of that analysis are used in this study.

2.1.1 Radar Rainfall Data for June 1998

Archived U.S. NEXRAD weather radar data with a 10 Ghz scanning frequency for the entire month of June 1998 was used in the weather radar analysis completed for CPR. The radar data have a spatial resolution of approximately 2 km by 2 km and cover a rectangular area bounded by the following coordinates: -75° longitude to the west, -72° longitude to the east, 45.5° latitude to the north, and 43.5° latitude to the south. This rectangular area is roughly centered on Port Douglas and was selected to be large enough to encompass several rain gauges for calibration purposes. The reflected radar energy was converted into precipitation estimates by using the relation developed by Professor J.S. Marshall in the late 1940's. A gauge-to-radar adjustment was also made by using a Gauge/Radar precipitation ratio for a given hour as a corrective factor to all unadjusted radar-derived precipitation for that particular hour.

Figure 2-2 shows the final adjusted radar dataset of the total precipitation for the month of June 1998. It can be seen near the Port Douglas site the total accumulation for the month of June was a fairly uniform 13 inches (330 mm). For the month of June the rainfall was greater than 300% of the norm 3.02 inches (77mm). This total accumulation exceeded the 100-year return period by over 4 inches (102 mm) when using the Peru Station's long-term records for comparison. The large area of very low precipitation located to the northeast of Burlington is actually an area of radar shadow caused by mountains. Therefore, all the data shown within the area northeast of Burlington are not representative of the actual rainfall.

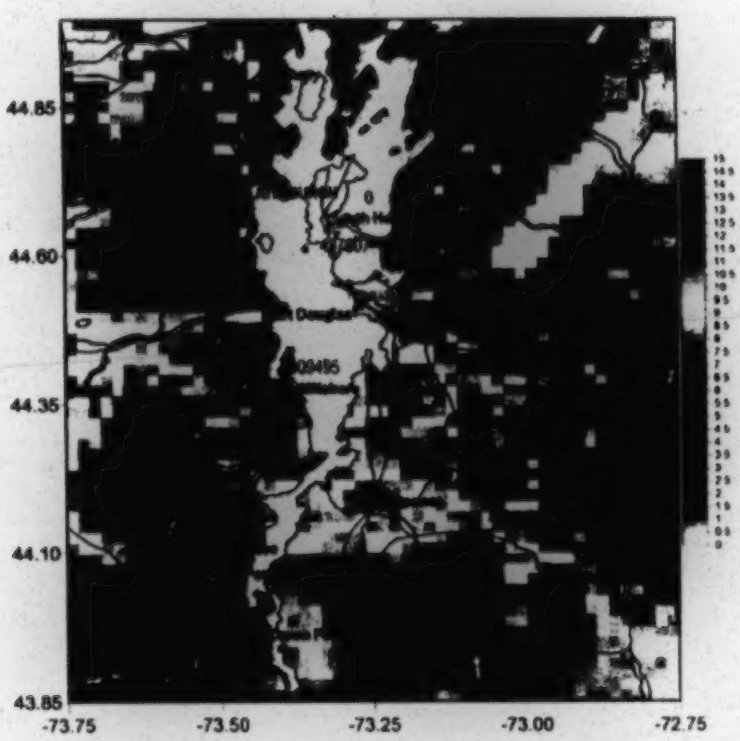

Figure 2-2 Total precipitation in June 1998 from final adjusted radar data (Unit: inch)

Figure 2-3 presents the total daily precipitation for June 1998 over the Port Douglas study site. The graph indicates ten inches (254 mm) of rainfall had already accumulated prior to the 26th of June. Also of particular interest are the period of continuous daily rainfall from June 11 to 19 and the three-day period with over 1.7 inches/day (44 mm/day) of rainfall on June 25, 26 and 27. Figure 2-4 shows the estimate of hourly sequence of the precipitation at Port Douglas from 06:00 on June 25 to 09:00 on June 27. This graph shows that the precipitation was practically continuous for this 51-hour period. The total accumulation for this period was nearly 5.5 inches (140 mm).

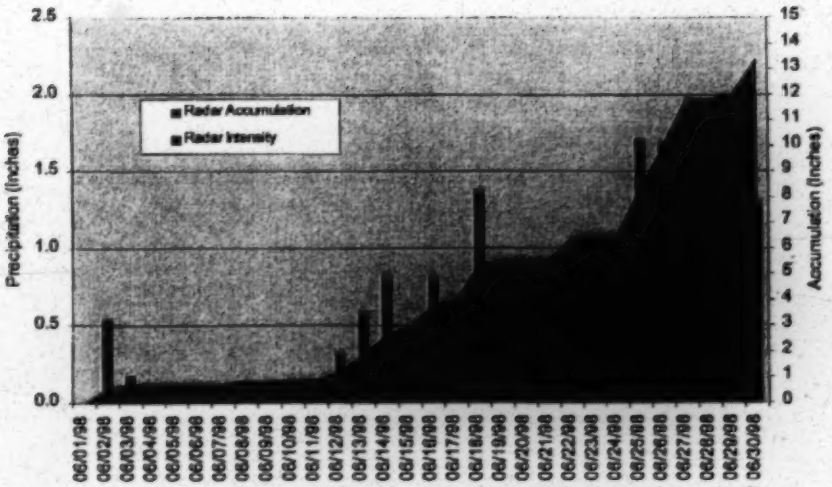

Figure 2-3 Radar daily rainfall data for June 1998

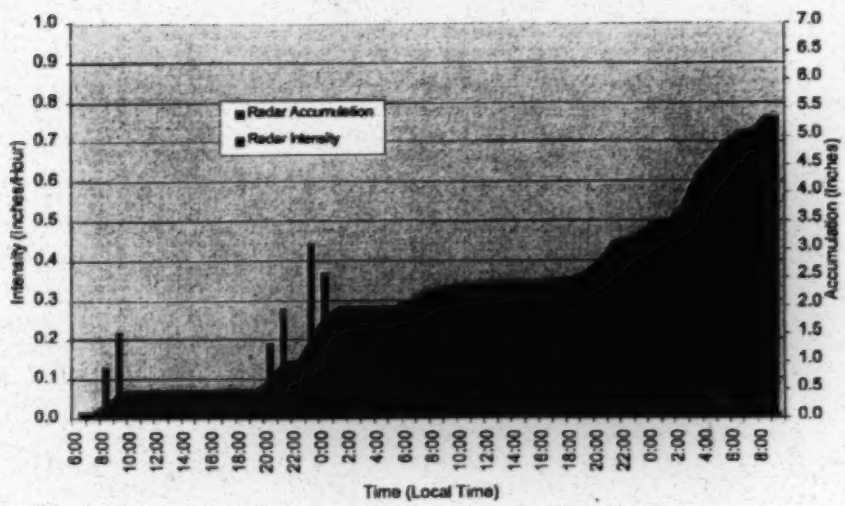

Figure 2-4 Radar hourly rainfall data from June 25th to June 27th 1998

2.1.2 Potential Sources of Error for Radar-derived Rainfall Data

Radar energy and any precipitation estimates derived from this energy can be affected by quite a number of things, some being inherent to the technology itself. The main sources of errors that can potentially affect radar-derived precipitation measurements include

attenuation through precipitating cloud formations, attenuation from wet radome, precipitation particle state discrimination, ground attenuation, orographic & structural reflections, earth curvature, minimum sensing threshold, scanning displacement, and computational plane versus ground catch (Zawadzki, 1984). For the radar-derived rainfall in Port Douglas, June 1998, a detailed discussion of these sources of error and the approaches to mitigate their impacts is presented in the report prepared for CPR. A calibrated weather radar system is capable of producing precipitation estimates with less than 30% average absolute error in the near real time acquisition mode, as was demonstrated at the Marshall Weather Radar Research Station in Montreal (Zawadzki, 1984). It should be noted, however, that in Hong Kong this approach gave greater errors than those reported for Port Douglas (Morgenstern, pers. comm.).

2.1.3 Rainfall Data for Early July 1998

The rain gauge data for early July 1998 were obtained from the National Oceanic and Atmospheric Administration. The rainfall data used in this study, presented in Figure 2-5, are assumed based on the rain gauge data at the Burlington WSO AP station, which is located approximately 15 miles from Port Douglas and across Lake Champlain (see Figure 2-1).

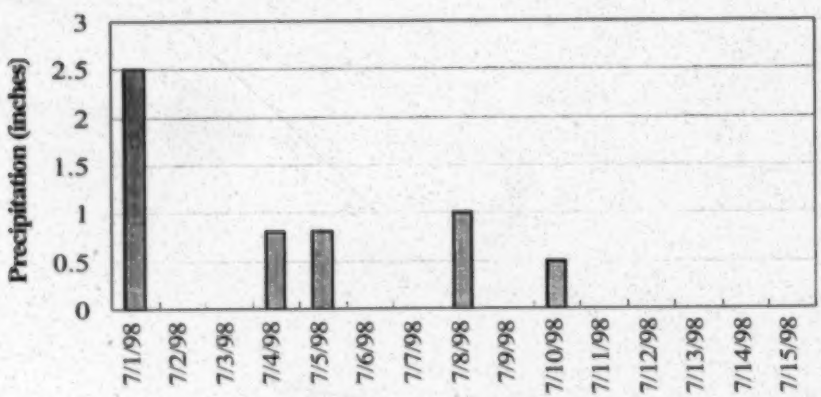

Figure 2-5 Rainfall data for early July, 1998 used in this study

2.2 Geological Setting

The Port Douglas event site is located on the eastern boundary of the Adirondack Mountains, immediately adjacent to Lake Champlain. The mountains immediately to the west rise to a maximum of about 370 meters above the lake level. The drainage patterns are well developed, with flow towards the north and east, into Lake Champlain. The streams were conveyed through the railway embankment with masonry or metal pipe culverts. The embankment slopes and the surrounding area are heavily vegetated with a variety of deciduous trees and dense undergrowth.

Along this section of the west shore of Lake Champlain, the track is located 20 m to 45 m above the lake shore. This track traverses bedrock outcrops, colluvial and dense till side slopes, alluvial and lacustrine sand (with some silt and trace find gravel) terraces, and lacustrine silt (with some find sand and clay) deposits, as shown in Figure 2-1. The embankment hazards were primarily in the areas of erodible lacustrine silts and of sand and silt fills and natural deposits.

2.3 Watershed Delineation in the ArcGIS Program

In order to evaluate the culvert's capacity to carry the water flow during the prolonged precipitation period and to understand the causes of the railway embankment overland flow erosion, a knowledge of the stream network and watershed boundaries is required. In this research, GIS technology was used to find the flow paths and to delineate the watersheds by using DEM, which is a cell-based representation of a continuous surface of the earth.

2.3.1 Obtaining a Digital Elevation Model

A digital elevation model with a 10-meter by 10-meter horizontal resolution for the Port Douglas study site was obtained from USGS online resources at http://data.geocomm.com/dem/ and is presented in Figure 2-6. This DEM model was

used to analyze the hydrologic characteristics upstream of the railway line with the help of a hydrology modeling tool in the ArcGIS program.

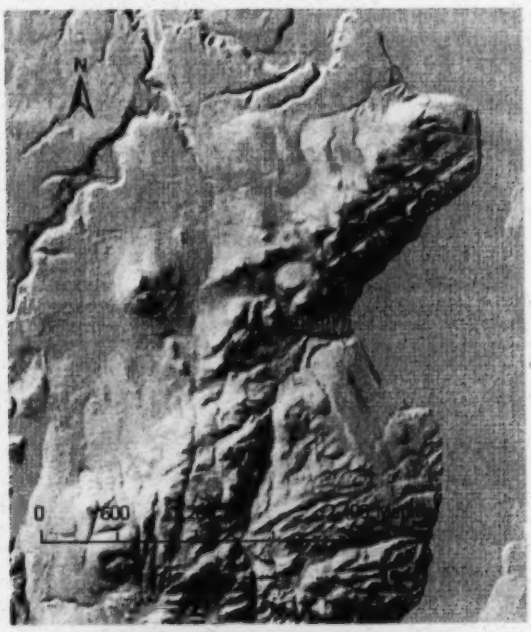

Figure 2-6 Digital elevation model for the study site from USGS

2.3.2 Procedures to Derive Hydrologic Characteristics

In the ArcGIS program, the procedure to derive the surface characteristics by using the hydrology modeling tool is shown in Figure 2-7 and explained in the following sections.

2.3.2.1 Determining Flow Directions

One of the keys to deriving the hydrologic characteristics of a surface is to determine the direction of the flow from every cell in the raster by using the *Flow Direction* function. This function takes a raster DEM model as input and outputs a raster showing the direction of the flow out of each cell (see Figure 2-8). The direction of the flow is determined by finding the direction of the steepest descent from each cell by calculating the maximum drop. If the maximum descent to several cells is the same, the

neighborhood is enlarged until the steepest descent is found. When a direction of the steepest descent is found, the output is coded with the value representing that direction.

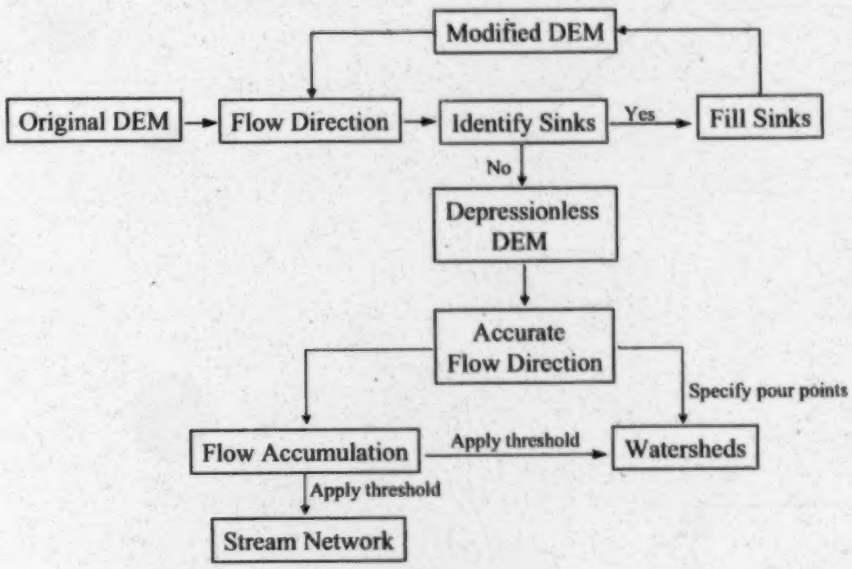

Figure 2-7 Outline of deriving surface characteristics from a DEM (modified from ArcGIS Help)

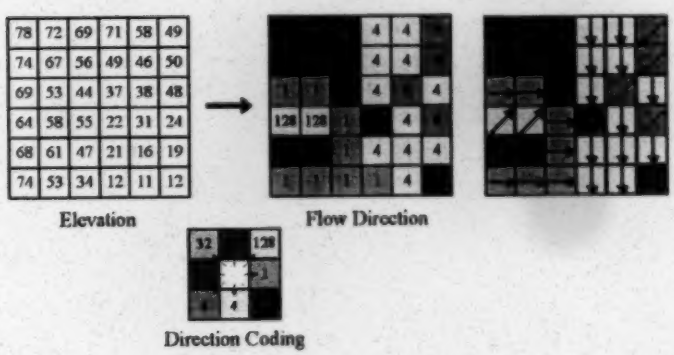

Figure 2-8 Determining flow direction from a DEM (from ArcGIS help)

2.3.2.2 Finding and Filling Sinks

A sink is an area lower than all the surrounding areas. Some of these may be legitimate sinks, but many are imperfections in the DEM. The morphology of the area must be understood well enough to know which features may truly be sinks on the surface of the earth and which are merely errors in the data. The presence of sinks may result in an erroneous flow-direction raster. Errors of sinks should be removed before attempting to derive any surface information.

Sinks can be identified by using the *Identify Sinks* function, which requires a direction raster created by the *Flow Direction* function. The result is a raster that identifies any existing sinks in the data. Finding the depth of a sink or group of sinks can be useful to determine an appropriate z-limit for the *Fill Sinks* function, to understand the type of errors present in the data, and to decide whether some of the sinks are legitimate morphological features.

Sinks can be filled by using the *Fill Sinks* function, which requires an input DEM surface, a fill limit, and an output DEM surface. When a sink is filled, it is filled to its pour point, which is the minimum elevation along its watershed boundary. After a sink is filled, the boundaries of the filled area may create new sinks, which then need to be filled. The identification and removal of sinks are an iterative process carried out until a depressionless DEM is obtained.

An accurate flow direction raster can be derived from the depressionless DEM. Once the direction of the flow out of each cell is known, which and how many cells flow into any given cell can be determined. This information can be used to define the watershed boundaries and stream network.

2.3.2.3 Identifying Stream Network

To define a stream network, not only the direction of water flows from cell to cell, but also how much water flows through a cell must be known. The *Flow Accumulation* function calculates the number of upslope cells that flow into each cell from a flow

direction raster (see Figure 2-9). When enough water flows through a cell, then the location is considered to have a stream passing through it. By applying a threshold value to the results of the flow accumulation, a linear stream network can be obtained.

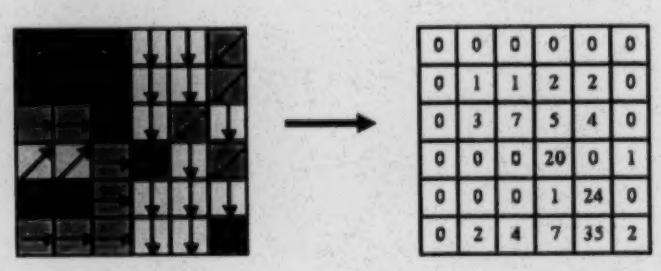

Figure 2-9 Calculating flow accumulation (from ArcGIS help)

2.3.2.4 Delineating Watersheds

A watershed is the upslope area contributing flow to a given location. A subwatershed is simply part of a hierarchy, implying that a given watershed is part of a larger watershed. Watersheds can be delineated by the *Watershed* function, which requires a flow direction raster and pour points to determine their contributing area. As well, a flow accumulation raster and a flow accumulation threshold value can be used to define a watershed for which the pour points will be the junctions of a stream network derived from the flow accumulation raster.

2.3.3 Result of Stream Network and Watershed Boundaries

The result of the delineation of the stream network and watershed boundaries in the Port Douglas study area is provided in Figure 2-10. From the results, the watershed area, length and gradient of a stream and cross section of a stream can be determined within the ArcGIS program and used in the hydrology modeling for a rainfall event.

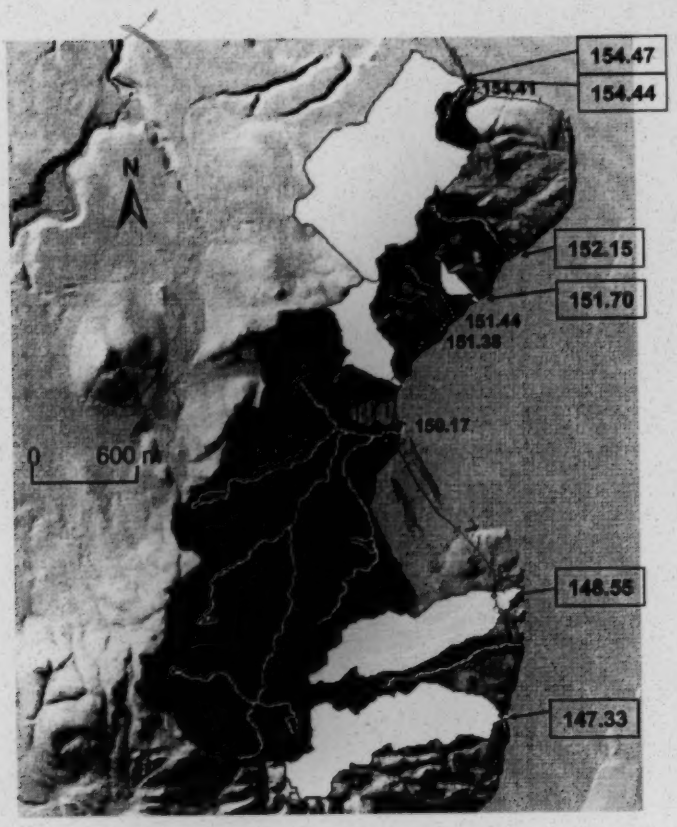

Figure 2-10 Result of stream network and watershed boundaries from DEM

2.4 Classification of Rainfall-induced Railway Ground Hazards

2.4.1 Railway Ground Hazard Classification System by Keegan

Keegan (2003) developed a functional Railway Ground Hazard Classification System (RGHCS) intended to provide a means to categorize relevant railway ground hazards for avoidance, control, or remediation. Figure 2-11 presents Keegan's classification system, which is based on the material involved in the processes and the movement types that may occur. The railway ground hazards are grouped as landslides (including earth slides, rock slides and debris slides), hydraulic erosion, subsidence, avalanches and frost. According to Keegan's statistics, of the various railway ground hazards, earth slides, rock

slides, and hydraulic erosion are the major hazards encountered by railway systems. These three together account for 67 percent of the total ground hazards along railways.

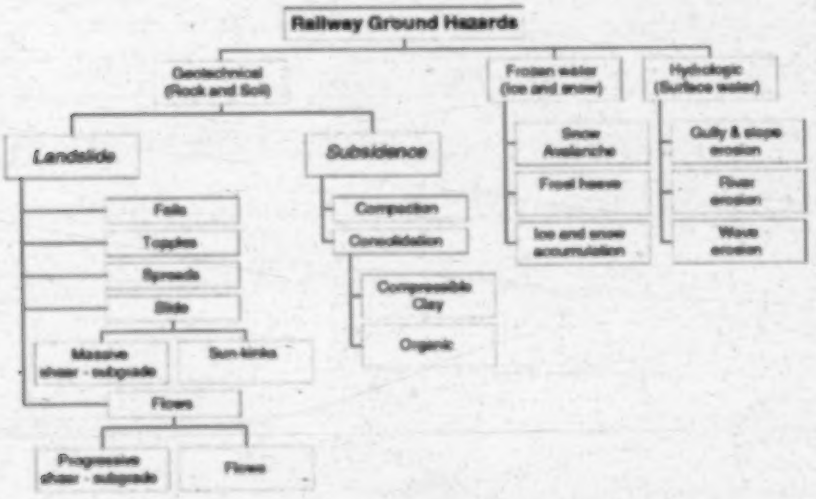

Figure 2-11 Railway ground hazard classification system (after Keegan, 2003)

2.4.2 Classification of Rainfall-induced Railway Ground Hazards

According to Keegan's Railway Ground Hazards Classification System, the embankment damage sites in the CPR Port Douglas area during June and early July 1998 were categorized into overland flow erosions, earth slides, shallow earth slides and other ground hazards. A detailed description of each kind of railway ground hazard in the Port Douglas region is presented in the following section.

2.4.2.1 Major Overland Flow Erosions

One of the major overland flow erosions occurred at Mile Post 154.47 where the earth embankment crossed a stream valley, with a stone box culvert 1.2 m wide and 0.9 m high through the base of the embankment to provide drainage. The embankment, composed of lacustrine silt with fine sand materials, was about 12 m high and had side slopes of approximately 1.4H:1V. On the night of June 27, 1998, the embankment and culvert were partially eroded (see Figure 2-12). The failure extended over a length of around 35 m at

the track level and the erosion depth was about 17 m. This overland flow erosion site was the largest in the Port Douglas event. The CPR's inventory recorded that this area endured previous overland flow erosion damage.

Close to the site 154.47, another embankment overland flow erosion was also investigated at MP 154.44 at the end of June 1998. At the site 154.44 a stream went through the earth embankment in a stone box culvert, which was 1 m wide and 0.9 m in height, to provide drainage. The embankment was built of local lacustrine silt and fine sand materials with a height of 12 m and side slopes of approximately 1.4H:1V. As shown in Figure 2-13, the erosion length at the track level was around 23 m and the failure depth was 12 m.

The embankments at MP 154.47 and 154.44 had similar geometry and fill materials and were typical embankments with lacustrine silt with fine sand material. Seepage and stability analyses of the embankments were carried out and are presented in Chapter 3.

Figure 2-12 Embankment overland flow erosion at MP 154.47, looking south (Canadian Pacific Railway, photograph taken in June 1998)

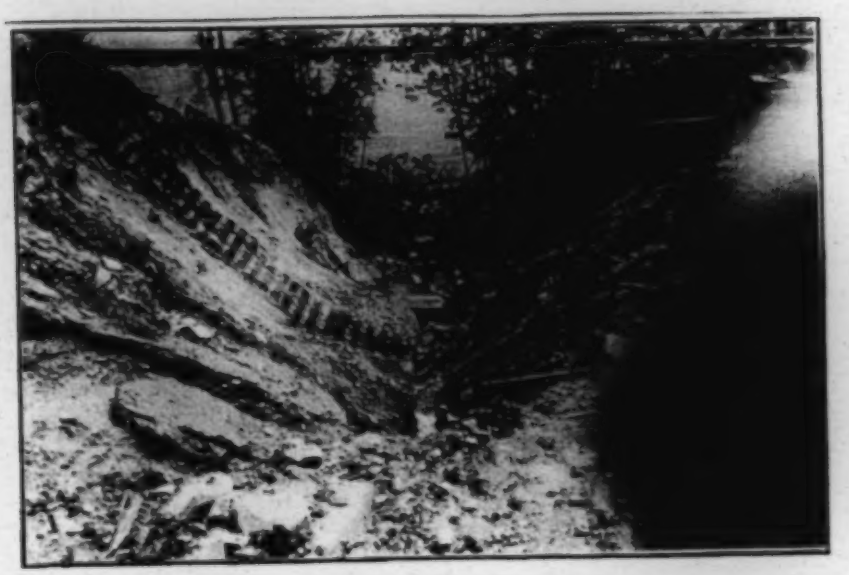

Figure 2-13 embankment overland flow erosion at MP 154.44, looking west
(Canadian Pacific Railway, photograph taken in July 1998)

Table 2-1 Summary of the overland flow erosion sites

Mile Post	Slope Height	Side Slope	Failure Length x depth	Surficial Geology	Culvert (rise x span)
154.47	12m	1.4:1	35m x 17m	Lacustrine Silt	Stone Box 0.9m x 1.2m
154.44	12m	1.4:1	23m x 12m	Lacustrine Silt	Stone Box 0.9m x 1.0m
152.15	14m	1.4:1	24m x 15m	Glacial Till	Stone Box 0.9m x 1.2m
151.70	7.5m	3:1	24m x 5m	Glacial Till	No existing culvert.
148.55			12m x 3m		Stone Box 0.9m x 0.6m
147.33			25m x 18m		metal pipe 0.9m diameter

Other railway embankment major erosions near Port Douglas were inspected at the end of June and early July 1998, and details about these erosion sites are presented in Appendix A. Table 2-1 summarizes the information for all the major erosion sites. Of the

six major overland flow erosions, the largest one occurred at MP 154.47 and was a 35 m long and 15 m deep complete failure. The photographs of the overland flow erosion sites clearly show that the erosion failures were triangular or trapezoid in shape in sections along the railway line.

2.4.2.2 Railway Embankment Earth Slides

- Embankment Earth Slide at MP 150.17 (Derailment Site)

At MP 150.17, the railway grade crossed Little Trout Brook and was located on a high embankment with a length of around 120 m and a maximum height of 20 m. The embankment was constructed of material taken from a nearby source of fine to medium sand with some silt and trace fine gravel and had side slopes of approximately 1.5H:1V. Little Trout Brook was conveyed through the embankment by a horseshoe-shaped masonry arch culvert which was 4 m high and 3.7 m wide at the base. The culvert and embankment were constructed in 1886 and had performed satisfactorily prior to June 1998. At approximately 01:25am on the morning of June 26, 1998, Train 552-25 southbound from Rouse's Point was derailed while crossing this site. The slope on the east side of the embankment failed. One locomotive and 4 cars slid down to the toe of the embankment, as shown in Figure 1-3. The derailment site was inspected in the afternoon of June 26, 1998, about 12 hours after the event. At that time, the failure scarp reached a length of about 40 m along the railway tracks and extended to the western crest of the embankment, undermining the tracks. The west embankment slope was still intact. As shown in Figure 2-14, the failure scarp was centered over the masonry culvert and appeared nearly vertical at the top, flattening out somewhat at the base.

Several witnesses reported a strong odor of kerosene downstream from the railway embankment, prior to the derailment. Based on these reports, the fuel lines inside the culvert are believed to have broken prior to the derailment. It is suspected that the fuel lines were broken because the toe of the embankment failed first, damaging a section of the culvert near the outlet sufficiently to break the fuel line.

It was reported by CPR personnel that on the morning of June 26th, 1998, about 4 hours after the failure, the embankment soil exposed in the upper portion of the failure scarp appeared moist, but not saturated. No significant seepage was observed from the exposed surface.

Figure 2-14 View of failure scarp at MP 150.17, looking west
(Canadian Pacific Railway, photograph taken on June 27, 1998)

The embankment slopes and the surrounding area were heavily vegetated with a variety of deciduous trees and dense undergrowth. The cuts both north and south of the embankment show that the native soil around the derailment site consists of a dense glacial till, which is composed of a mixture of sand, gravel and occasional boulders in a matrix of sandy silt and silty clay. The Standard Penetration Number counts in the undisturbed till ranged from 30 to over 100, indicating that the till was very dense and hard. The available mapping indicates that the glacial till is underlain by well cemented, very hard quartzite. The valley at this location was formed by Little Trout Brook down-cutting through the glacial till. Further down-cutting at the location of the embankment was prevented by the presence of the underlying erosion-resistant bedrock.

In July 1998, three boreholes were drilled from the track level at a location south of the failure scarp. The borehole logs are presented in Figure B-7 in Appendix B. From the top down of borehole B-3, which was drilled near the south end of the failure scarp, the borehole encountered the following conditions:

0 to 43 feet	(0 to13.1 m)	Fill consisting of very loose to loose fine to medium silty sand
43 to 55feet	(13.1 to 16.8 m)	Native alluvial deposits of clayey silt, compact sandy gravel, and gravelly sand
55 to 57 feet	(16.8 to 17.4 m)	Very compact silt with sand and gravel glacial till
57 to 60.5feet	(17.4 to18.4 m)	Bedrock consisting of hard fresh quartzite

The gravel and sand deposits were either alluvial materials deposited by Little Trout Brook, or beach deposits from Lake Champlain and were native soils present prior to the construction of the embankment.

No groundwater table information is available for the periods prior to or during the failure. A standpipe piezometer was installed in borehole B-3. The water level was found to be at a depth of about 13.2 m on July 15, 1998 at this location, corresponding to 9 m above the invert of the culvert. However, it is difficult to extrapolate this water level to the area of the embankment failure because of the effects of the local topography and seepage patterns.

In this study, seepage and stability analyses were conducted for the embankment at MP 150.17, a typical embankment composed of local silty sand with gravel material.

- Embankment Slide at MP 150.10

This landslide was immediately south of the derailment site at MP 150.17(see Figure B-6 in Appendix B). The embankment was about 15 m high, and the east slope had a side slope 1.5H:1V. The east slope failed on July 5, 1998 at about 06:00am, while the MP

150.17 site was being restored. It was raining hard before and during the failure. A witness working on the restoration of MP 150.17 reported that the embankment appeared to fail from the bottom first and to slowly move in one piece. Figure 2-15 suggests a circular failure undermined the tracks. During inspection after the landslide event, multiple seeps were noted at the cut/fill interface, and seeps continued for weeks. Debris from the slide flowed approximately 120 m east of the track centerline, carrying a section of track with it.

Figure 2-15 Earth slide at MP 150.10, looking south
(Canadian Pacific Railway, photograph taken in July 1998)

Borehole B-3 was at the north end of the failure at MP 150.10 and the south end of the failure at MP 150.17 (see Figure B-6 in Appendix B). Boreholes B-1 and B-2 were located at the south end of the landslide at MP 150.10. From the borehole logs and cross-sections information provided by CPR, the cross section of the embankment at MP 150.10 was developed, and seepage and stability modeling were performed to analyze the came of the failure.

- Embankment Slide at MP 154.41

This earth slide was immediately next to the embankment overland flow erosion at MP 154.47 and MP 154.44 (see the site topography shown in Figure B-1 in appendix B). The

embankment had a height of 12 m and a east side slope estimated to be 1.4H:1V. The earth slide occurred on the east slope and appeared to be a circular failure, as shown in Figure 2-16. The failure length was measured to be as long as 60 meters.

Figure 2-16 Earth slide at MP 154.41, looking north
(Canadian Pacific Railway, photograph taken in June 1998)

- Embankment Slides at Other Sites

Other embankment slides occurred in the Port Douglas area, like the one indicated in Figure 2-17. No detailed descriptions are presented due to the lack of enough information.

Figure 2-17 Embankment slide along railway (from Canadian Pacific Railway)

2.4.2.3 Shallow Earth Slides

Shallow earth slides refer to that surface soils become saturated and slide off the slope of a railway embankment.

Table 2-2 presents a summary of some of the railway embankment surface shallow earth slides according to the inspection on July 13, 1998. The majority of these sites were within the lacustrine silt region. The shallow earth slides all occurred on the east slope of the embankments.

Several upslope surface earth slides (on the west side of the tracks and above the track level) were noticed on July 2, 1998. The debris blocked the drainage swale and flowed onto the tracks, affecting the safety of the railway operation. Figure 2-18 shows a photograph of an upslope embankment shallow earth slide. A review of the upslope earth slides is given in Table 2-3.

Figure 2-18 Upslope shallow earth slide at MP 151.30, looking west
(Canadian Pacific Railway, photograph taken in July 1998)

Table 2-2 Summary of the railway embankment shallow earth sldies

Mile Post	Slope Ht. Side Slope	Failure Height	Failure Length	Notes
155.35	9m 1.7H:1V	0.8m	n/a	Rip Rap had been placed in the past. Seeps were visible at toe.
155.30	7.5m 1.7H:1V	0.6m	20m	Slope had medium to heavy rip rap with small rip rap at top.
155.18	6m 1.4H:1V	0.6m	18m	Slope had medium to large rip rap at top, and heavily vegetated mid-slope and toe.
155.06	n/a	n/a	36m	
154.87	n/a	4.6m	3m	
154.83	n/a		24m	
154.77	n/a	0.6m	9m	
154.72	11m 1.7H:1V	n/a	7.5m	There was evidence that water had flowed over the tracks from west to east.
154.70	n/a	6m	3m	
154.65	10.5m 1H:1V	n/a	23m	This slump occurred at the top1/3 of the slope. Evidence of water rising above the tracks and flowing to east was observed.
154.63	10.5m 2H:1V	n/a	21m	There was evidence of water rising above the tracks from west to east.
151.11	n/a	n/a	15m	

Table 2-3 Upslope embankment shallow earth slides

Mile Post	Slope Ht. Side Slope	Failure Length x Height	Surficial Geology	Notes
152.20	6m 1H:1V	8.5m 3m	Glacial Till	No seeps were visible. Drainage swale at top of slope was filled with debris.
152.00	5m 1.5H:1V	24m 5m	Glacial Till	Seeps were visible as high as 3.5 m on exposed face. West drainage swale had stagnant water, possibly due to slope failure blocking swale.
151.30	4.5m 1.5H:1V	34m 4.5m	Glacial Till	Slope had a 75mm layer of topsoil with vegetation. Seeps were visible. Additionally, 0.6m high slump occurred directly to the north over a 30m length.

2.4.2.4 Others (Settlement and Piping)

On July 2, 1998, track settlement at the east slope was observed at MP 151.38, and the scarp was directly below the ties approximately 8.5 m long and 1.5 m deep (see Figure 2-19). At this site, the embankment was 15 m high and had a side slope of 1.75H:1V. It appeared that the scarp was caused by subsidence of the stone box culvert within the embankment. Evidence of piping soils near the outlet of the existing stone box culvert was also observed.

Similarly, at MP 151.44, track settlement at the east slope occurred with cracking at the toe of the rail bed ballast. The railway grade at this site was located on a 21m-high embankment which had a side slope of 1.75H:1V. The scarp was approximately 46 m

long and 0.6 m deep. The settlement was likely due to the subsidence of the existing culvert within the embankment.

Figure 2-19 Scarp due to settlement at MP 151.38
(Canadian Pacific Railway, photograph taken in July 1998)

2.4.2.5 Review of Rainfall-induced Ground Hazards Classification

To classify the types of railway ground damages in the Port Douglas region during the prolonged rainfall in June 1998, a classification was carried out on the basis of the severity of the damage, according to Keegan's Railway Ground Hazards Classification System. Figure 2-20 shows the classification of the railway embankment damage types triggered by heavy rainfall. Embankment overland flow erosion is the most serious failure type, since the railway subgrade is washed out and leaves the track unsupported. This kind of damage usually occurs at a site where the embankment crosses a stream valley. It may result from both embankment soil strength decrease and water erosion. Earth slide refers to shear failure of the railway subgrade, which means that the overall factor of safety of the embankment is less than 1. Shallow earth slide is a common failure type for railway embankments during a period of heavy rainfall. This type of damage is

less severe than embankment overland flow erosion and landslide. A shallow earth slide causes the embankment to fail locally in the surface region due to rainfall infiltration and erosion while the overall stability of the embankment is secure. Occasionally, other types of ground hazards occur such as settlement and piping during a rainfall period. At Port Douglas, embankment shallow earth slides accounted for around 54 percent of the railway ground damage. Overland flow erosion and earth slides accounted for 21 percent and 18 percent, respectively. Settlement of the embankment accounted for only 7%.

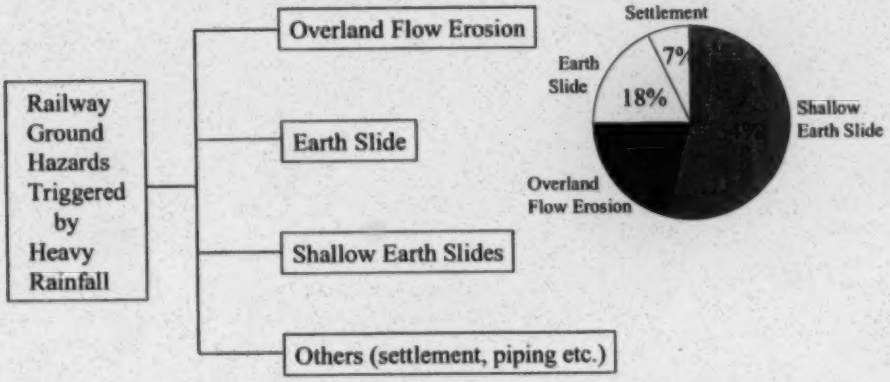

Figure 2-20 Classification of rainfall-induced railway ground hazards found at Port Douglas CPR site

Chapter 3 Railway Embankment Stability Analysis

In this chapter, the stability of the railway embankments during the prolonged period of rainfall is assessed using unsaturated soil theory. First, as background information, the components of a railway track structure are introduced. Then the embankment stability analysis method is presented, including a seepage analysis with SEEP/W to obtain the pore water pressure distribution and a slope stability analysis with SLOPE/W. The embankment at MP 154.47, a typical embankment with lacustrine sandy clayey silt material, and the embankment at MP 150.17, a typical embankment with silty sand with gravel material, are modeled and analyzed.

3.1 Components of Railway Track Structure

The railway track structure is made up of the subgrade, sub-ballast, ballast, ties and rail as illustrated in Figure 3-1 (Hay, 1982). Each of these contributes to the primary function of the track structure, which is to safely conduct the applied loads from train traffic across the subgrade. The subgrade is the foundation for the track structure and can be existing natural soil or placed soil. Its main function is to provide a stable foundation with limiting deflections for the track structure. Thus it is important that adequate subgrade strength and stiffness be available on a year-round basis, particularly during the spring thaw and following heavy precipitation events. Ballast is crushed gravel placed as the top layer of the substructure to retain the track's position and provide resiliency and energy absorption for the track. The purpose of the subballast is to form a transition zone between the ballast and the subgrade to avoid migration of soil into the ballast and to reduce the stresses applied to the subgrade.

In the following analysis, railway subgrade stability is considered, and the ballast and subballast are omitted since they provide good drainage and have little effect on the embankment stability during a rainfall season.

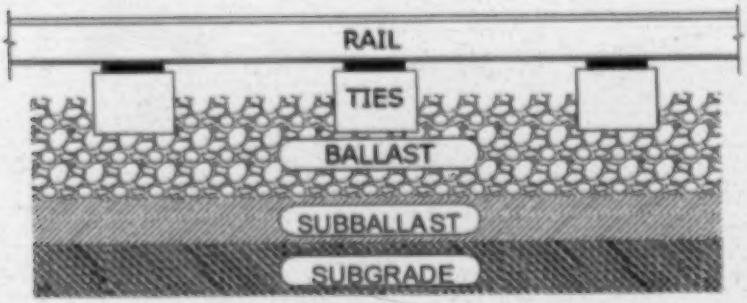

Figure 3-1 Components of the track structure (Hay, 1982)

3.2 Method for Assessment of Embankment Stability

Figure 3-2 illustrates a typical railway embankment and the factors affecting its stability, e.g. soil profile, groundwater table, precipitation and evaporation.

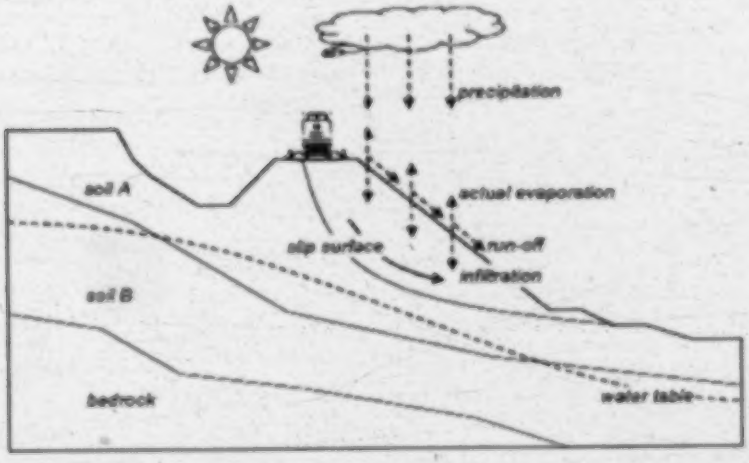

Figure 3-2 Factors affecting the stability of railway embankment (after Gitirana, 2005)

Embankment stability can be assessed with the program SLOPE/W based on limit equilibrium theory. In the rainfall-related embankment stability problem, changes in the shear strength within the soil mass take place in response to moisture fluxes at the soil-

atmosphere boundary. The pore-water pressures are important in establishing the correct shear strength in the stability analysis. Due to the importance of pore-water pressures in this problem, a seepage analysis is carried out with the SEEP/W program to determine the changes in the pore-water pressure throughout the embankment. Using the pore-water pressure results from SEEP/W as input, a slope stability analysis using the limit equilibrium method is conducted with the SLOPE/W program.

3.2.1 Seepage Analysis with SEEP/W

The general governing differential equation for two-dimensional seepage, known as Richard's equation, can be expressed as (Cedergren, 1977; Lim, et al., 1996; and Gasmo, et al., 2000)

$$\frac{\partial}{\partial x}\left(k_x \frac{\partial H}{\partial x}\right) + \frac{\partial}{\partial y}\left(k_y \frac{\partial H}{\partial y}\right) + Q = \frac{\partial \theta_w}{\partial t}, \qquad (1)$$

where, H = the total head

k_x = the hydraulic conductivity in the x-direction,

k_y = the hydraulic conductivity in the y-direction

Q = the applied boundary flux

θ_w = the volumetric water content, and

t = time.

Equation (1) states that the rate of change of the volumetric water content is equal to the sum of the rates of change of the flows in the x- and y- directions plus the external applied flux.

SEEP/W is formulated for conditions of constant total stress; that is, no loading or unloading of the soil mass occurs (Krahn, 2004). SEEP/W also assumes that the pore-air pressure remains constant at atmospheric pressure during transient processes (Krahn, 2004). Changes in the volumetric water content are consequently dependent only on

changes in the pore-water pressure, which can be given as (Fredlund, et al., 1993; Barbour, 1998; and Fredlund, 2002)

$$\partial\theta_w = m_w \partial u_w, \tag{2}$$

where, m_w = the slope of the storage curve.

u_w = pore-water pressure.

Combing Equations (1) and (2), the final form of the governing equation of the water flow through an unsaturated media is obtained and presented as Equation (3)

$$\frac{\partial}{\partial x}\left(k_x \frac{\partial H}{\partial x}\right) + \frac{\partial}{\partial y}\left(k_y \frac{\partial H}{\partial y}\right) + Q = m_w \gamma_w \frac{\partial H}{\partial t}, \tag{3}$$

where, γ_w = the unit weight of water.

Under unsaturated conditions, the hydraulic conductivity with respect to the water of a soil is a non-linear function of the volumetric water content of the soil. Similarly, the negative pore-water pressure is dependent on the volumetric water content of the soil in a non-linear fashion. From the above, it can be concluded that Equation (3) is highly non-linear. The finite element method is used in SEEP/W to solve the non-linear equation. For the numerical solution of Equation (3), the volumetric water content versus the negative pore-water pressures function, the hydraulic conductivity versus the negative pore-water pressures function and the boundary flux are required. Finally, the initial condition of the problem (the initial hydraulic head at any point of the initial time step) must also be defined.

The volumetric water content function describes the capacity of the soil to store water under changes in the pore-water pressures. A typical function for a drying soil is shown in Figure 3-3.

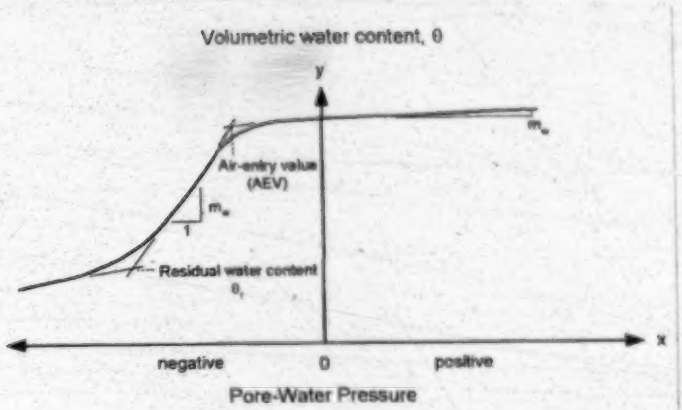

Figure 3-3 Volume water content function (Fredlund, 1993; 1994)

The volumetric water content function describes what portion or volume of the voids remain water-filled as the soil drains. The three main features that characterize the volumetric water content function are the air-entry value (AEV), the slope of the function for both the positive and negative pore-water pressure ranges (designated as m_w), and the residual water content or saturation (θ_r). These three features of the volumetric water content function are most strongly influenced by the size of the individual soil particles and the distribution of particle sizes in the soil (Fredlund, et al., 1993; Fredlund, et al., 1994; and Barbour, 1998).

In this research, the daily precipitation rate is modeled as a unit flux boundary function, q = q(t), along the edges of the elements at the ground surface. During the solution procedure, SEEP/W translates the unit flux boundary (q) into a nodal boundary (Q) and then calculates the hydraulic head at each node. In order to avoid any ponding phenomena, which are unlikely to take place in sloping ground, the software performs a check so that once a node at the ground surface is found with a positive pore-water pressure at the end of the calculation for each time step, then that node is set to have a head equal to the elevation and the problem is resolved.

The seepage analysis presented in this work has two limitations. The first limitation is that no evaporation was considered during the dry periods of each simulation. The second limitation is the assumption that the hysterisis of the soil-water characteristic curve between the wetting and the drying phase is not significant.

3.2.2 Slope Stability Analysis with SLOPE/W

SLOPE/W uses the theory of limit equilibrium of forces and moments to compute the factor of safety against failure based on effective stress analysis.

The shear strength equation for unsaturated soils is an extension of the Mohr-Coulomb failure criterion into the third dimension and can be expressed as (Fredlund et al., 1978; Fredlund, et al., 1993; and Fredlund, et al., 1996)

$$\tau_{ff} = c' + (\sigma_f - u_a)_f \tan\phi' + (u_a - u_w)_f \tan\phi^b, \qquad (4)$$

where, τ_{ff} = shear stress on the failure plane at failure

c' = effective cohesion

ϕ' = effective angle of internal friction

σ_{ff} = total normal stress on the failure plane at failure

u_{wf} = pore-water pressure on the failure plane at failure

u_{af} = pore-air pressure on the failure plane at failure

ϕ^b = angle indicating the rate of increase in shear strength relative to the matric suction, $(u_a - u_w)_f$.

In SLOPE/W, ϕ^b is treated as a constant value, but this parameter actually varies with the degree of saturation. For practical purposes, ϕ^b can be taken to be about $1/2\phi'$ (Krahn, 2004).

There are a number of different methods of stability analysis available, in terms of the conditions of the static equilibrium satisfied and the assumption regarding the interslice forces. Morgenstern and Price (1965) described a method of analysis in which it is assumed that the interslice shear forces X are related to the interslice normal forces E by

$$X / E = \lambda \cdot f(x), \tag{5}$$

where $f(x)$ is a function which varies continuously across the slip, and λ is a scaling factor. For a given function $f(x)$, the values of λ and the factor of safety F are found for which the overall force equilibrium and overall moment equilibrium are satisfied. In this thesis, Morgenstern and Price method is used for the railway embankment stability analysis.

In slope stability analysis, pore-water pressures are very important in establishing the correct effective shear strength. SLOPE/W is able to read the seepage results directly from SEEP/W in order to compute the actual pore-water pressures applied on each slice. To use the finite element computed pore-water pressures, SLOPE/W first finds the element that encompasses the slice base center. Next, the local element coordinates (r, s) are determined at the slice base. The pore-water pressures are determined at the element nodes either directly from the finite element results or by mapping the Gauss point values to the nodes. The nodal pore-water pressures and local r-s coordinates together with the inherent finite element interpolating functions are then used to compute the pore-water pressure at the slice base center. The advantage of this approach is that the pore-water pressures can have any irregular distribution and represent transient conditions at various times (Krahn, 2004).

3.3 Seepage and Stability Modeling Results

The 12m-high embankment at MP 154.47 is taken as a typical medium-high embankment with lacustrine sandy clayey silt material. The 20m-high embankment at MP 150.17 is

considered as a typical high embankment with silty sand with gravel material. These two embankments were selected, and their seepage and stability during the period of prolonged rainfall in June 1998 were modeled. In this thesis, different scenarios were considered in order to account for the uncertainties in the material properties and the embankment initial conditions. The embankment landslide at MP150.10 was also modeled and discussed.

3.3.1 MP 154.47 Embankment Stability Analysis

The embankments at MP 154.47 & 154.44 had similar geometries and soil profiles. The following analysis and results represent are for both embankments. The embankment at MP 154.47 was 12 m high and had side slopes of 1.4H:1V (35.5°), with an embankment crest width of 3 m (see Figure 3-4 (a)). The location and size of the culvert are also shown in figure 3-4(a). The culvert, however, was not modeled in the seepage and stability modeling. The analysis lateral and bottom edges of the embankment were located at a distance of 10 m and 11 m from the toe and base of the embankment, respectively, in order to avoid any influence of the boundary conditions on the seepage process within the embankment area. A fine finite element mesh was designed, as shown in Figure 3-4 (b), with a total of 966 elements. Tsaparas (Tsaparas et. al., 2002) found that a fine mesh design was required for transient seepage analysis in order to overcome unstable solutions related to the non-linearity of the water flow equation and to use of steep permeability functions.

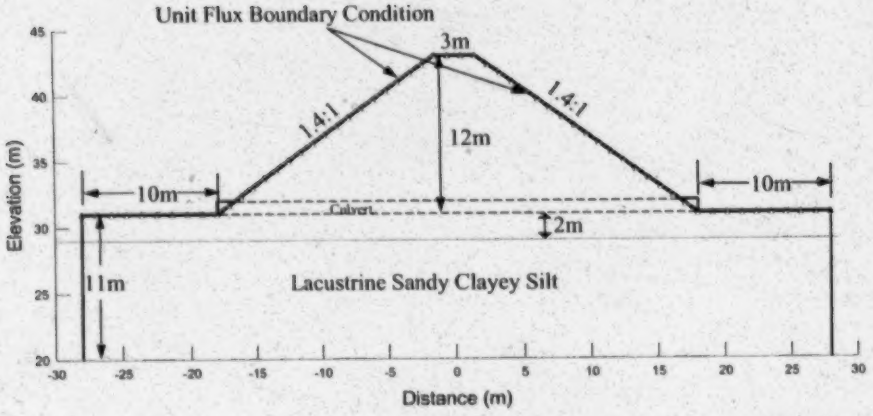

(a) embankment geometry

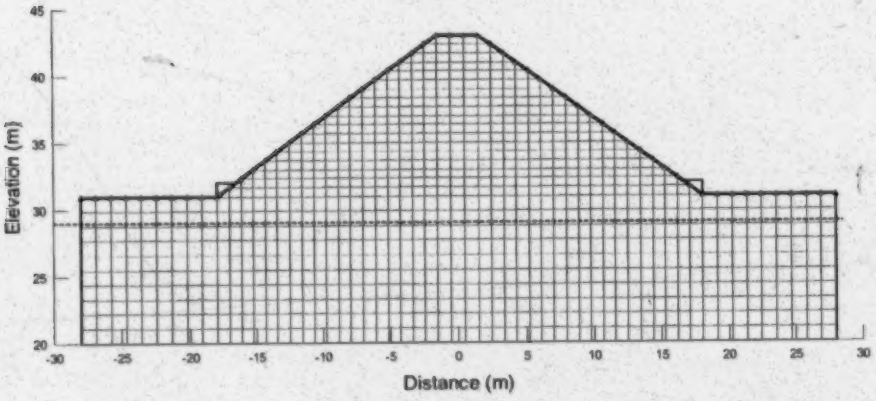

(b) finite element mesh

Figure 3-4 Geometry and finite element mesh for embankment at MP 154.47

A homogeneous embankment was used. Available test pits at the nearest site, MP 154.41, discovered that the top 3.5 m was sandy clayey silt underlain by clayey silt. Grain size distributions of these materials were not available. It is reasonable to assume that the embankment was local. The soil properties for the seepage analysis were estimated according to material # 23 (sandy clayey silt) in the SEEP/W soil function database (see Figure B-3 in Appendix B for the soil functions of material #23). A volumetric water

content at saturation of 0.4 was assumed. Three different saturated hydraulic conductivities with respect to water, 5E-8 m/s, 1E-7 m/s, and 5E-7 m/s, were considered in order to investigate their effect on the development of the pore-water pressures with time. Among these three values, a saturated hydraulic conductivity value of 1E-7 m/s was taken as a mean value for the silt embankment material. Figure 3-5 gives the volume water content and hydraulic conductivity functions used in this study. As mentioned in the previous section, the difference between drying and wetting soil-water characteristic curves was not taken into consideration.

The initial pore-water pressure distribution in the embankment was established based on a combination of hydrostatic distributions and minimum pore-water pressure values. An initial water table of 2 m below the embankment base was assumed. Two minimum negative pore-water pressure conditions were considered, a minimum pore-water pressure head of -8 m to represent a relatively dry embankment and a minimum pore-water pressure head of -4 m to represent a relatively wet embankment. The pore-water pressures below the groundwater table were assumed to be hydrostatic. Above the ground water table, the pore-water pressures become negative until they reach the appropriate limiting values, and after that they remain constant.

The radar-derived daily precipitation data from June 1, 1998 to June 27, 1998, as reproduced in Figure 3-6, were applied to the embankment surface as a unit flux boundary function. A no-flow condition was specified along the remaining boundaries.

For the slope stability analysis, the Morgenstern-Price limit equilibrium method was used. The pore-water pressures determined in the seepage analysis by SEEP/W were used as input data for the slope stability analysis. In order to investigate the sensitivity of the strength parameters on the slope stability, it was assumed that the soil had an effective cohesion c' of 3 kPa to 5 kPa, an effective angle of internal friction Φ'of 25° to 27°, and a Φ^b angle of 12°. A total unit weight of 18 kN/m^3 was used. Figure 3-7 shows the analysis scenarios for the embankment at MP 154.47.

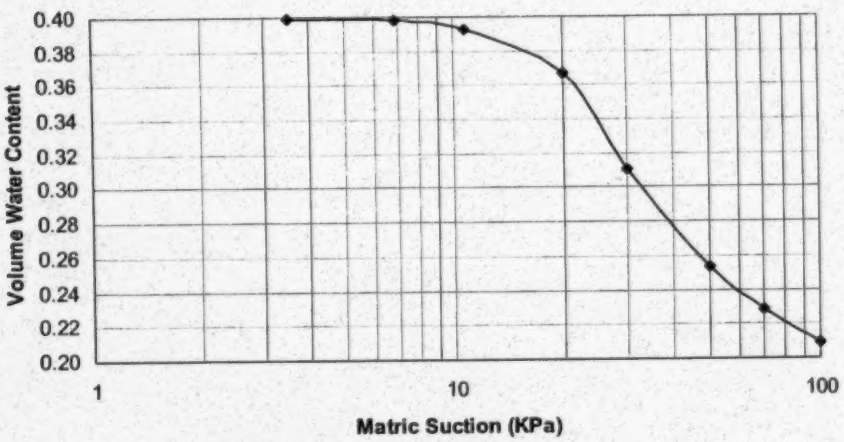

(a) volume water content vs. matric suction

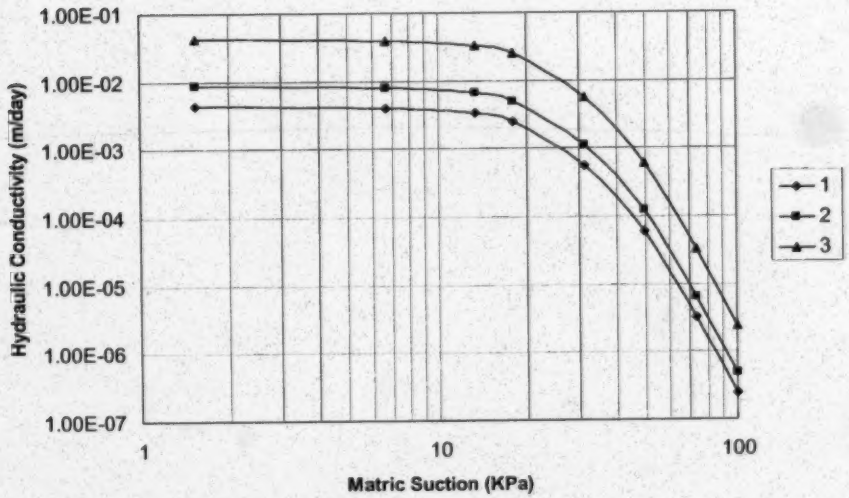

1: Ks=5E-8m/s; 2: Ks=1E-7m/s; 3: Ks=5E-7m/s

(b) hydraulic conductivity vs. matric suction

Figure 3-5 Volume water content and hydraulic conductivity functions of clayey silt embankment at MP 154.47

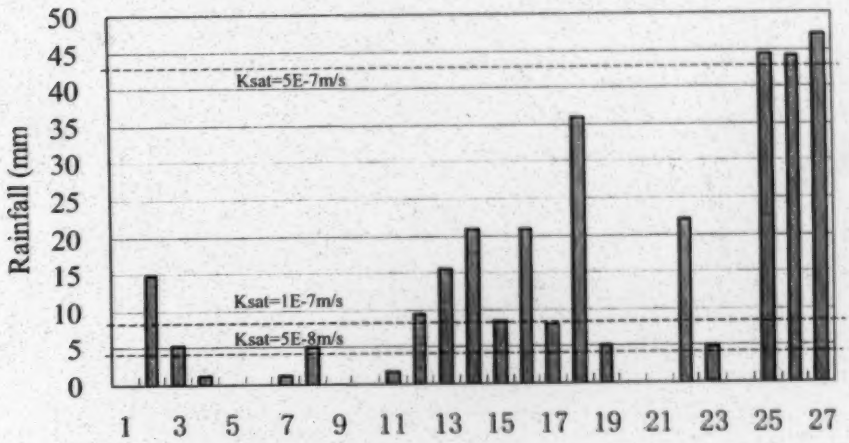

Figure 3-6 Rainfall data for seepage analysis of embankment at MP 154.47

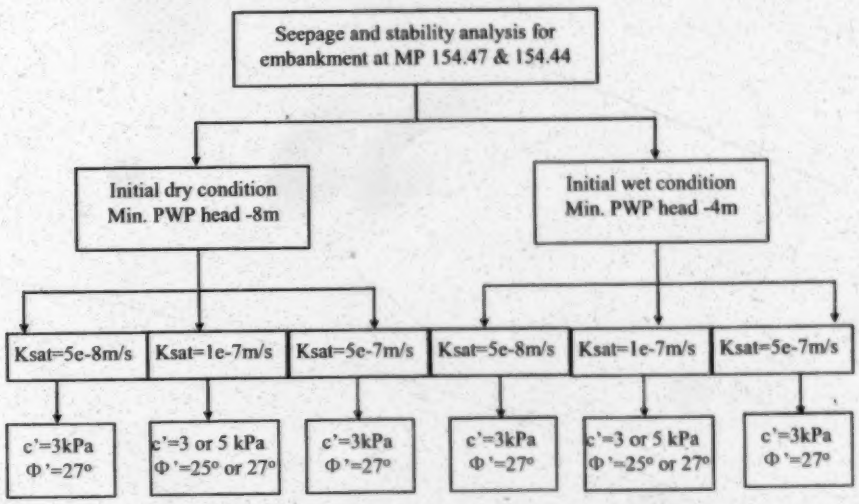

Figure 3-7 Analysis scenarios for embankment at MP 154.47

The seepage modeling results are presented in Figures 3-8, 3-9 and in Appendix C. Figures 3-8 and 3-9 illustrate the final pore-water pressure profile after June 27 for the initially dry and wet embankments, respectively. These figures show that the pore-water pressure distributions had similar patterns for all analysis scenarios. As expected, near the

embankment surface, the matric suction decreased due to the applied rainfall, and the core of the embankment presented higher suctions than the region near the ground surface. The figures also show that for the same initial condition and the same distribution of rainfall, the higher the value of K_{sat}, the greater the decrease of the matric suctions from the initial condition and the deeper the wetting front.

For the initially dry embankment, the changes in the pore-water pressure with time are given in Figures C-1 to C-4 in Appendix C. From Figures C-1 to C-3, it clearly shows that the wetting front developed downward gradually with time and Figure C-4 shows that horizontally, the wetting front advanced inward with time. The higher the hydraulic conductivity, the deeper the wetting front was. After June 27, in vertical direction, the wetting front reached 2.6 m depth, 3.3 m depth, and 4.0 m depth, respectively, for the Ksat =5E-8 m/s, Ksat = 1E-7 m/s, and Ksat = 5E-7 m/s scenarios. For the Ksat=5E-8 m/s and Ksat = 1E-7 m/s cases, the pore-water pressure at the embankment surface reached a saturated state (PWP = 0) on June 2, dropped back to a negative value, and then reached a saturated state again for most of remainder of June. The saturated pore-water pressures at the embankment surface resulted from a rainfall rate higher than the saturated hydraulic conductivity (refer to Figure 3-6). In the case of Ksat = 5E-7 m/s, the pore-water pressure at the embankment surface did not reach a saturated state until June 25. From Figure C-1, it can also be found that during dry periods (i.e., when either no rainfall or only a very small amount of rainfall occurred), the water in the soil voids still could flow downward due to the hydraulic gradient, resulting in an increase of the matric suction at the top of the embankment and a decrease of the mtatric suction in the region below. After June 27, the ground water table in the middle of the embankment did not change for the Ksat = 5E-8 m/s and Ksat = 1E-7 m/s cases, and the water table rose at the toes of the embankment and in the foundation outward away from the embankment toes. In the case of Ksat = 5E-7 m/s, a slight rise of the ground water table in the middle of the embankment and a dramatic rise of water table at the toes of the embankment occurred.

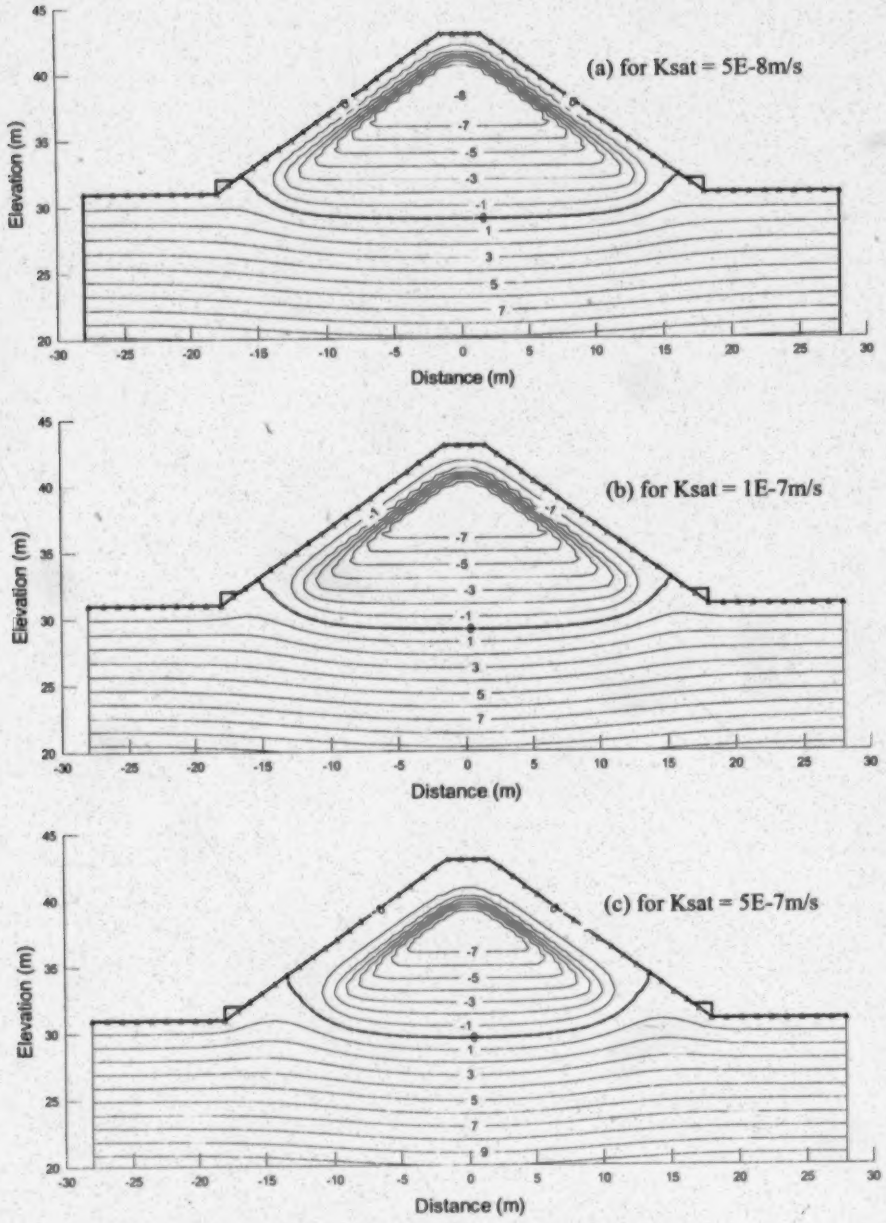

Figure 3-8 Pore-water pressure head profiles after June 27
for initially dry embankment at MP 154.47 (contour unit: meters)

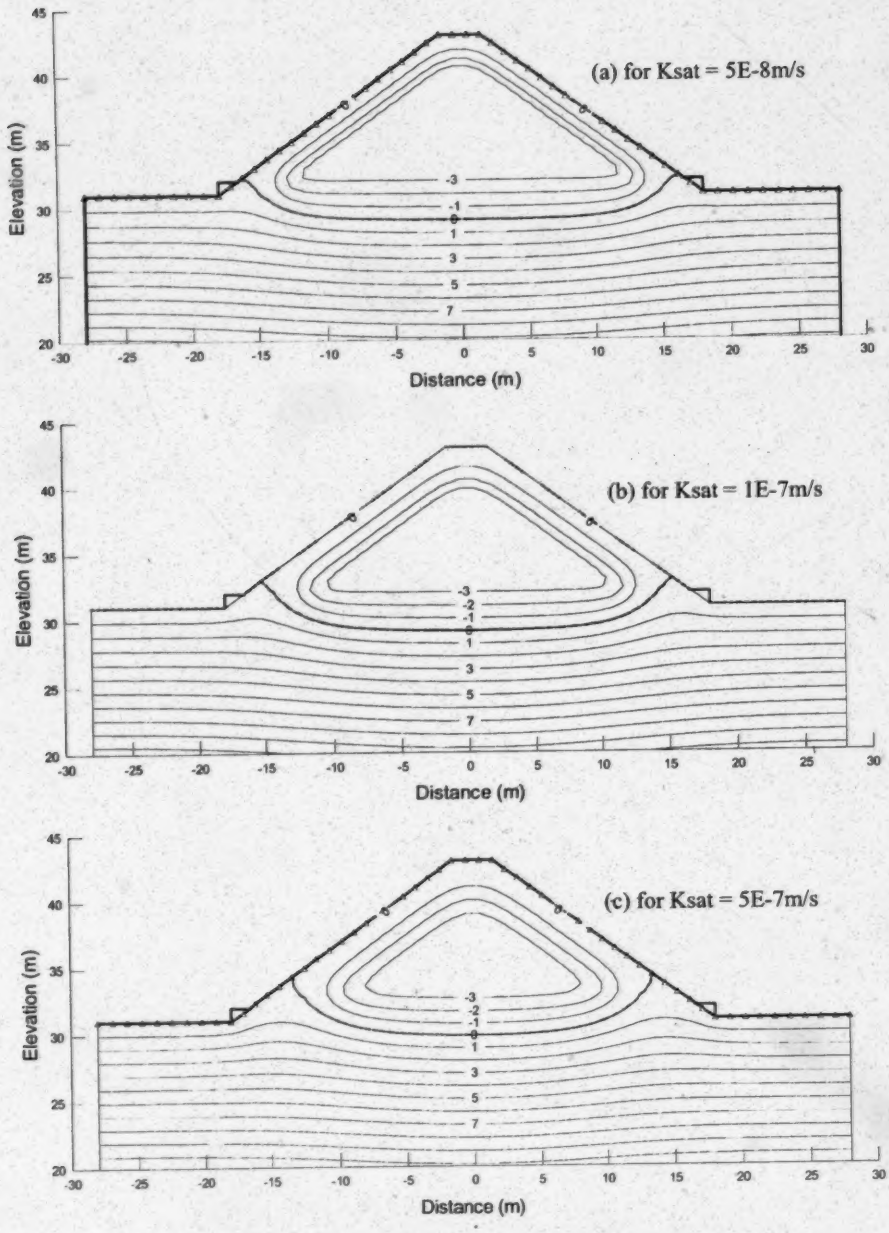

Figure 3-9 Pore-water pressure head profiles after June 27
for initially wet embankment at MP 154.47 (contour unit: meters)

For the initially wet embankment, the detailed seepage modeling results are provided in Figures C-5 to C-8 in Appendix C. The results again show that for a higher hydraulic conductivity material, the rainfall infiltration wetting front went deeper than that for a lower hydraulic conductivity case. After June 27, the wetting front reached 4 m depth, 4.6 m depth and 6.6 m depth for the Ksat = 5E-8 m/s, Ksat = 1E-7 m/s, and Ksat = 5E-7 m/s cases, respectively. For the Ksat = 5E-8 m/s and Ksat = 1E-7 m/s scenarios, since the saturated hydraulic conductivity was smaller than the rainfall intensity in most days in June (see Figure 3-6), a saturated surface was reached on June 2, a negative pore-water pressure developed due to drainage during the dry periods, and then a saturated state was reached again for most of the remainder of June. In the case of Ksat = 5E-7 m/s, the pore-water pressure at the embankment surface did not reach a saturated state until June 25. After June 27, almost no change occurred in the ground water table in the middle of the embankment for the Ksat =5E-8 m/s and Ksat = 1E-7 m/s cases, and the water table rose much as 0.8m in the case of Ksat = 5E-7 m/s. At the toes of the embankment, the water table rose considerably in all the scenarios. It can be found that in the Ksat = 5E-7 m/s case, after June 27, the whole embankment was affected by the rainfall and had pore-water pressure head values higher than -4m throughout the embankment.

Compared to the initially dry embankment with the same hydraulic conductivity function, the initially wet embankment had lower matric suction and a deeper wetting front since the hydraulic conductivity of the soil increased with the decrease in the matric suction.

For the slope stability analysis, if the soil matric suction is not considered, the factor of safety of the embankment would be 0.95 if the shear strength parameters c'= 3 kPa and $\Phi'=27^{o}$ were used and the critical slip surface was relatively shallow, as is shown in Figure 3-10. This indicates that the embankment would be unstable if no soil matric suction existed.

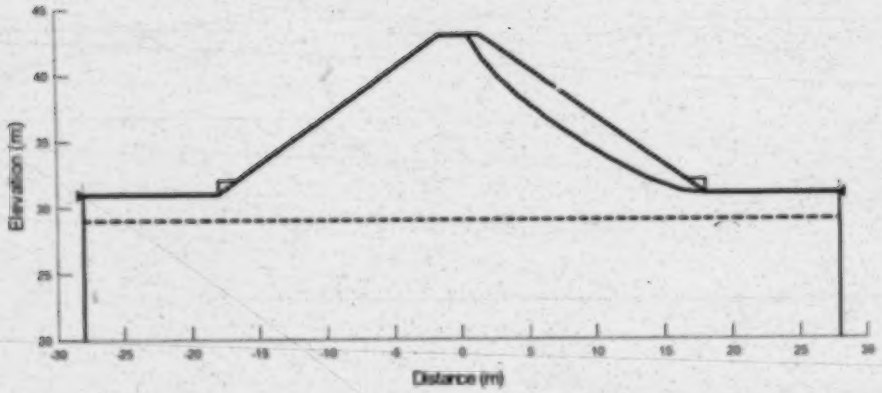

Figure 3-10 Critical slip surface for embankment at MP 154.47 if matric suction not considered

The stability results obtained when considering the soil matric suction are presented in Table 3-1 for both the initially dry and wet embankment conditions on June 1 (i.e., before the rainfall in June) and on June 27 (i.e., after heavy rainfall) by using soil strength parameters of c'= 3 kPa, Φ'= 27° and Φ^b=12°. The initial factors of safety equaled 1.38 and 1.27 for the initially dry and wet embankments, respectively, indicating that in both of the conditions, the embankment was relatively stable. For the initially dry embankment, after June 27 the factor of safety decreased by 11%, 18% and 26%, respectively, for the Ksat = 5E-8 m/s, Ksat = 1E-7 m/s and Ksat = 5E-7 m/s cases. This decrease resulted from the decrease in the soil matric suction due to the rainfall infiltration and, hence, the decrease of the soil shear strengths. The embankment was in a marginally stable condition after June 27 with a factor of safety of 1.13 and 1.02 for the Ksat = 1E-7 m/s and Ksat = 5E-7 m/s scenarios. For the initially wet embankment, the factor of safety decreased by 10%, 16% and 22% for the cases of Ksat = 5E-8 m/s, Ksat = 1E-7 m/s and Ksat = 5E-7 m/s, respectively. Again, the rainfall infiltration drove the embankment into a marginally stable or unstable condition. Figure 3-11 shows the critical slip surfaces for both the initially dry and wet embankments. For the initially dry embankment, the critical slip surface on June 1 was slightly deeper than that of the initially wet embankment. In both circumstances, the critical slip surface moved toward the ground surface with time due to the rainfall infiltration.

It is important to mention that if the hourly rainfall data instead of the daily rainfall data were used in the modeling, the results would be slightly different since the actual rainfall was not continuous.

Table 3-1 Factors of safety of embankment at MP 154.47
by using strength parameters c'=3kPa, Φ'=27°, Φ^b=12°

Initially Dry Embankment				
	June 1	June 27 Ksat = 5E-8m/s	June 27 Ksat = 1E-7m/s	June 27 Ksat = 5E-7m/s
FoS	1.38	1.23	1.13	1.02
% of FoS Decrease		11%	18%	26%
Initially Wet Embankment				
	June 1	June 27 Ksat = 5E-8m/s	June 27 Ksat = 1E-7m/s	June 27 Ksat = 5E-7m/s
FoS	1.27	1.15	1.07	1.00
% of FoS Decrease		10%	16%	22%

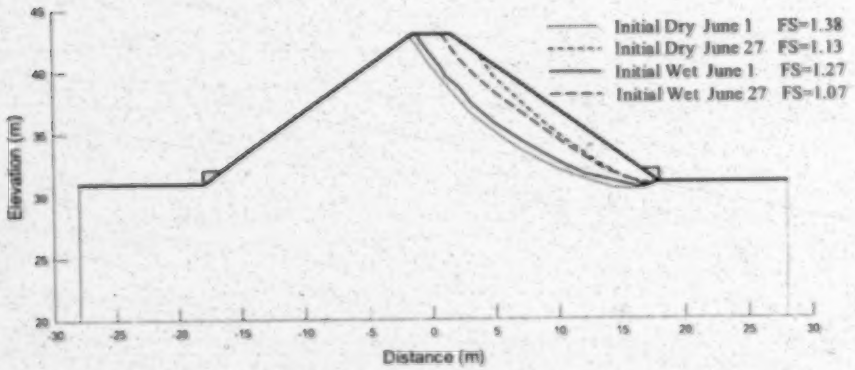
Initial Dry June 1 FS=1.38
Initial Dry June 27 FS=1.13
Initial Wet June 1 FS=1.27
Initial Wet June 27 FS=1.07
Elevation (m)
Distance (m)

Figure 3-11 Critical slip surfaces for initially dry and wet embankments at MP 154.47
by using c'=3kPa, Φ'=27°,and Φ^b=12°

The change in the embankment stability with time was modeled by taking the day-to-day pore-water pressure distribution as an input for the stability analysis. The results for the initially wet embankment with Ksat = 1E-7 m/s and using c'=3 kPa, $\Phi'=27^{\circ}$ and $\Phi^{b}=12^{\circ}$ are presented in Figure 3-12, together with the rainfall data. From Figure 3-12, the 14 mm rainfall on June 2 decreased the factor of safety of the embankment by 1.6% from 1.272 to 1.252. From June 3 to June 11, the factor of safety almost remained unchanged since either no rainfall or only a very small amount of rainfall occurred in this period. Then a continuous decrease in the factor of safety occurred until June 19, from a value of 1.25 on June 11 to 1.18 on June 19, a decrease of 5.2% resulting from the continuous rainfall infiltration from June 12 to June 19. After June 19, the factor of safety increased slightly during the dry period of June 20 and 21 and then decreased due to the rainfall on June 22 and 23. A high-intensity rainfall of more than 44 mm per day occurred between June 25 and June 27. After the three days heavy rainfall on June 25, 26 and June 27, the factor of safety of the embankment decreased by 6.6% from 1.15 to 1.07. The effect of these three days of heavy rainfall accounted for 41% of the total decrease of the factor of safety of the embankment for the 27-day period from June 1 to June 27. The prolonged antecedent rainfall from June 2 to June 24 also had an influence on the embankment instability by accounting for 59% of the total decrease of the factor of safety of the embankment.

Figure 3-13 presents the evolution of the critical slip surface with time for the Ksat = 1E-7 m/s initially wet embankment, using parameters of c'=3 kPa, $\Phi'=27^{\circ}$ and $\Phi^{b}=12^{\circ}$. It shows a relatively deep critical slip surface on June 1. As the rainfall infiltrated and the matric suction in the near ground surface region decreased rapidly, the critical slip surfaces moved towards the ground surface.

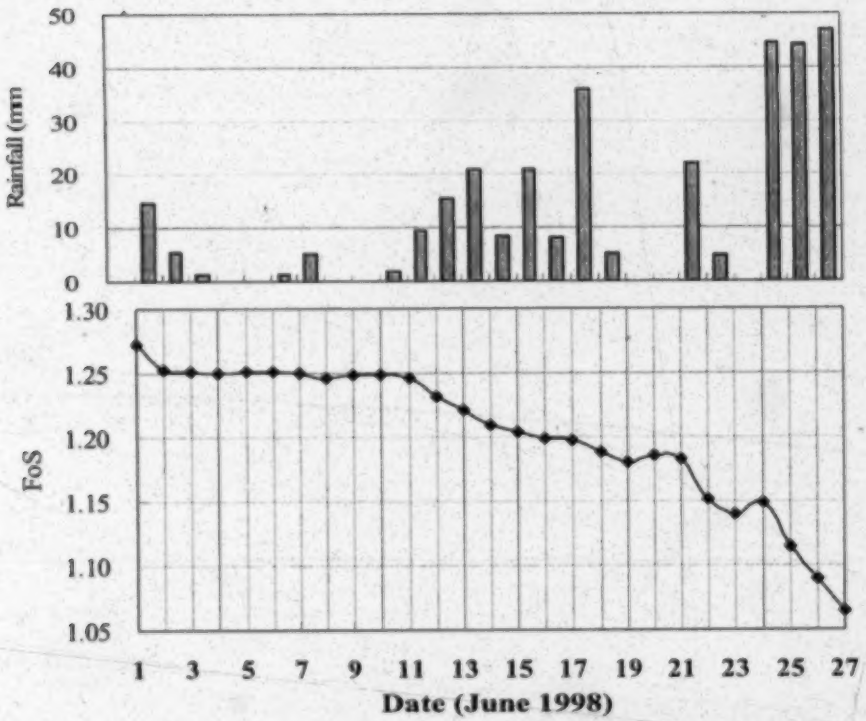

Figure 3-12 Change in the factor of safety with time for initially wet embankment at MP 154.47 by using Ksat = 1E-7m/s, c'=3kPa, $\Phi'=27^{\circ}$ and $\Phi^{b}=12^{\circ}$

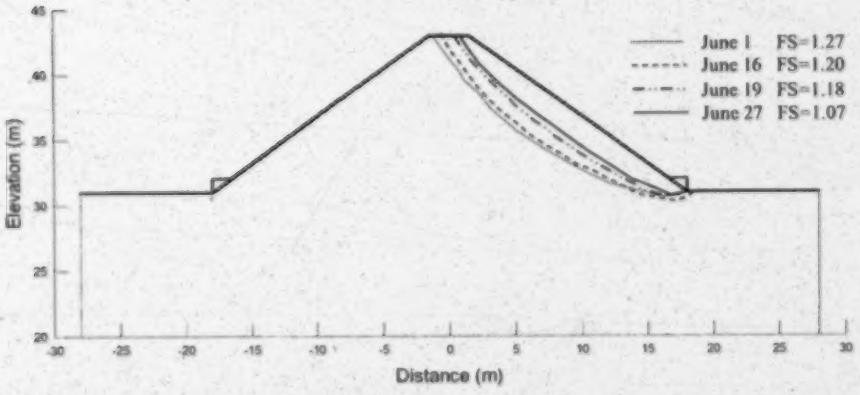

Figure 3-13 Evolution of critical slip surfaces for initially wet embankment at MP 154.47 by using Ksat = 1E-7m/s, c'=3kPa, $\Phi'=27^{\circ}$, $\Phi^{b}=12^{\circ}$

A parametric study including the uncertainty in the shear strength parameters was performed, and the results are provided in Table 3-2 for the Ksat = 1E-7 m/s condition. It can be seen from Table 3-2 that the shear strength parameters, effective friction angle and effective cohesion, had an influence on the factor of safety regardless of the atmospheric conditions. For example, by increasing the effective cohesion from 3 kPa to 5 kPa, the factor of safety of the initially wet embankment would be increased by 5.8% on June 1 and by 11.5% after the rainfall on June 27.

Table 3-2 Factors of safety with different strength parameters for embankment at MP 154.47 using Φ^b=12° for all the calculations

Factor of Safety		Initial Dry Condition Ksat = 1E-7m/s		Initial Wet Condition Ksat = 1E-7m/s	
		June 1	June 27	June 1	June 27
c=3kPa	Φ=25°	1.29	1.08	1.20	1.01
	Φ=27°	1.38	1.13	1.27	1.07
% of FoS change		6.6%	4.2%	6.4%	6.0%
Φ=27°	c=3kPa	1.38	1.13	1.27	1.07
	c=5kPa	1.45	1.27	1.35	1.19
% of FoS change		5.2%	12.5%	5.8%	11.5%

Finally, to consider the different initial ground water conditions, an analysis of an initial ground water table right at the base of the embankment was conducted, using the hydraulic conductivity function with Ksat = 1E-7 m/s and the shear strength parameters of c'=3kPa, Φ'=27° and Φ^b=12°. The pore-water pressure distribution and slope stability results are presented in Figure 3-14, which reveals that at the toes of the embankment, the ground water table rose due to the rainfall infiltration. The slope stability results indicate that the local area of the toes of the embankment failed first.

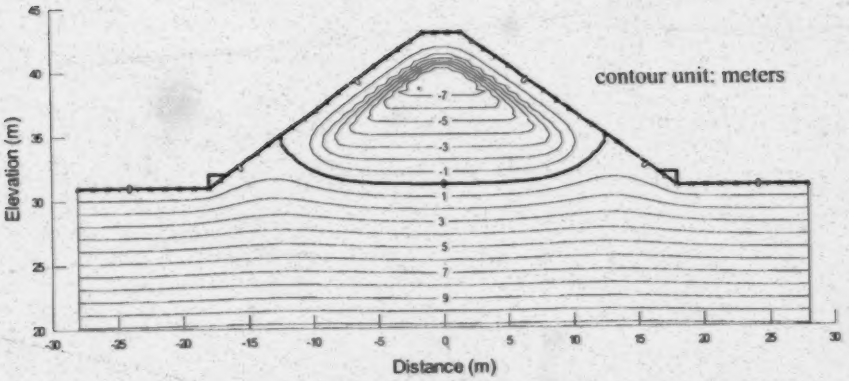

(a) Pore-water pressure head distribution after June 27 for initially dry embankment

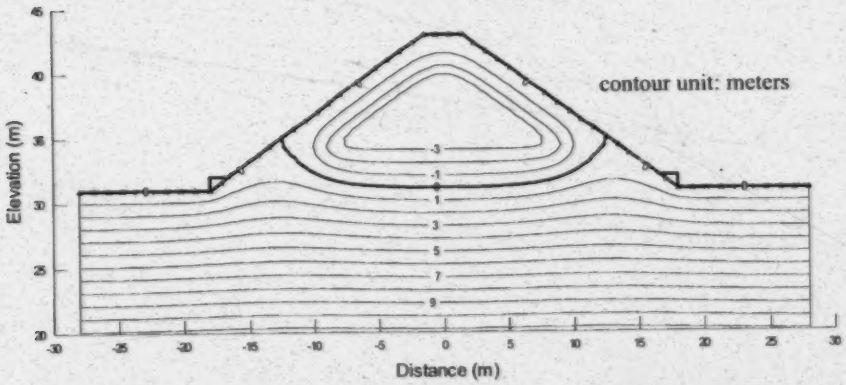

(b) Pore-water pressure head distribution after June 27 for initially wet embankment

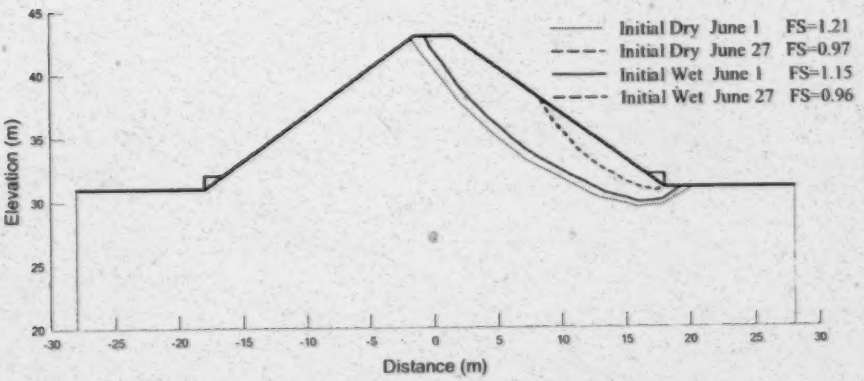
Initial Dry June 1 FS=1.21
Initial Dry June 27 FS=0.97
Initial Wet June 1 FS=1.15
Initial Wet June 27 FS=0.96
Elevation (m)
Distance (m)

(c) Evolution of critical slip surface

Figure 3-14 Seepage and stability results for embankment at MP 154.47 with an initial groundwater table at the base of the embankment

3.3.2 MP 150.17 Embankment Stability Analysis

The slope on the east side of the embankment at MP 150.17 failed on the morning of June 26, 1998, resulting in the derailment of a train. A stability analysis was conducted in order to evaluate the reasons for the embankment failure.

Figure 3-15 presents the embankment geometry and finite element mesh. The embankment was 19 m high with an crest width of 3 m and side slopes of 1.5H:1V (33.7°). The embankment was built of fine to medium sand, with some silt and traces of fine gravel (refer to Figure B-8 in Appendix B for grain-size curves) over a hard bedrock foundation. The embankment was discretized into a fine finite element mesh for seepage analysis with a total of 1446 elements.

The soil properties for the seepage analysis were estimated on the basis of material #6 (silty sand) and material #3 (sandy loam) in the SEEP/W soil function database. The grain size curves of the embankment material and materials #6 and #3 in the SEEP/W database, were compared, and the results are provided in Figure B-9 in Appendix B. Figures B-10 and B-11 in Appendix B provide the soil functions for materials #6 and #3 in the SEEP/W database. A volumetric water content at saturation of 0.42 was assumed for the embankment soil, and three values for the saturated hydraulic conductivity with respect to water, 5E-7 m/s, 1E-6 m/s and 5E-6 m/s, were considered. A saturated hydraulic conductivity value of 1E-6 m/s was taken as a typical value for the embankment silty sand material. The volume water content and hydraulic conductivity functions used in this study are presented in Figure 3-16.

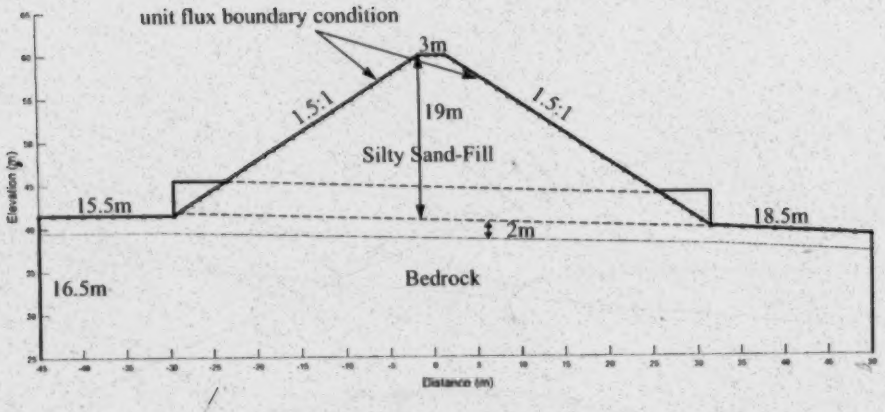

(a) Embankment geometry

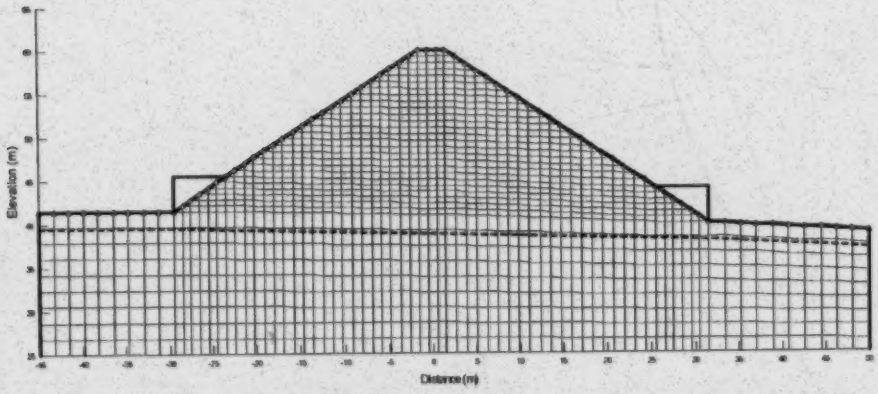

(b) Finite element mesh

Figure 3-15 Geometry and finite element mesh for embankment at MP 150.17

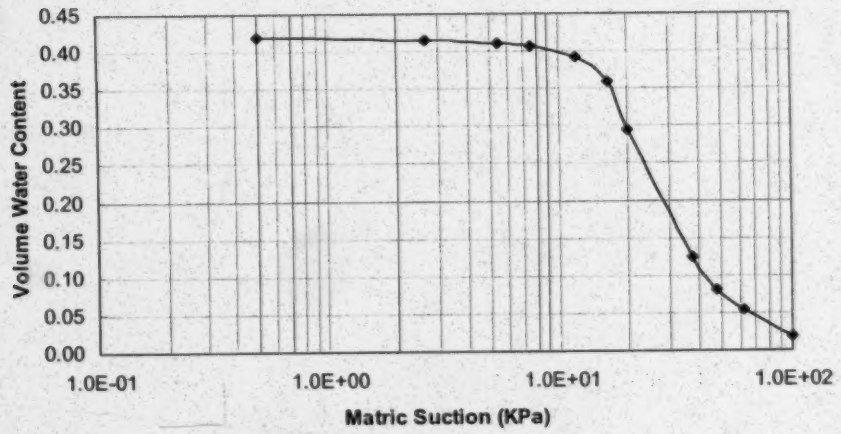

(a) Volume water content function

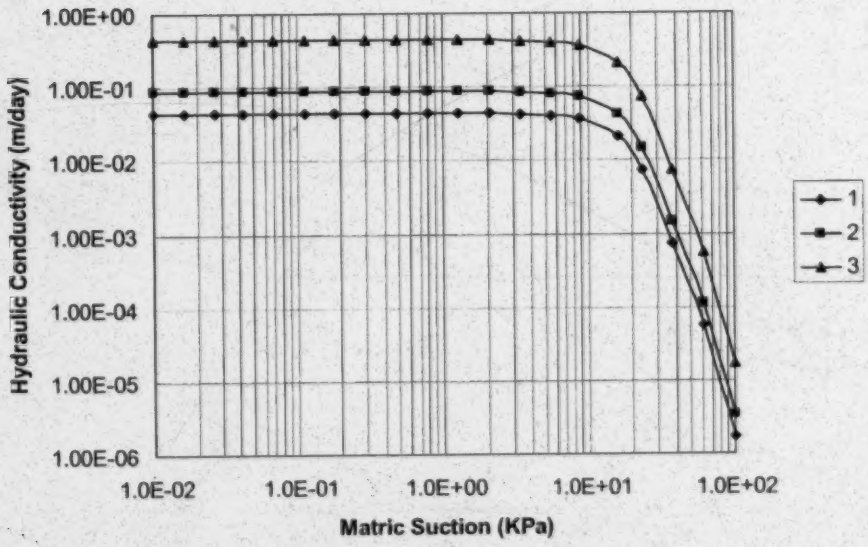

1: Ks=5E-7m/s; 2: Ks=1E-6m/s; 3: Ks=5E-6m/s

(b) Hydraulic conductivity function

Figure 3-16 Volume water content and hydraulic conductivity functions for embankment fill at MP 150. 17

The initial pore-water pressure distributions were established based on a combination of a hydrostatic distribution and a minimum pore-water pressure value. An initial water table 2 m below the embankment base was assumed. Two minimum negative pore-water pressure conditions were considered, namely a minimum pore-water pressure head of -8 m to represent a relatively dry embankment and a minimum pore-water pressure head of -4 m to represent a relatively wet embankment.

The radar-derived daily precipitation data from June 1, 1998 to June 25, 1998 were applied to the embankment surface as a unit flux boundary condition. Since the embankment failed on the morning of June 26 around 01:00am, only the time period from June 1 to June 25 was considered. A no-flow condition was selected for the remaining boundaries.

For the slope stability analysis, Morgenstern-Price limit equilibrium method was used. It is assumed that the soil had a zero effective cohesion and an effective angle of internal friction Φ' of 28° to 32°. A Φ^b angle of 15°, equal to approximately half of the internal friction angle, was assumed, and a total unit weight of 18 kN/m^3 was used in the analysis. The analysis scenarios for the embankment at MP 150.17 are shown in Figure 3-17.

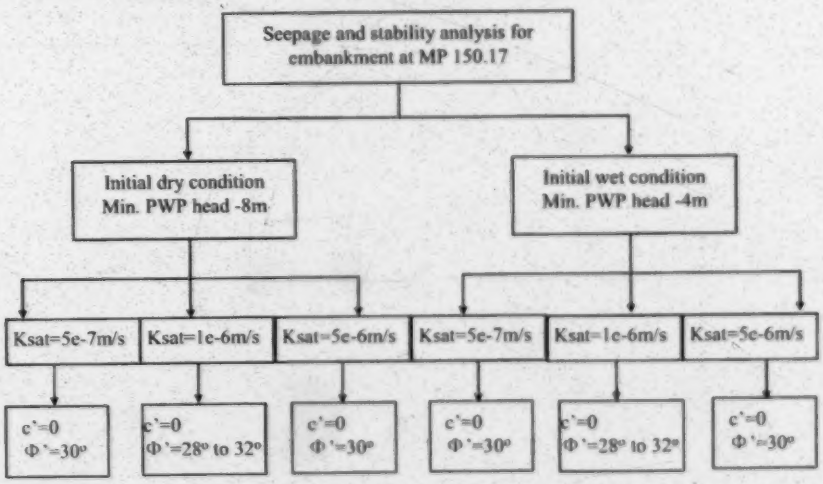

Figure 3-17 Analysis scenarios for embankment at MP 150.17

The seepage modeling results are given in Figures 3-18 and 3-19 and in Appendix C. Like the pore-water distribution of the embankment at MP 154.47, the pore-water pressure distribution of the embankment at MP 150.17 had similar styles for all analysis scenarios. The core of the embankment presented higher suctions than those near the ground surface. For the same initial condition and the same distribution of rainfall, higher hydraulic conductivity created a greater decrease in the matric suction from the initial condition and deeper wetting front.

The detailed seepage results are provided in Figures C-9 through C-16 in Appendix C to demonstrate the evolution of the pore-water pressures in the embankment. These figures clearly show that the wetting front developed gradually downward in a vertical direction and inward in a horizontal direction. It can also be found that the higher the hydraulic conductivity, the deeper the wetting front was.

From Figures C-9 and C-11 in Appendix C, for the initially dry embankment, the wetting front after June 25 developed downward, reaching 2.2 m depth, 3.0 m depth and 4.4 m depth for the cases of Ksat =5E-7 m/s, Ksat = 1E-6 m/s, and Ksat = 5E-6 m/s, respectively. For initially wet embankment, it can be observed from Figures C-13 and C-15 that after June 25, the wetting front reached 3 m depth, 4 m depth and 5.2 m depth for the Ksat =5E-7 m/s, Ksat = 1E-6 m/s, and Ksat = 5E-6 m/s cases, respectively.

For the embankment at MP 150.17, in both the initially dry and wet conditions, the embankment surface region did not reach saturation during June 1 to June 25, with the exception of the Ksat = 5E-7 m/s scenario in which a saturated embankment surface appeared after the 44 mm of heavy rainfall on June 25. This result occurred because the rainfall intensities were lower than the saturated hydraulic conductivity. In the case of a high hydraulic conductivity of Ksat = 5E-6 m/s relative to the rainfall intensity, for the initially wet embankment, the matric suction head at the crest of the embankment increased by 0.7 m during June 5 to June 9 when no rainfall or only a small amount of rainfall occurred (refer to Figure C-13 (d) in Appendix C).

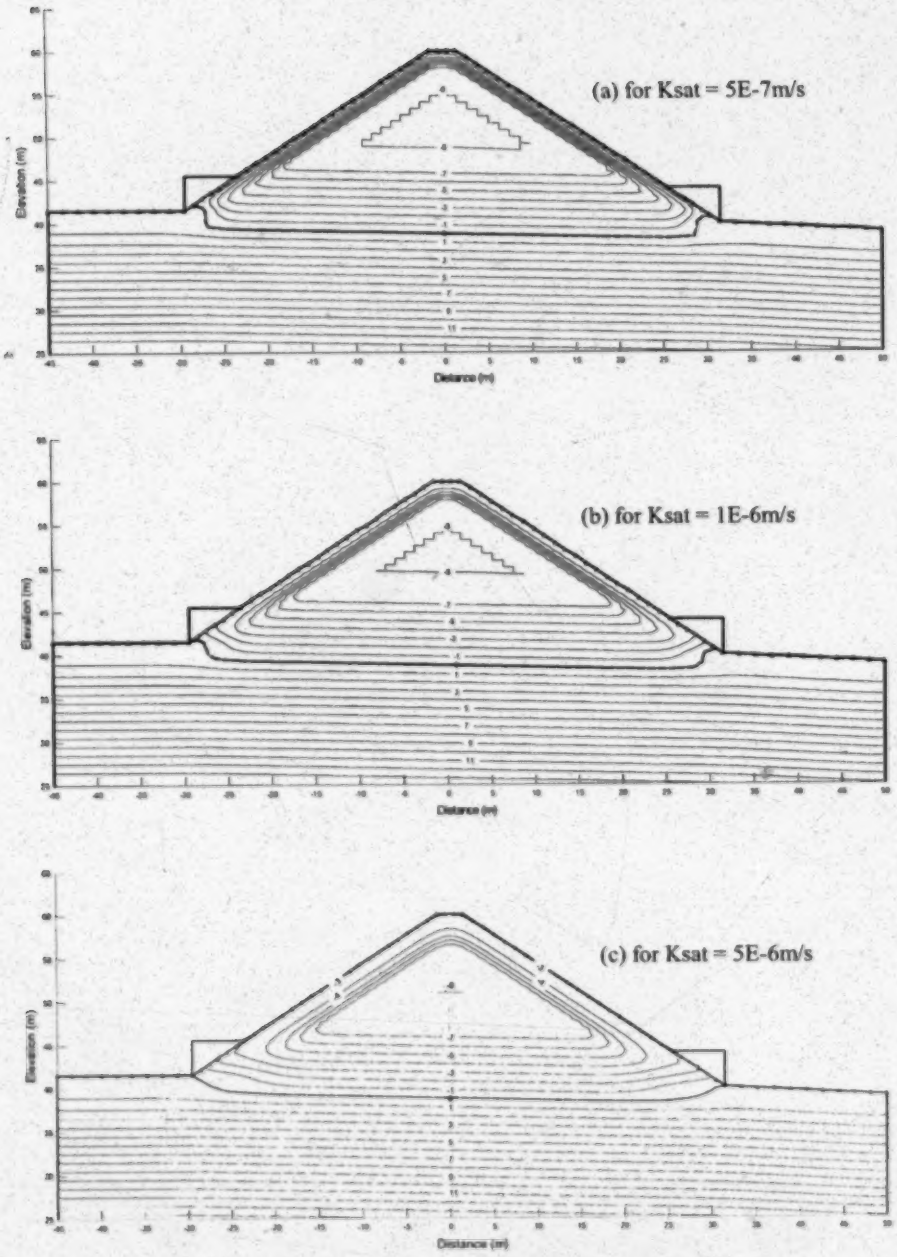

Figure 3-18 Pore-water pressure head profiles after June 25
for initially dry embankment at MP 150.17 (contour unit: meters)

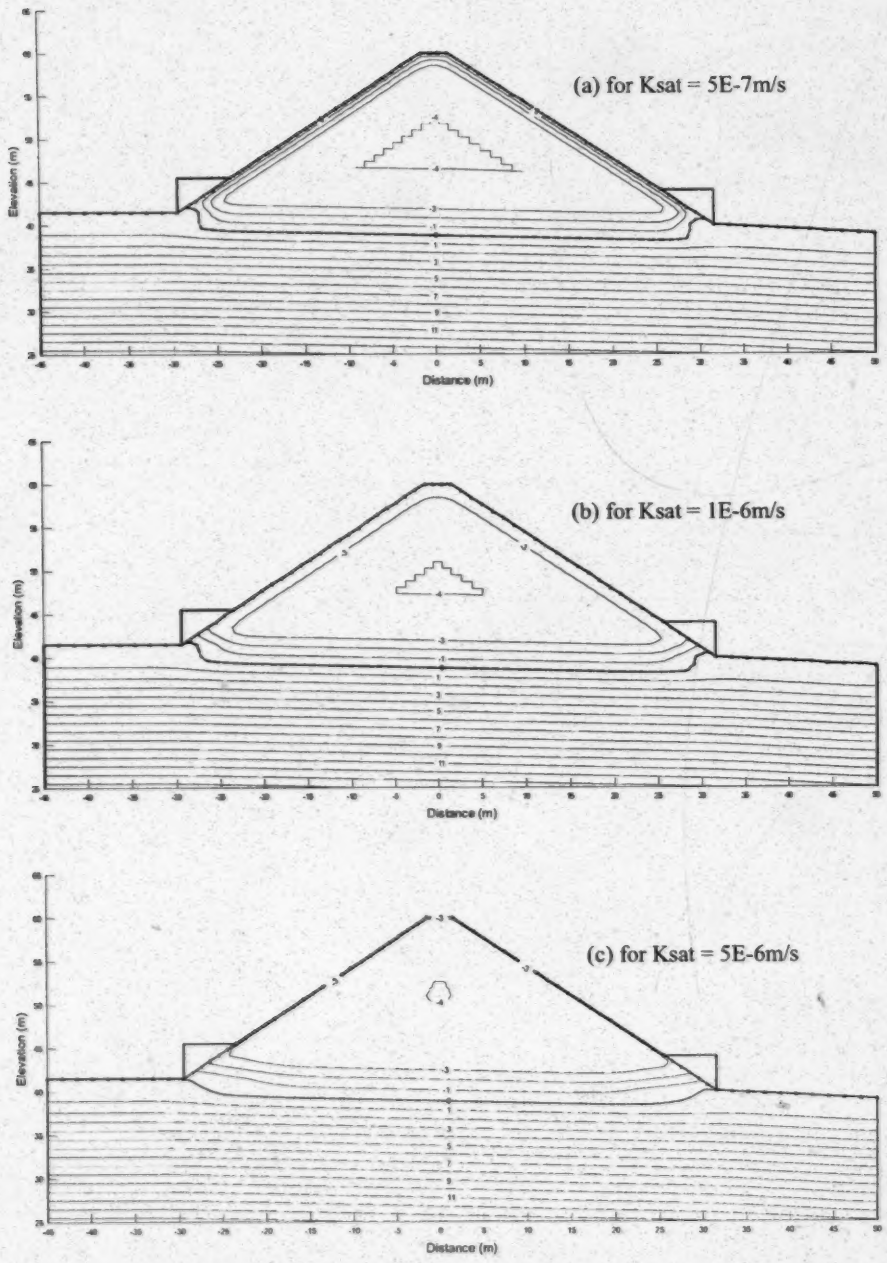

Figure 3-19 Pore-water pressure head profiles after June 25 for initially wet embankment at MP 150.17 (contour unit: meters)

Figures C-10 and C-11 in Appendix C show that for the initially dry embankment, the ground water table in the middle of the embankment did not change due to the rainfall from June 1 to June 25, while the water table at the toes of the embankment rose. Figures C-14 and C-15 in Appendix C show that for the initially wet embankment, the water table both in the middle and at the toes of the embankment rose.

Compared with the initially dry embankment having the same hydraulic conductivity function, the initially wet embankment had a lower matric suction result and a deeper wetting front.

If the soil matric suctions were not taken into account in slope stability analysis and if the shear strength parameters of $c'=0$ and $\Phi'=30^{\circ}$ were used, the factor of safety of the embankment would turn out to be less than one. This suggests that soil matric suction plays a role in the embankment stability.

Table 3-3 provides the factors of safety for the initially dry and wet embankments. The results in this table were prepared by considering the increase of soil strength due to matric suction and by using the shear strength parameters $c'=0$, $\Phi'=30^{\circ}$ and $\Phi^{b}=15^{\circ}$. The initial factors of safety of 1.44 for the initially dry embankment and 1.29 for the initially wet embankment show that under both conditions the embankment was stable. After June 25, the factor of safety of the initially dry embankment decreased by 2.1%, 2.2% and 3.2%, respectively, for Ksat = 5E-7 m/s, Ksat = 1E-6 m/s and Ksat = 5E-6 m/s cases. The factor of safety of the initially wet embankment decreased by 2.8%, 3.0%, 3.8%, respectively, for Ksat = 5E-7 m/s, Ksat = 1E-6 m/s and Ksat = 5E-6 m/s scenarios. These results show that the intermittent rainfall from June 1 to June 25 reduced the stability of the embankment slightly and that the embankment would have remained stable if only the rainfall infiltration had acted on it. Figure 3-20 illustrates the critical slip surfaces for the initially dry and wet embankments with a saturated hydraulic conductivity of 1E-6 m/s and using the mean shear strength values. It can be observed that the initially dry embankment presented a deeper critical slip surface than the initially wet embankment. After the precipitation event from June 1 to June 25, the critical slip surfaces of both the

initially dry and wet embankments slightly moved toward the ground surface. For the Ksat = 5E-7 m/s and Ksat = 5E-6 m/s cases, the critical slip surfaces had similar trends.

Table 3-3 Factor of safety for embankment at MP 150.17 using c'=0, Φ'=30°, and Φ^b=15°

Initially Dry Embankment				
	June 1	June 25 Ksat = 5E-7m/s	June 25 Ksat = 1E-6m/s	June 25 Ksat = 5E-6m/s
FoS	1.44	1.41	1.41	1.39
% of FoS Decrease		2.1%	2.2%	3.2%
Initially Wet Embankment				
	June 1	June 25 Ksat = 5E-7m/s	June 25 Ksat = 1E-6m/s	June 25 Ksat = 5E-6m/s
FoS	1.29	1.25	1.25	1.24
% of FoS Decrease		2.8%	3.0%	3.8%

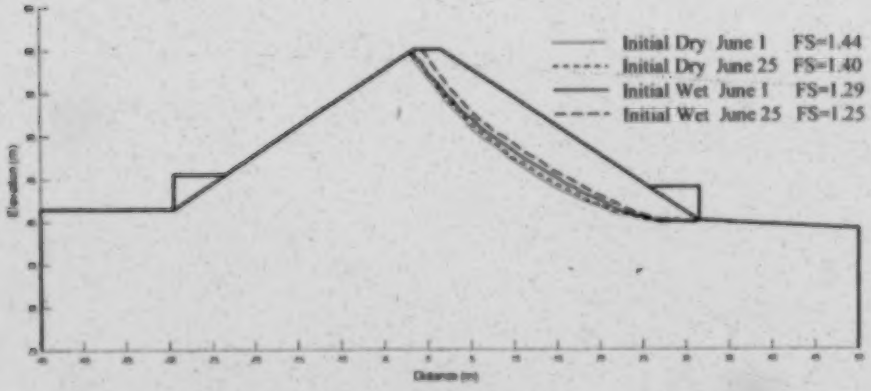

Figure 3-20 Critical slip surfaces for initially dry and wet embankments at MP 150.17 by using Ksat = 1E-6m/s, c'=0, Φ'=30°, and Φ^b=15°

The change in the embankment stability with time was calculated by taking the day-to-day pore-water pressure distribution as an input for the stability analysis. The results for the initially wet condition obtained by using the parameters c'=0, Φ'=30°, Φ^b=15°, are

presented in Figure 3-21, together with the rainfall data. The figure shows that the factor of safety of the embankment decreased gradually with time due to the precipitation. The factor of safety increased slightly during the dry periods of June 5, June 6, June 9, June 10, June 20 and June 21. It can also be noted that the 44 mm rainfall on June 25 reduced the stability of the embankment significantly. The prolonged antecedent rainfall from June 2 to June 24 also had an influence on the embankment stability. In Figure 3-21, the three lines for the different hydraulic conductivity cases show that the higher the hydraulic conductivity of the embankment material, the faster the decreased of the embankment stability.

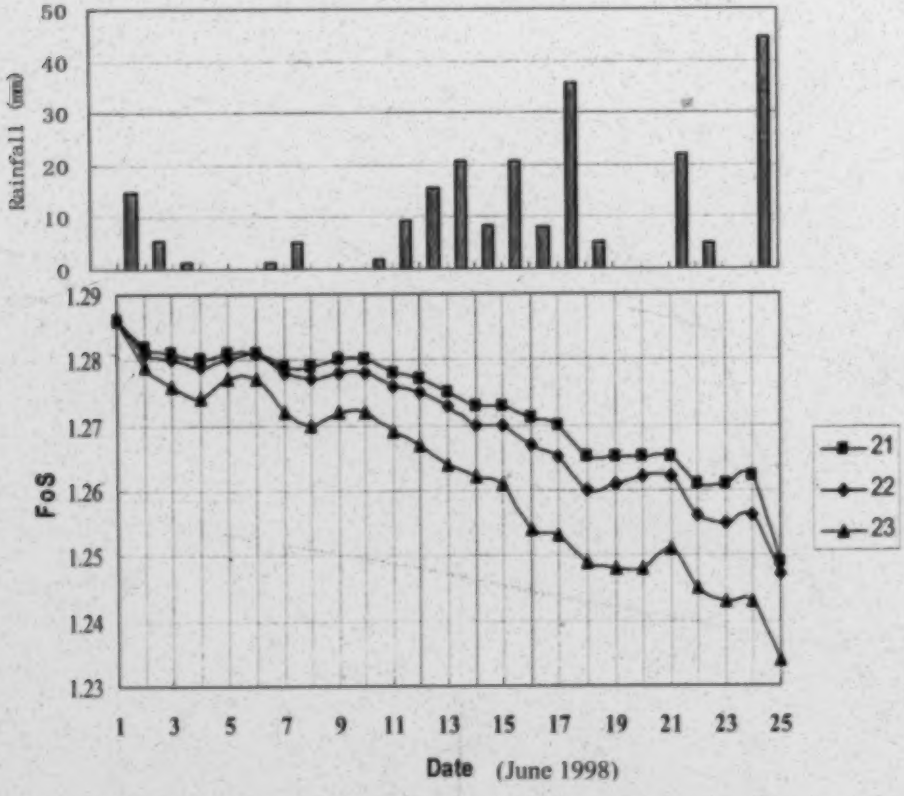

Note: 21: Ks=5E-7m/s; 22: Ks=1E-6m/s; 23: Ks=5E-6m/s

Figure 3-21 Change in factor of safety with time of initially wet embankment at MP 150.17

Table 3-4 gives the factors of safety of the embankment by using different strength parameters for the Ksat = 1E-6 m/s condition. It can be seen that the stability of the embankment was influenced by the shear strength parameters regardless of the atmospheric conditions.

Table 3-4 Factors of safety of embankment at MP 150.17 using different strength parameters

Factor of Safety		Initially Dry Embankment Ksat = 1E-6m/s		Initially Wet Embankment Ksat = 1E-6m/s	
		June 1	June 27	June 1	June 27
c'=0	Φ'=28°	1.35	1.32	1.20	1.17
	Φ'=30°	1.44	1.40	1.29	1.25
	Φ'=32°	1.52	1.49	1.37	1.33

To simulate the effect of train loading on the embankment stability, an external load of 40 kPa and 60 kPa distributed along 2 meters was applied on the embankment crest. The results are summarized in Table 3-5 and Figure 3-22, which show that a train loading of 60kPa could bring the initially wet embankment into a marginally stable condition with a factor of safety of 1.15. The train loading was likely to have been a contributory factor in the slope failure at MP 150.17.

Table 3-5 Effect of trainload on the stability of embankment at MP 150.17

Factor of Safety	Initially Dry Embankment Ksat = 1E-6m/s June 27			Initially Wet Embankment Ksat = 1E-6m/s June 27		
	1	2	3	1	2	3
c'=0 Φ'=30°	1.40	1.36	1.31	1.25	1.21	1.15

Note: 1: without trainload; 2: with trainload 40kPa; 3. with trainload 60kPa.

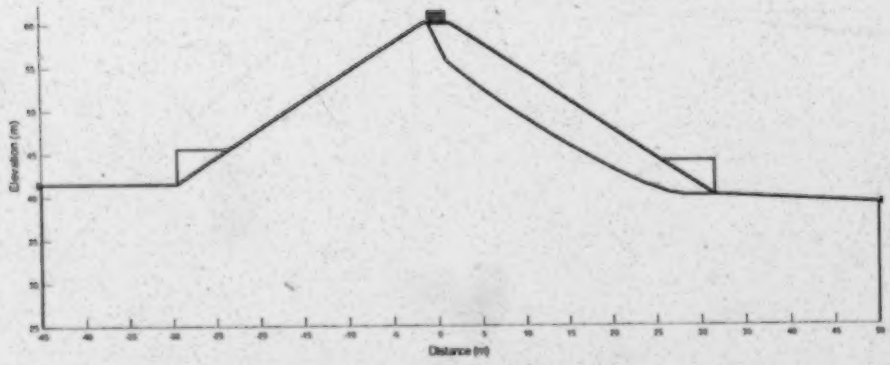

Figure 3-22 Critical slip surface for initially wet embankment at MP 150.17 with a train loading 60kPa (FS=1.15)

Finally, to consider different initial ground water conditions, an analysis of an initial ground water table right at the base of the embankment was conducted. In this analysis, the hydraulic conductivity function with Ksat = 1E-6 m/s and the shear strength parameters of c'=0, $\Phi'=30^{\circ}$ and $\Phi^{b}=15^{\circ}$ were used. The pore-water pressure distributions and slope stability results are presented in Figure 3-23, which shows that the toes of the embankment most likely failed first after the prolonged rainfall from June 1 to June 25. An assumed upstream water level rise is provided in Figure 3-24 (a) and its effect on the embankment stability was analyzed. From Figure 3-24 (b), it can be seen that upstream water level change had little effect on the downstream slope stability because of the low hydraulic conductivity of the embankment material. Figure 3-25 shows the critical slip surfaces after June 25 for the initially wet embankment when a train loading of 40 kPa or 60 kPa distributed along 2 meters at the embankment crest was included. The factors of safety of the embankment reached 1.13 and 1.10 with a 40 kPa and 60 kPa train loadings, respectively, indicating a barely stable condition. This finding suggests again that the train loading might have contributed to the slope failure at MP 150.17.

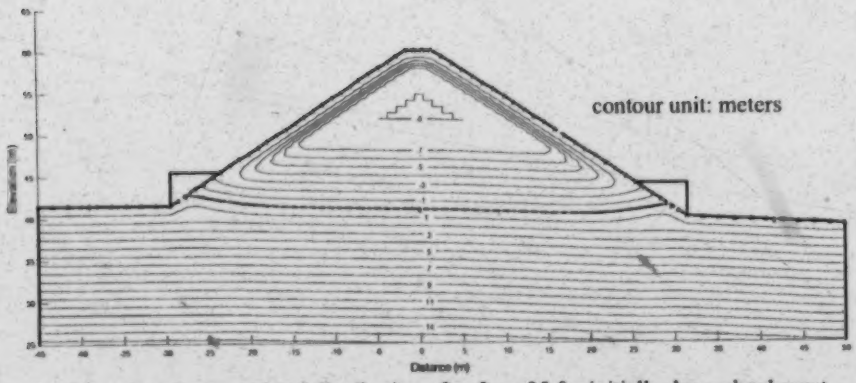

(a) Pore-water pressure head distribution after June 25 for initially dry embankment

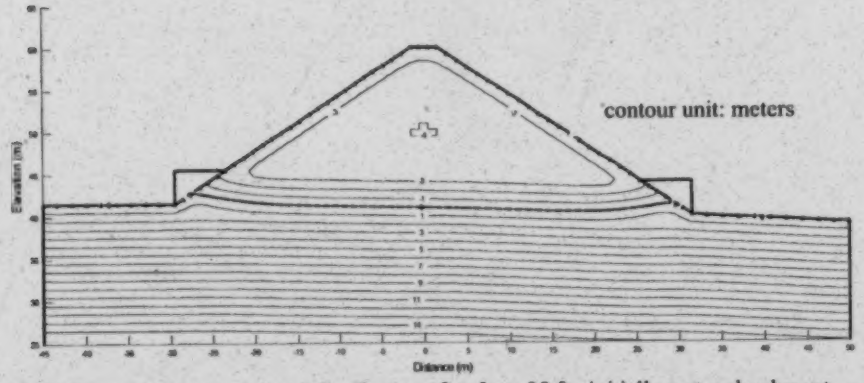

(b) Pore-water pressure head distribution after June 25 for initially wet embankment

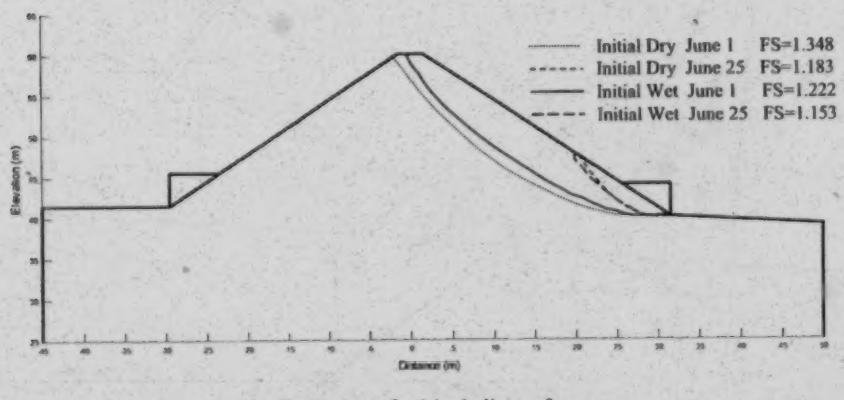
Initial Dry June 1 FS=1.348
Initial Dry June 25 FS=1.183
Initial Wet June 1 FS=1.222
Initial Wet June 25 FS=1.153
Elevation (m)
Distance (m)

(c) Evolution of critical slip surfaces

Figure 3-23 Pore-water pressure distributions and slope stability results for embankment at MP 150.17 with an initial groundwater table at the base of the embankment

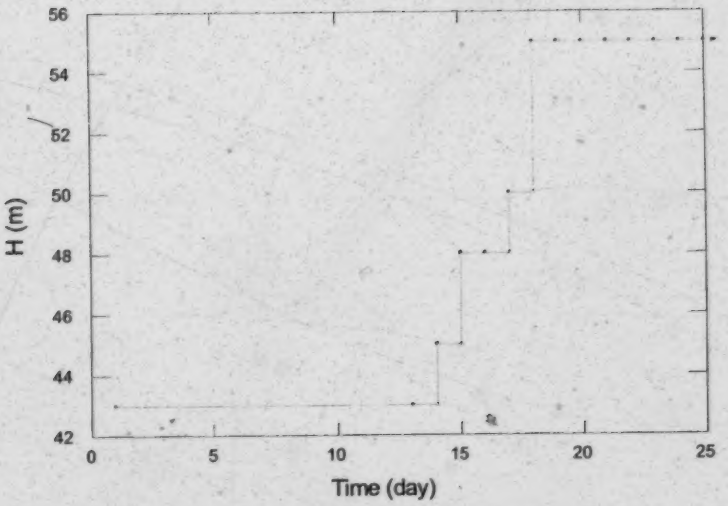

(a) Assumed upstream water level change

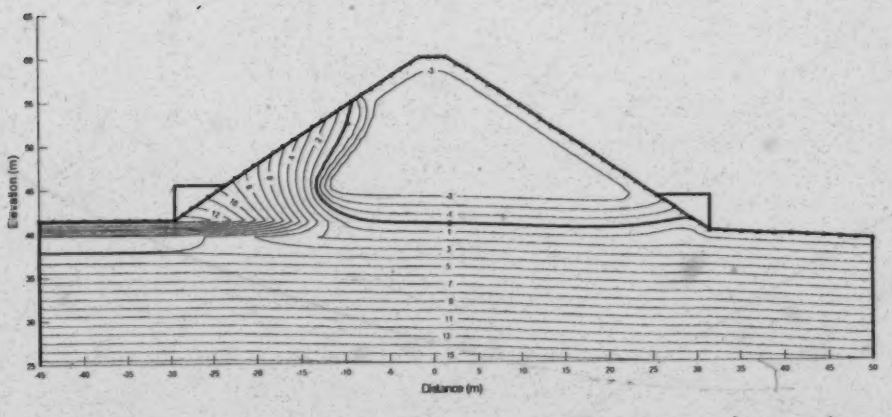

(b) Pore-water pressure head distribution after June 25 (contour unit: meters)

Figure 3-24 Effect of upstream water level on the slope stability of downstream slope at MP 150.17 for initially wet embankment with an initial groundwater table at base of embankment

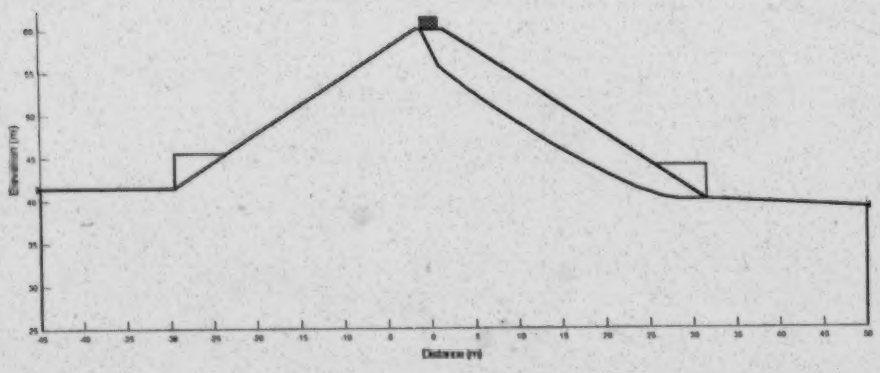

Figure 3-25 Critical slip surface for initially wet embankment at MP 150.17 with an initial groundwater table at the base of embankment when considering train loading (Trainload = 40kPa, FS=1.13; Trainload = 60kPa, FS = 1.10)

3.3.3 MP 150.10 Embankment Stability Analysis

At MP 150.10, the east slope failed on July 5, 1998 at about 06:00am while the MP 150.17 site was being restored.

The embankment soil profile and finite element mesh are presented in Figure 3-26. At MP 150.10, from the top down, the embankment consisted of silty sand fill, native silty sand and dense glacial till. An initial water table depth was assumed. A saturated hydraulic conductivity of 7.5E-7 m/s was specified for the native silty sand material and the silty sand fill was assumed to have a saturated hydraulic conductivity of 1E-6 m/s. The volume water content and hydraulic conductivity functions for the three materials are shown in Figure 3-27. The soil water characteristic curve for material # 11, compacted glacial till, from the SEEP/W database was used in this analysis for the glacial till material in the embankment at MP 150.10 .The shear strength parameters used in this study for the embankment materials are summarized in Table 3-6. An initially dry embankment with a minimum negative pore-water pressure head of -8 m and an initially wet embankment with a minimum negative pore-water pressure head of -4 m were modeled for the time period of June 1 to July 5.

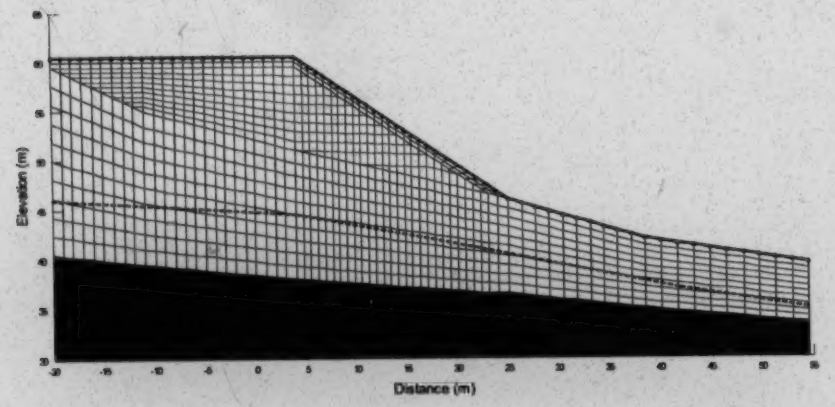

Figure 3-26 Finite element mesh for embankment at MP 150.10

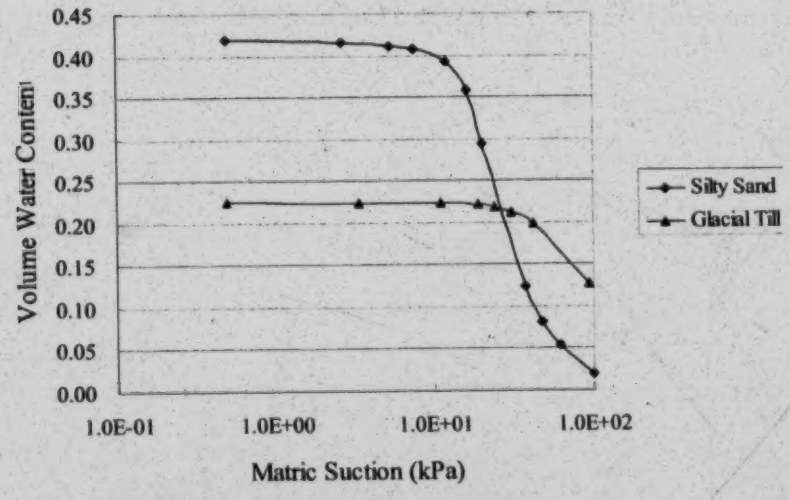

(a) Volume water content functions

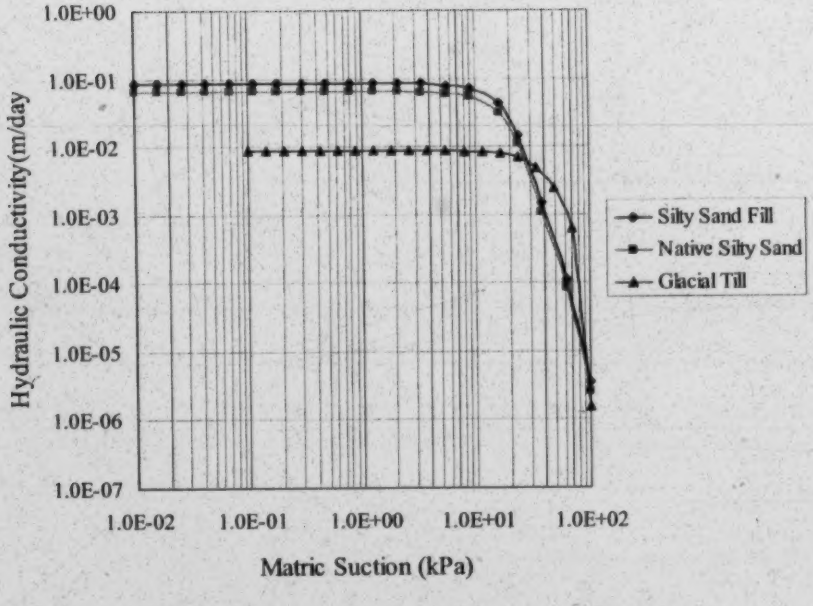

(b) Hydraulic conductivity functions

Figure 3-27 Volume water content and hydraulic conductivity functions for embankment materials at MP 150.10

Table 3-6 Shear strength parameters for embankment materials at MP 150.10

	c' (kPa)	Φ'	Φ^b	Unit weight (kN/m^3)
Silty Sand Fill	0	30°	15°	18
Native Silty Sand	0	30°	15°	18
Glacial Till	15	24°		20

The numerical modeling results are presented in Figures 3-28, 3-29 and Table 3-7. Figure 3-28 shows the final pore-water pressure profile for the initially dry and wet embankments. Near the ground surfaces rainfall infiltration reduced the soil matric suction and a high matric suction region was in the middle of the embankment.

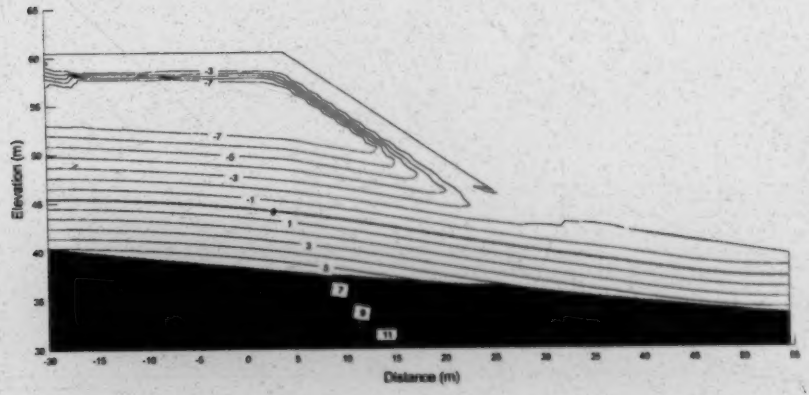

(a) for initially dry embankment

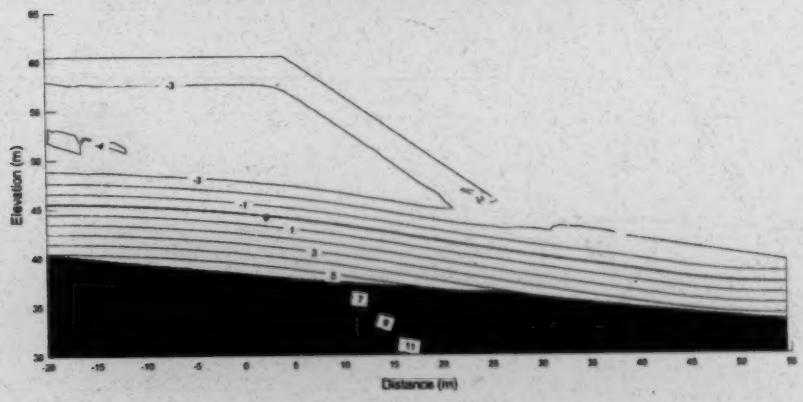

(b) for initially wet embankment

Figure 3-28 Final pore-water pressure head profiles after July 5
for initially dry and wet embankments at MP 150.10 (contour unit: meters)

As can be seen in Table 3-7, the factor of safety of the embankment gradually decreased with time. The initial factors of safety were 1.56 and 1.41 for the initially dry and wet embankments, respectively, indicating a fairly stable condition. After the rainfall on July 5, the factor of safety decreased to 1.37 for the initially dry embankment and 1.26 for the initially wet embankment. A great decrease in the factor of safety occurred due to the prolonged rainfall. The numerical results, however, show that the embankment appeared to have been still safe in terms of its overall stability. Figure 3-29 shows the change in the

depth of the critical slip surfaces with time. In both the initially dry and wet embankments, the critical slip surfaces moved toward the ground surface with time.

Table 3-7 Change of factor of safety with time for embankment at MP 150.10

Date	Initially Dry Embankment FoS	Initially Wet Embankment FoS
June 1	1.558	1.405
June 2	1.556	1.404
June 10	1.551	1.400
June 19	1.538	1.380
June 24	1.534	1.370
June 25	1.531	1.364
June 26	1.525	1.356
June 27	1.523	1.344
July 1	1.511	1.302
July 4	1.399	1.273
July 5	1.368	1.264

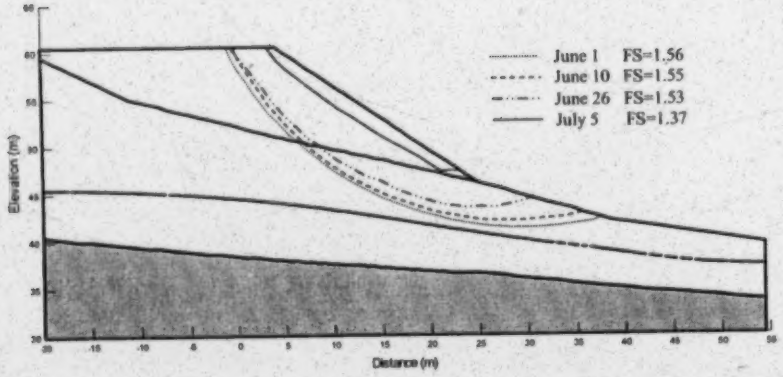

(a) for initially dry embankment

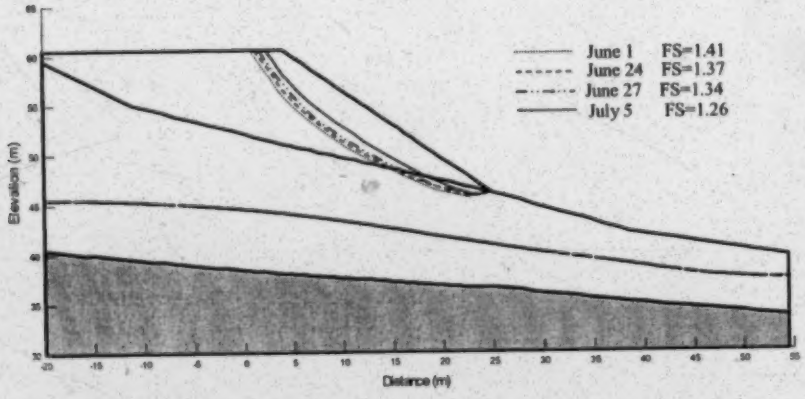

(b) for initially wet embankment

Figure 3-29 Move of critical slip surface with time for embankment at MP 150.10

3.4 Discussion

During periods of heavy rainfall, a railway embankment can be affected in three ways:

1) Rainfall infiltration decreases matric suction in the embankment soils and hence, decreases soil shear strengths and the stability of the embankment.

2) The impact of rainfall and surface water runoff along the embankment surface can erode away the surface soil and compromise the embankment.
3) Where an embankment crosses a river valley, the river water level may elevate during or following rainfall event and then decline after, possibly affecting the stability of the embankment. In an extreme case, the river level may overtop the embankment if the culvert capacity is not adequate to carry the water flow. The overland flow can erode the embankment crest and even completely erode the embankment.

In reality, the three soil-water interaction systems presented above may come into effect simultaneously. Sometimes, one or two of the mechanisms may control. In this study, only the first mechanism, i.e. the rainfall infiltration was considered. However, the modeling results can still provide some insights into the rainfall-induced ground hazards problem.

All the seepage modeling results presented in the previous section show that the surface of an embankment is strongly influenced by rainfall infiltration and has less matric suction than the core of the embankment. On one hand, the surface region has less shear strength and, thus, a lower local factor of safety than other regions of the embankment, particularly when a high rainfall intensity is greater than the saturated hydraulic conductivity of the embankment material. In this condition, a thin layer of the embankment surface will become saturated. On the other hand, the moist and loose embankment surface is more susceptible to erosion by the rainfall and by surface water runoff down the embankment surface. For both of the above reasons, the surface region of an embankment during a rainfall period is easily damaged and is likely to be the region most affected by the rainfall. This is why shallow earth slide and slope erosion are common railway ground hazards during a prolonged or heavy rainfall event.

At Port Douglas, numerous shallow earth slides have occurred between MP 154 and 155.3 where the railway embankments are composed of lacustrine silt with some fine sand and clay. This phenomenon may be explained by the following points. The sandy clayey silt material has a low hydraulic conductivity, and, as a result, infiltration is low

and runoff is high. In terms of erosion, silt and fine sand are the most erodible materials because the particles are very fine and cohesionless (ASCE, 1975 and Raudkivi, 1998). The surface runoff down the embankment can detach the soil particles easily and carry them away. With time slope erosion and shallow earth slides can develop. In the rest of the sections at Port Douglas, the embankments consist mainly of natural deposits of glacial till and fill materials from local glacial till (fine to medium sand with trace of clayey silt and fine gravel), which are coarser than the sandy silt material between MP 154 and MP 155.3. In the natural deposits, cohesion also developed with time. In general, this kind of material is less erodible than silt and fine sand. Therefore, most of the slope erosion and shallow earth slides occurred in the lacustrine silt area rather than the other areas.

Since the embankments near MP 154.5 were built mainly with fine silt and sand materials, it was reasonable to assign a low effective friction angle of 27° and a cohesion value of 3kPa in the analysis. The analysis results show that before the prolonged rainfall in June 1998, the embankments at MP 154.47 and 154.44 had a factor of safety of 1.27 to 1.38. The rainfall from June 1 to June 27 decreased the stability of the embankments, yielding a factor of safety of near 1.0. This finding indicates that only the first mechanism, rainfall infiltration itself, could bring the embankments into a marginally stable condition. The landslide at MP 154.41 may have been caused by rainfall infiltration. The gully erosion at MP 154.47 and 154.44 may have resulted from slope failure by rainfall infiltration and then overland flow erosion by the overland water flow.

The modeling results for the embankments at MP 154.47 and MP 150.17 also show that a region around the toes of the embankment had been saturated by rainfall infiltration. Therefore a collapse may have first occurred at an embankment toe, weakening the overall stability of the embankments. In this circumstance, if the embankments were subjected to a sudden loading, for example, the loading of a train, the overall slope may have failed suddenly. This possibility may explain why the embankment at MP 150.17 failed when a train came even though the overall stability of the embankment, as indicated by the numerical modeling, appeared to be a stable condition. The evidence that

the fuel lines were broken prior to the derailment may confirm that the toe of the embankment failed first, damaging a section of the culvert near the outlet and breaking the fuel line. The train loading may have triggered the overall failure of the slope.

The circular slope failure at MP 150.10 can be related to the presence of the fill material on the top of the embankment with a cut-fill interface at an inclination of 14° to horizontal dipping out of the slope. The fill materials may have a higher hydraulic conductivity than the native soil and can more easily become moist and fail. The numerical modeling gave a factor of safety of 1.26 on July 5, which indicates a relatively stable condition. This discrepancy is probably because the analysis is only a two-dimensional analysis when, in reality, the groundwater is controlled by the local topography, or some assumptions in the analysis might have been inappropriate.

In summary, the choice of material for a railway embankment is essential for ensuring its drainage and stability and the surface and toes of the embankment may be the most vulnerable regions during periods of rainfall. It is noted that the embankments in the Port Douglas area were constructed 100 years ago when geotechnical knowledge was in its infancy. The properties and characteristics of the subsurface layer might not have been fully understood at that time. Current measures can be taken to protect the embankments against heavy rainfall. At MP 150.10 and 150.17, CP Railway reconstructed the embankments with clean free-draining materials and geogrids, and french drains were built beneath the embankments to reduce the pore-pressure buildup. Where embankment surface slump occurred in the Port Douglas area, CP Railway armored the embankment surfaces with rip rap or used erosion blanket. The toes of the embankments were buttressed with pervious rock drains.

Chapter 4 Hydrology and Hydraulic Modeling

This chapter reports on the use of hydrology and hydraulic modeling to analyze the major erosions of the railway embankments. Where the embankment was eroded, the peak flow at the outlet of the watershed was determined, and the capacity of the culvert to handle the peak flow was checked by using hydrology modeling with the HEC-HMS (Hydrology Modeling System) program and hydraulic modeling with the HEC-RAS (River Analysis System) program.

4.1 Hydrology and Hydraulic Modeling Method

4.1.1 Hydrology Modeling with HEC-HMS

Within a watershed, during a given rainfall event, a portion of the rainfall soaks into the ground, a portion are lost by evaporation, and the rest becomes runoff, which eventually joins a stream and flows out through the outlet of the watershed. The simulation of this precipitation-runoff-routing is called hydrology modeling. The hydrologic modeling system HEC-HMS, a product of the US Army Corps of Engineers, Hydrologic Engineering Center, was used to calculate the discharge hydrograph of each watershed within the Port Douglas region. Figure 4-1 illustrates a typical HEC-HMS representation of watershed runoff.

HEC-HMS includes seven hydrologic elements: the subbasin, reach, reservoir, junction, diversion, source, and sink. The elements are connected in a dendritic network to simulate runoff processes. The computation proceeds from upstream elements in a downstream direction.

The subbasin element represents a watershed. A watershed is simply simulated by three separate processes: loss, transform, and baseflow. A loss method represents rainfall infiltration and evaporation. In this study, losses are considered as zero. Groundwater flow that returns to

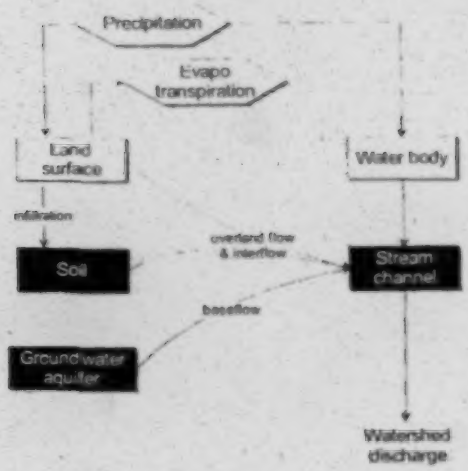

Figure 4-1 Typical HEC-HMS representation of watershed runoff (Haestad Methods Inc., 2001)

the stream channel or land surface from underground is called return flow or baseflow. In this study, it is considered that no baseflow occurred. Rainfall that does not infiltrate nor evaporate becomes direct runoff and moves across the watershed surface and eventually reaches the watershed outlet. All runoff processes are represented as pure surface routing by using a transform method. In this study, the kinematic wave method was used to compute direct runoff from excess precipitation. This method uses the continuity equation and the steady, uniform flow approximation of the momentum equation to transform precipitation to flow. In this method, a conceptual model of planes and channels, as shown in Figure 4-2, is used. The flow from the planes is combined and then uniformly distributed along the main channel as lateral inflow. The kinematic wave overland flow model represents behavior of overland flow on the plane surfaces as a wide rectangular channel of unit width. In one dimensional, the momentum equation for flow over the plane surfaces is

$$S_f = S_0 - \frac{\partial y}{\partial x} - \frac{V}{g}\frac{\partial V}{\partial x} - \frac{1}{g}\frac{\partial V}{\partial t}, \qquad (6)$$

where S_f is energy gradient, S_0 is bottom slope, V is velocity, y is hydraulic depth, x is distance along the flow path, t is time, g is gravity acceleration. The energy gradient can be estimated with Manning's equation, which can be written as

$$Q = \frac{CR^{2/3} S_f^{1/2}}{N} A, \tag{7}$$

where Q is flow, R is hydraulic radius, A is cross-sectional area, and N is a resistance factor that depends on the cover of the planes (note that this is Manning's n). For shallow flow, bottom slope and the energy gradient are approximately equal and acceleration effects are negligible, so the momentum equation simplifies to

$$S_f = S_0. \tag{8}$$

The one-dimensional representation of the continuity equation for shallow flow over a plane can be simplified as

$$\frac{\partial A}{\partial t} + \frac{\partial Q}{\partial x} = q \tag{9}$$

where q is lateral flow per unit length of channel.

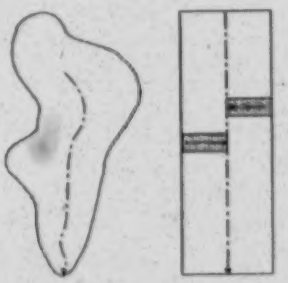

Figure 4-2 Conceptual model of a watershed (left) with the kinematic wave method (right) (Haestad Methods Inc., 2001)

The reach element can be used to represent the flow of water in open channels. Inflow requires a certain amount of time to travel down the reach, and, as it passes through the reach, a flood wave is attenuated by friction and channel storage. The travel time and attenuation characteristics vary widely between different streams. Many models have been developed under different assumptions and for different stream types. The kinematic wave method employed in this study uses the continuity equation and the steady, uniform flow approximation of the momentum equation. Theoretically, the method models the flow with translation and no attenuation by computing the velocity from the flow depth and channel parameters specified by the user. However, the equations are solved using a finite difference approximation, and some numerical attenuation is inevitable (Haestad Methods Inc., 2001). The required parameters for a reach element include the stream length, energy slope, bottom width or diameter, side slope and manning's n..

The junction element and sink element were also used in this study. A junction element is used to represent a confluence of streams. All inflows are added together to obtain the outflow by assuming zero storage at the junction. A sink is an element with one or more inflows but no outflow. Multiple inflows are added together to determine the total amount of water entering the element. Sink element can be used to represent the outlet of the basin model.

In this research, the watershed and stream network information obtained from the ArcGIS program are used to develop hydrologic model for a watershed. Most of the input data for the hydrology modeling was also determined with the help of GIS tools. The areas of each watershed was calculated in the *Field Calculator*. The length data required for HEC-HMS, such as the stream length and the length of overland flow, were approximately measured by the *Length Measuring* tool. The slope data including those for the channel slope and overland flow slope were derived from the length values and the elevation values, which were identified from DEM. The cross section of a channel was extracted from DEM by using the *Create Profile Graph* tool in the *3D Analyst Geoprocessing* toolbox, and, subsequently, the shape, width and side slope of a channel cross section were determined.

4.1.2 Culvert Modeling in HEC-RAS

In order to assess the capacity of each culvert within the embankments, a hydraulic analysis was carried out for each culvert by using the HEC-RAS program. HEC-RAS is an integrated package of hydraulic analysis program developed by the Hydrology Engineering Center of US Army Corps of Engineers. The system is capable of performing steady and unsteady flow water surface profile calculations (Haestad Methods Inc., 2002).

Four cross sections are required for a complete culvert model, as illustrated in Figure 4-3 (Haestad Methods Inc., 2002). These include one cross section sufficiently downstream from the culvert such that flow is not affected by the culvert (Cross Section 1), one at the downstream end of the culvert (Cross Section 2), one at the upstream end of the culvert (Cross Section 3), and one cross section located far enough upstream that the culvert again has no effect on the flow (Cross Section 4). The use of additional cross sections both upstream and downstream of the culvert is suggested in order to prevent any user-entered boundary conditions from affecting the hydraulic results through the culvert.

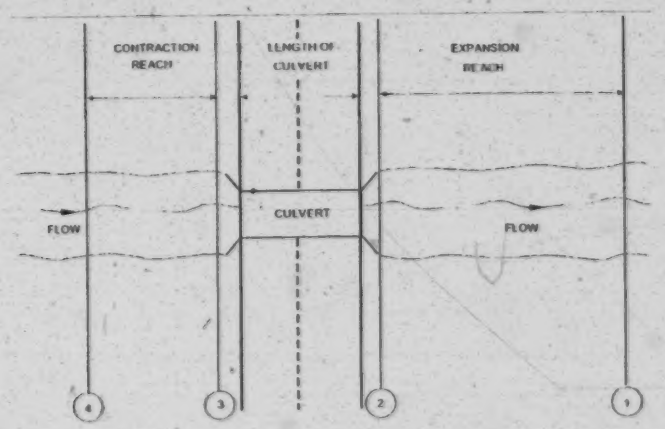

Figure 4-3 Cross section layout for culvert (Haestad Methods Inc., 2002)

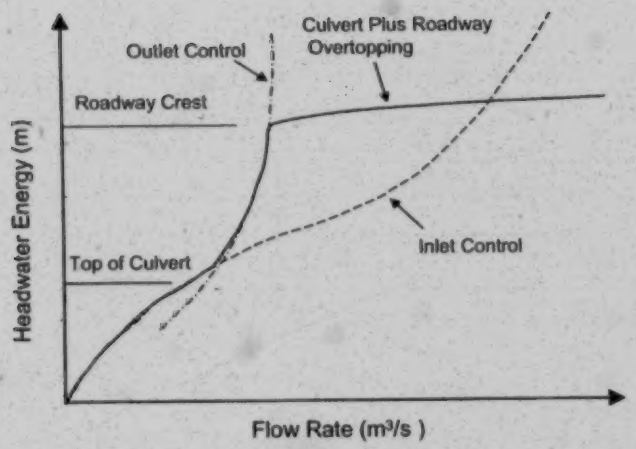

Figure 4-4 Culvert performance curve with roadway overtopping (Haestad Methods Inc., 2002)

The analysis of the flow in a culvert is quite complicated, but usually simplified into "inlet control" and "outlet control". Inlet control flow occurs when the flow capacity of the culvert depends primarily on the geometry of the culvert entrance. For inlet control, the required upstream energy is computed by assuming that the culvert inlet acts as a sluice gate. Outlet control flow occurs when the culvert flow capacity is limited by downstream conditions (high tailwater) or by the flow-carrying capacity of the culvert barrel. For outlet control, the required upstream energy is calculated by performing an energy balance from the downstream section to the upstream section and considering the entrance losses, friction losses in the culvert barrel, and exit losses at the outlet. For a given flow rate and tailwater condition, the HEC-RAS culvert routines compute the upstream energy required for both inlet control and outlet control conditions, and the higher upstream energy determines the type of flow in the culvert, as illustrated in Figure 4-4.

At first, an assumption is made that all of the flow is going through the culvert barrels. Once a final upstream energy is obtained, the program will check if weir flow (overtopping) will occur. If the computed energy is less than the minimum elevation for weir flow, then no overtopping will occur, and the solution is final. If the computed

energy is greater than the minimum elevation for the weir flow, overtopping will occur, and then the program will perform an iterative procedure to determine the amount of flow over the weir and through the culverts. The program will continue to iterate until it finds a flow split that produces the same upstream energy (within the error tolerance) for both the weir and culvert flows.

4.2 Hydrology and Hydraulic Modeling Results

Watersheds 154.47, 154.44, 152.15, 151.70 and 147.33 were modeled and analyzed. At the outlets of these watersheds, the culverts and railway embankments had failed due to overland flow erosion. Hydrologic modeling within HEC-HMS was carried out to determine the peak flow during the period of the highest intensity of rainfall from June 25 to June 27 by using the radar-derived hourly rainfall data. Since a prolonged antecedent period of rainfall before June 25 likely saturated the soil, no precipitation loss (infiltration) was considered in this study. The kinematic wave method was applied in both surface routing and open-channel routing. The baseflow was considered to be zero in this study. Steady flow analysis was employed in the HEC-RAS program to obtain the capacity of the culvert at the outlet of each watershed. The input parameters for hydrologic and hydraulic analysis were measured approximately from the Digital Elevation Model in the ArcGIS program and are presented in Tables 4-1, 4-2 and 4-3.

Table 4-1 Hydrology modeling parameters for watershed 154.47

Watersheds	Sub_1	Sub_2	Sub_3	Sub_4	Sub_5	Sub_6
Drainage Area (km^2)	1.500	0.434	0.232	0.541	0.304	1.040
Overland Roughness	0.2	0.2	0.2	0.2	0.2	0.2
Channel Length (m)	2500	1250	470	1150	850	1100
Channel Slope (m/m)	0.053	0.08	0.026	0.07	0.023	0.038
Manning's n	0.02	0.02	0.02	0.02	0.02	0.02
Bottom Width(m)	10	8	15	10	0	10
Side Slope (xH:1V)	12	7.5	9	10	10	6

Table 4-2 Input parameters for hydrology modeling

Watersheds	154.44	152.15	151.70	147.33
Drainage Area (km^2)	0.294	0.744	0.145	2.694
Overland Roughness	0.2	0.2	0.2	0.2
Channel Length (m)	1250	1300	550	1000
Channel Slope (m/m)	0.10	0.10	0.231	0.086
Manning's n	0.02	0.02	0.02	0.02
Channel Shape	Trapezoid	Trapezoid	Trapezoid	Trapezoid
Bottom Width (m)	5	13	10	5
Side Slope (xH:1V)	18	2.8	1.3	0.8

Table 4-3 Input parameters for culvert modeling

watersheds	154.47	154.44	152.15	147.33
Culvert Type	Box	Box	Box	Circular
Culvert Span (m)	1.2	1.1	1.2	Diameter 0.9m
Culvert Rise (m)	0.9	0.9	0.9	
FHWA Chart Number	8	8	8	2
Scale Number on Chart	1	1	1	1
Manning's n	0.015	0.015	0.015	0.015
Culvert Entrance Coefficient	0.5	0.5	0.5	0.5
Culvert Length (m)	40	40	42.5	23
Culvert Slope	0.05	0.05	0.10	0.05
Upstream Channel Slope	0.04	0.11	0.10	0.10

(a) subbasin delineation for watershed 154.47 from GIS

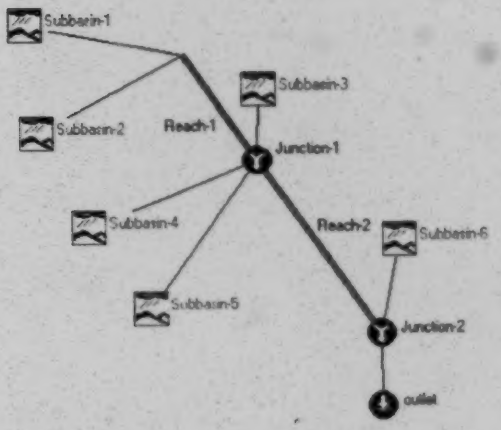

(b) hydrologic model for watershed 154.47

Figure 4-5 Subbasin delineation and hydrologic model for watershed 154.47

Figure 4-5 shows the hydrologic model for watershed 154.47. In this model, six subbasin elements are used. The hourly hydrograph at the outlet of watershed 154.47 and the water surface profile near the culvert are represented in Figures 4-6 and 4-7, respectively. From Figure 4-6, it can be seen that the peak flow at the outlet of watershed 154.47 was 14m^3/s at around 3:00am on June 27, 1998. The flow capacity of the culvert was 9 m^3/s (see Figure 4-7). This figure indicates that the culvert was not large enough to convey the water flow.

The hydrology and hydraulic results for all the watersheds are provided in Appendix D, and a summary of the results are given in Table 4-4 which shows that for watersheds 154.47 and 147.33, the flow capacities of the culverts were less than the peak flows, so overtopping and erosion of embankment could occur. However, for watershed 154.44 and watershed 152.15, the culverts were large enough to handle the water flows. This finding suggests that overland flow erosion occurred at both culverts that were adequate and inadequate to handle the water flow.

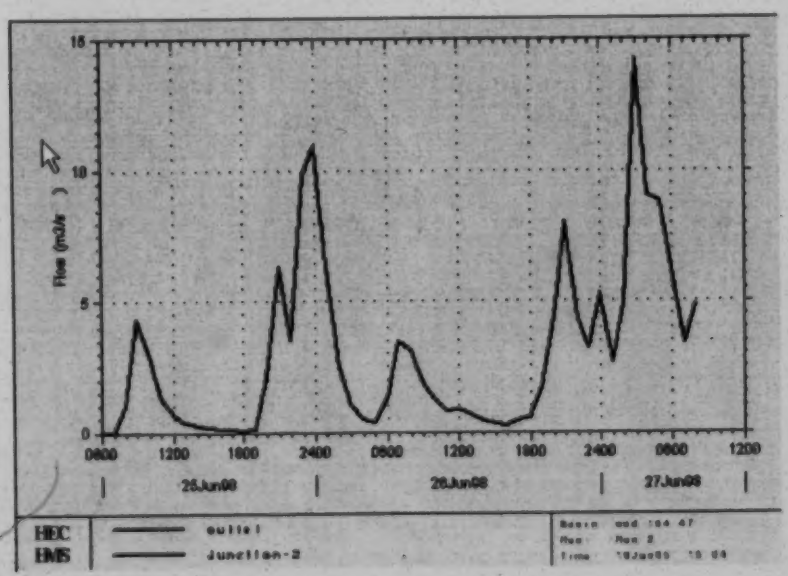

Figure 4-6 Modelled hydrograph at outlet of watershed 154.47

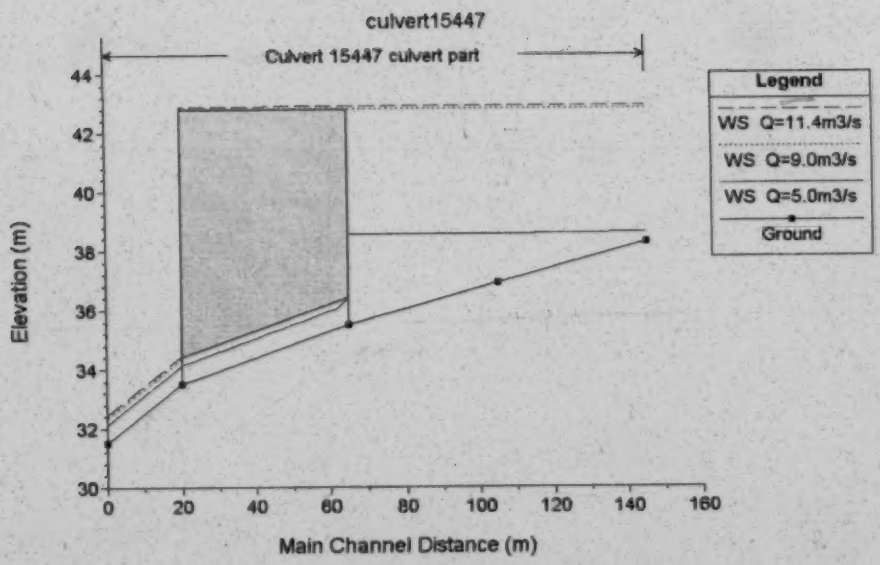

Figure 4-7 Modelled water surface profile at culvert 154.47

Table 4-4 Summary of peak flow and culvert capacity results

Watersheds	Drainage Area (km^2)	Peak Flow (m^3/s)	Existing Culvert	Flow Capacity of Culvert (m^3/s)
154.47	4.060	14.0	Stone Box 3.0ft x 4.0 ft	9
154.44	0.294	1.2	Stone Box 3.0ft x 3.5ft	8
152.15	0.746	3.0	Stone Box 3.0ft x 4ft	11
151.70	0.145	0.6	No existing culvert	n/a
147.33	2.694	10.6	Culvert pipe 3.0ft diameter	6

4.3 Discussions

During the prolonged rainfall event, small-scale erosion and surface sloughing of the railway embankments were likely to have become relatively common, and debris might have blocked the culverts, so the culverts could not handle the flow generated by the unusually intense rainfall. Alternatively, the landslide failure of the embankments might have occurred first and the stream water flow washed the remaining materials away.

The results of the stability modeling and hydraulic modeling suggest that the embankment erosions at MP 154.47 and MP 154.44 likely resulted from a combination of a landslide and the subsequent overland flow erosion. The stability results indicate that the embankments reached a marginally stable condition due to the reduction of the shear strengths induced by the rainfall infiltration from June 1 to June 27. From the hydrology and hydraulic modeling results, the water flow at MP 154.47 was higher than the culvert capacity for more than 3 hours during the high intensity rainfall between June 25 and June 27, so overtopping flow could occur. At MP 154.44, the culvert had an adequate capacity but the embankment surface slump and failure could have plugged the culvert and resulted in over-embankment flow and erosion. The site MP 154.47 had a history of problems which may have been related to the low factor of safety of the embankment stability and an inadequate culvert capacity.

At MP 152.15, the embankment was constructed with local glacial till materials, and its complete erosion was inspected on July 2, 1998. The hydraulic analysis demonstrated that the culvert capacity was sufficient to convey the water flow generated by the heavy rainfall provided the culvert capacity was not compromised. The erosion might have resulted from a blocked or partially blocked culvert. At MP 151.70, the stream changed course and washed out the embankment 5 meters deep. This finding indicates that maintaining a clear route for water flow and adequate drainage is very important for a railway track.

In the Port Douglas case, the fact that embankments were washed out at the places with an adequate calculated culvert capacity suggests that blocked or partially blocked culverts can occur during the rainfall season. Track maintenance and inspection employees should be aware of this problem. In addition, using free-draining materials, constructing french drains at the base of an embankment, and removing the debris from drainage swales are also good practices for improving the drainage of railway embankments.

Chapter 5 Conclusions and Recommendations

In this thesis, the background of the rainfall-induced CPR railway ground hazards in Port Douglas area was explained and a classification of the damages was carried out according to Keegan's Railway Ground Hazards Classification System. A methodology for evaluating rainfall-induced railway ground hazards was developed by using GIS technology, hydrology and hydraulic analysis linked to GIS, seepage and slope stability analysis. Numerical modeling of the seepage and stability of typical embankments was carried out by using the unsaturated soil theory with the help of the SEEP/W and SLOPE/W programs, and the mechanisms of the embankment failure were analyzed. Later, the capacities of the culverts at the base of the embankments were checked by using hydrology and hydraulic modeling, and the possible reasons for the plugged culverts and their effect on the stability of the embankments were pointed out.

5.1 Conclusions

From the results of the analysis and discussion, the following conclusions can be reached about the stability of railway embankments during periods of heavy rainfall.

In general,

1. Unsaturated soil theory can be used effectively to assess the stability of an embankment during periods of rainfall.
2. The soil matric suctions in an embankment are reduced by rainfall infiltration, and, hence, the shear strength and stability of the embankment decrease. During a period of continuous rainfall, the stability of the embankment decreases continuously. The critical slip surfaces of the embankment move towards the ground surface gradually with time during a period of rainfall.
3. The initial pore-water pressure distribution throughout an embankment and the hydraulic conductivity of embankment material have a significant influence on the stability of the embankment during periods of heavy rainfall.

4. The surface region of embankment is susceptible to rainfall weather conditions and presents lower matric suctions and less shear strength than the core of the embankment. The impact of rainfall drops and surface water runoff along the embankment surface can also jeopardize the slope surface by eroding surface soils away. This explains why surface slumps frequently occur during periods of heavy rainfall. Debris from a surface slump can block a culvert and result in serious consequences such as a major erosion of an embankment. It is suggested that during rainfall season, track maintenance and inspection employees should assure that the flow in culvert is not impeded.
5. After a period of rainfall, a build-up of the ground water level occurs at the toes of an embankment, making the toes of the embankment less stable. The toes may fail first, and, hence, the shear stresses in the upper part of the embankment increase, and an overall failure may occur.

For the Port Douglas case,

1. Most of the surface slump hazards occurred in the embankments with lacustrine silt and fine sand materials. The reason is likely to be that silts and fine sands are highly erodible.
2. The three-day heavy rainfall between June 25 and June 27, 1998 greatly decreased the stability of the embankments at MP 154.47 and 154.44 and played an important role in the final failures. However, the antecedent prolonged rainfall from June 2 to June 24 also had a influence on the stability of the embankments, especially the continuous rainfall from June 11 to June 19.
3. The embankments at MP 154.47 and 154.44 reached a marginally stable condition due to the reduction of the shear strengths induced by rainfall infiltration from June 1 to June 27. The embankment erosion likely resulted from a landslide and subsequent overland flow erosion.
4. In terms of its overall stability, the embankment at MP 150.17 was still safe after June 25. The toe of the embankment might have failed first and led to an overall failure. The loading of the train might contribute to the final slope failure.

5. Embankment erosion occurred both where the culvert capacity was not enough to convey the water flow and where an adequate culvert capacity existed. A plugged culvert resulting from the surface slump and the failure of an embankment could have caused the overtopping flow and the erosion of the embankment.

5.2 Recommendations for Future Research

In order to further improve our understanding into the railway geo-hazards triggered by rainfall, as well as our ability to manage them proactively, it is recommended that

1. The soil-water characteristic curve, which is essential for seepage analysis, be obtained through laboratory experiments. The saturated hydraulic conductivity value of a soil can be obtained in a laboratory. The direct measurement of a volumetric water content function can be done with a pressure plate cell. The task of measuring the unsaturated hydraulic conductivity function directly can be overcome by predicting the unsaturated hydraulic conductivity from a measured volumetric water content function and a measured value of the saturated hydraulic conductivity.
2. A more detailed seepage analysis of railway embankments can be made through VADOSE/W by considering the precipitation and evaporation by using hourly precipitation data and temperature information. Moreover, the hystersis of the soil-water characteristic curve may have an important role in the soil-atmosphere fluxes and can also be considered.
3. The selection of soil shear strength parameters is crucial for the stability analysis, and laboratory tests are recommended to determine the shear strength parameters.
4. If the water level in a stream is observed, an analysis of the effect of water level change on the stability of embankment can be modeled.
5. For a specific embankment, the threshold for a landslide can be determined through a number of trials by varying the rainfall amount and rainfall patterns. Such information can be used to warn of a possible subgrade collapse in the railway corridor.

References

American Society of Civil Engineers. 1975. Sedimentation Engineering. Headquarters of the Society, New York.

Anderson, M.G. and Richards, K.S.1987. Slope Stability. New York: John Wiley & Sons Ltd.

Barbour, S.L. 1998. The soil-water characteristic curve: a historical perspective. Canadian Geotechnical Journal, Ottawa, Vol. 35, pp. 873-894

Bunce, C.M., Mackay, C.H. and Martin, C.D. 2003. Severe weather warning levels for geotechnical railway hazards, the 3rd Canadian Conference on Geotechnique and Natural Hazards, Edmonton, Canada

Cedergren, H.R. 1977. Seepage drainage and flow nets. John Wiley & Sons, New York.

Childs, E.C., and Collis-George, N., 1950. The permeability of porous materials. Proceedings of Royal Society, pp. 392-405

Fredlund, D.G., and Krahn, J. 1977. Comparison of slope stability methods of analysis. Canadian Geotechnical Journal, Vol.14, pp. 429-439.

Fredlund, D.G., Morgenstern, N.R., and Widger, R.A. 1978. The shear strength of unsaturated soils. Canadian Geotechnical Journal, Vol. 15, pp. 313-321

Fredlund, D.G., Rahardjo, H.. 1993. Soil Mechanics for Unsaturated Soils. New York: John Wiley & Sons.

Fredlund, D.G. 2000. The 1999 R.M. Hardy Lecture: The implementation of unsaturated soil mechanics into geotechnical engineering. Canadian Geotechnical Journal, Vol. 37, pp. 963-986

Fredlund, D.G. 2002. Use of soil-water characteristic curves in the implementation of unsaturated soil mechanics. Proc. of the 3rd Int. Conf. on Unsaturated Soils, March 10-13, Recife, Brazil, Vol. 3, pp. 1-23

Fredlund, D.G., Xing.A., and Fredlund, M.D. 1996. The relationship of the unsaturated shear strength to the soil-water characteristic curve. Canadian Geotechnical Journal, Vol. 33 (3), pp. 440-448

Fredlund, D.G., Xing, A., and Huang, S. 1994. Predicting the permeability function for unsaturated soil using the soil-water characteristic curve. Canadian Geotechnical Journal, Vol. 31 (4), pp. 533-546

Fredlund, M.D. 1999. The role of unsaturated soil property functions in the practice of unsaturated soil mechanics. Ph.D. Thesis, University of Saskatchewan, Saskatoon, Canada. 292p

Gasmo, J.M., Rahardjo, H., Leong, E.C. 2000. Infiltration effects on stability of a residual soil slope. Computers and Geotechnics, Vol. 26, pp.145-165

Gitirana Jr, G.F.N. 2005. Weather-related geo-hazard assessment model for railway embankment stability, Ph.D Thesis, University of Saskatchewan, Saskatoon, Canada. 439p

Hay, W.W. 1982. Railroad Engineering. New York: John Wiley & Sons.
Haestad Methods, Inc.. 2001. HEC-HMS Version 2.1, User's Manual and Technical Reference Manual.

Haestad Methods, Inc.. 2002. HEC-RAS Version 3.1, User's Manual and Technical Reference Manual.

Keegan, T. 2003. Chapter 3: Railway ground hazard classification system.

Krahn, J. 2004. Seepage modeling with SEEP/W. First Edition. GEO-SLOPE International Ltd., Calgary, Alberta

Krahn, J. 2004. Stability modeling with SLOPE/W. First Edition.GEO-SLOPE International Ltd., Calgary, Alberta

Lim, T.T., Rahardjo, H., Chang, M.F., and Fredlund, D.G. 1996. Effect of rainfall on matric suctions in a residual soil slope. Canadian Geotechnical Journal, Vol. 33, pp. 618-628

Morgenstern, N.R. and Price, V.E., 1965. The analysis of the stability of general slip surfaces. Geotechnique, Vol. 15, pp. 79-93.

Rahardjo, H., X.W. Li, Toll, D.G. and Leong, E.C. 2001. The effect of antecedent railfall on slope stability. Geotechnical and Geological Engineering, Vol. 19, pp. 371-399

Raudkivi, A.J. 1998. Loose Boundary Hydraulics. A.A. Balkema, Netherlands.

Tsaparas, I., Rahardjo, H., Toll, D.G., and Leong, E.C. 2002. Controlling parameters for rainfall-induced landslides. Computers and Geotechnics, Vol. 29, pp. 1-27

Zawadzki I., 1984. Factors affecting the precision of radar measurements of rain. Preprints of conference of Radar Meteorology. Sept.10th-13rd, 1984, Zwrich. P251-256

Appendix A Description of Overland Flow Erosion Sites

- Embankment Erosion at MP 152.15

The native surficial soil around site MP 152.15 consists of dense glacial till. The railway grade was located on a 14 m-high earth embankment which crossed a stream valley with a stone box culvert, 1.2 m wide and 0.9 m high, at the base. The embankment had side slopes of approximately 1.4H:1V. According to the inspection on July 2, 1998, the embankment and culvert were eroded, and the failure was as long as 24 m at the track level (see Figure A-1).There was evidence that the water level was above the racks at one time. Seeps were noted about 3 m below the rails. Seepage through the blind drain/culvert to the north was also observed.

Figure A-1 Embankment erosion at MP 152.15 (from Canadian Pacific Railway)

- Embankment Erosion at MP 151.70

Figure A-2 shows the embankment erosion at MP150.17. Glacial till surfacial material appears near site 151.70. A stream runs from west to east perpendicular to the tracks, with a culvert at the base of embankment. The embankment was about 7.5 m high and had a side slope of approximately 3H:1V. The stream changed course, creating a new

stream alignment. On July 2, inspectors found that the new alignment had washed out the embankment by 24 m wide and 3 m to 5 m deep.

Figure A-2 Embankment erosion at MP 151.70
(Canadian Pacific Railway, picture taken in July 1998)

- Embankment Erosion at MP 148.55

At MP 148.55, the earth embankment crossed a valley with a stone box culvert, which was 0.9 m wide and 0.6 m high, at the base of the embankment to convey the water flow. An overland flow erosion occurred, and the failure was around 12 m long at the track level and 3 m deep.

- Embankment erosion at MP 147.33

At site 147.33, the existing 0.9 m diameter metal pipe culvert and the embankment were completely washed out at the end of June 1998. The failure length reached around 25 m, and the failure depth was18 m. The culvert had been installed 2 years earlier after a previous overland flow erosion. Previously, the embankment had only a blind drain (i.e., the water flowed through large, open stone at the base of the embankment).

Figure A-3 Embankment erosion at MP 147.33

(Canadian Pacific Railway, picture taken in June 1998)

Appendix B Borehole Logs and Grain Size Curves

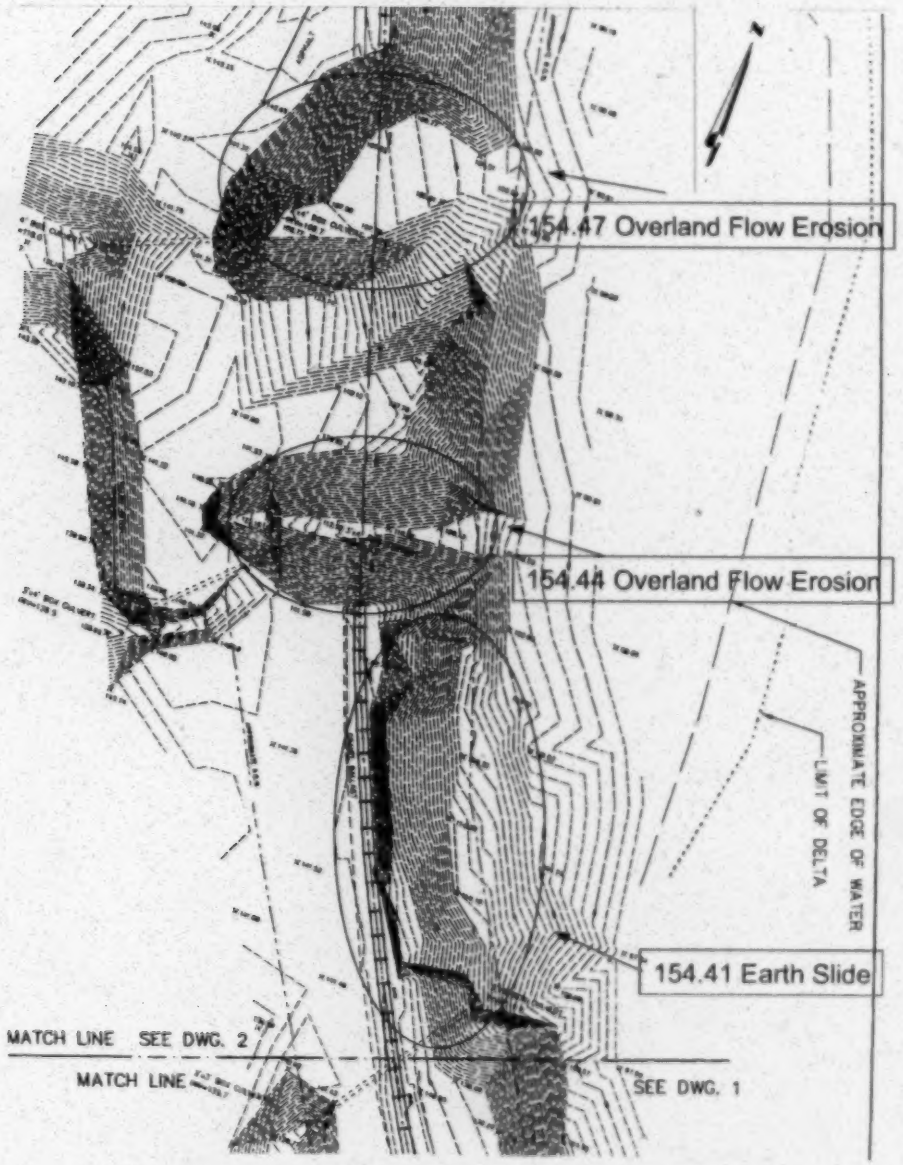

Figure B-1 Site topography for MP 154.5 overland flow erosion and landslide

CLOUGH, HARBOUR & ASSOCIATES LLP

Canadian Pacific Railway – Mile Post 154.41
SUBSURFACE LOG
TEST PIT NUMBER 1 through 7

PROJECT NUMBER: 6258.07.91 June, 1998 — Page 1 of 1

LOCATION: N4930946 E626824 East side scarp

CLIENT: Canadian Pacific Railway

CONTRACTOR: N/A

EQUIPMENT: Komatsu Excavator

DATE: 6/29/98 — INSPECTOR: WAH IV

SURFACE ELEV.: — CHECKED BY: WAH IV

PIT DIMENSIONS – TOP: N/A — BOTTOM: N/A

WATER LEVEL OBSERVATIONS DURING/AFTER EXCAVATION	DATE	TIME	WATER DEPTH	NUMBER OF BOULDERS ENCOUNTERED
				8" to 18" Diam: N/A Over 18" Diam: N/A

SAMPLE # AND DEPTH RANGE	ELEVATION (Feet)	DEPTH (Feet)	STRATA	DESCRIPTION AND CLASSIFICATION	WATER AND/OR SEEP ELEV.	Remarks on Character of Excavation Water seeps, etc.
		5		f.g. SAND, little silt, brown, v. compact, wet (SM)		Seven (7) test pits were excavated in the failure scarp at MP 154.41. This test pit log combines the information from the test pits to provide the stratigraphy of the failure scarp. Depth given is approximate depth below rail.
		10		f.g. SAND and SILT, brown, compact, saturated (SM)		Multiple seeps observed at various depths.
		15		Clayey SILT, little f.g. sand, gray with brown seams, soft to m.stiff, wet (ML)		
		20		Silty CLAY, trace f.c. gravel, trace f. sand, trace cobbles, gray, soft–m.stiff, wet (CL)		
		25				
		30				

Figure B-2 Subsurface log at MP 154.41

Table B-1 Properties of sandy clayey silt material from SEEP/W database

Sandy Clayey Silt	Ksat (m/s)	θs	AEV (kPa)	D10 (mm)	D60 (mm)
#23	1.50e-8	0.35	15	n/a	n/a

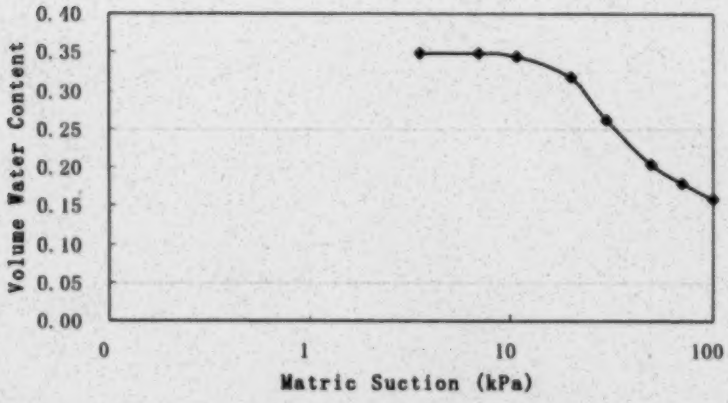

(a) volume water content function

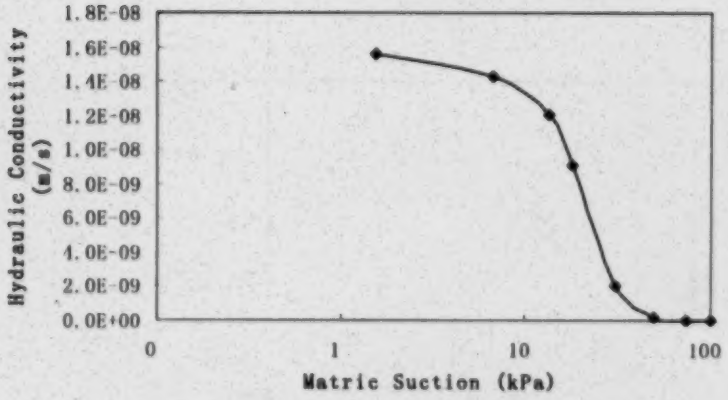

(b) hydraulic conductivity function

Figure B-3 Volume water content and hydraulic conductivity functions for sandy clayey silt material from SEEP/W database

CLOUGH, HARBOUR & ASSOCIATES LLP

Canadian Main Line – Mile Post 152.15
SUBSURFACE LOG
HOLE NUMBER B-3
Page 1 of 2

PROJECT NUMBER: 6258.07.90 July, 1998
LOCATION: CML Mile Post 152.15 – North Side
CLIENT: Canadian Pacific Railway
CONTRACTOR: Atlantic Testing
DRILLER: M. Childs | INSPECTOR: W. Harris
START DATE: 7/07/98 | FINISH DATE: 7/07/98
SURFACE ELEV.: | CHECKED BY:

DRILL FLUID: Water | DRILLING METHOD: 3"HW FJC-Spin

WATER LEVEL OBSERVATIONS DURING DRILLING	DATE	TIME	WATER DEPTH	CASING BOTTOM	HOLE BOTTOM
	07/07/98	AM	38.7 ft	60 ft	62 ft

SAMP./CORE NUMBER	SAMP. ADV. LEN CORE	RECOVERY	Blows Per 6" on Split Spoon Sampler	"N" VALUE	SAMPLE	DEPTH (Feet)	GRAPHICS	DESCRIPTION AND CLASSIFICATION	ELEVATION (Feet)	Remarks on Character of Drilling, water Return, etc.	WATER LEVELS AND/OR WELL DATA
S1	2.0'	0.58'	2-1-3-8	4		2 4 6 8 10		f.g.c. SAND, some f.c. Gravel, black, v.loose, moist (FILL)		Test boring was advanced between the ties, from track level, on the north side of the failure scarp. Numerous cobbles and boulders from 7'-13'.	
S2	2.0'	0.92'	2-2-1-2	3		12 14 16 18 20 22		f.g.c. SAND, some clayey Silt, little f.c. Gravel, brown, v.loose, saturated (SM)		Laboratory analysis performed on S2: %Gravel = 14% %Sand = 52% %Fines = 34% w% = 14.3%	
S3	2.0'	0.25'	7-3-4-4	7		24 26 28 30 32 34		Similar Soil (SM)			

Figure B-4 Borehole log at MP 152.15

CLOUGH, HARBOUR & ASSOCIATES LLP

Canadian Main Line – Mile Post 152.15
SUBSURFACE LOG
HOLE NUMBER B-3

PROJECT NUMBER: 6256.07.80 July, 1998 Page 2 of 2

SAMP./CORE NUMBER	SAMP. ADV. LEN CORE	RECOVERY	Blows Per 6" on SplitSpoon Sampler	N VALUE	SAMPLE	DEPTH (Feet)	GRAPHICS	DESCRIPTION AND CLASSIFICATION	ELEVATION (Feet)	Remarks on Character of Drilling, water Return, etc.	WATER LEVELS AND/OR WELL DATA
S4	2.0'	0.3'	5-6-3-6	9		36		Similar Soil (S4)			
						38					
						40					
						42					
						44		Similar Soil, becomes compact (S5)		Note: f.c. Gravel becomes angular, whereas previously rounded.	
S5	2.0'	0.92'	24-27-22-14	49		46				Laboratory analysis performed on S5:	
						48				50 Gravel = 46%	
						50		Similar Soil (S6)		15 Sand = 54%	
S6	2.0'	1.33'	14-23-9-12	34		52				37 Fines = 30%	
						54				LL=17.2 PL=12.3 PI=4.9	
						56				w% = 10.3%	
						58				Cobbles from 52'-57'.	
						60				Rock from 57'-62'. Hole collapsed to 60'.	
S7	0.3'	0	40/0.3' -bouncing	Ref		62		No recovery			
						64		End of Boring: 62'			
						66					
						68					
						70					
						72					

Figure B-4 Borehole log at MP 152.15 (Cont'd)

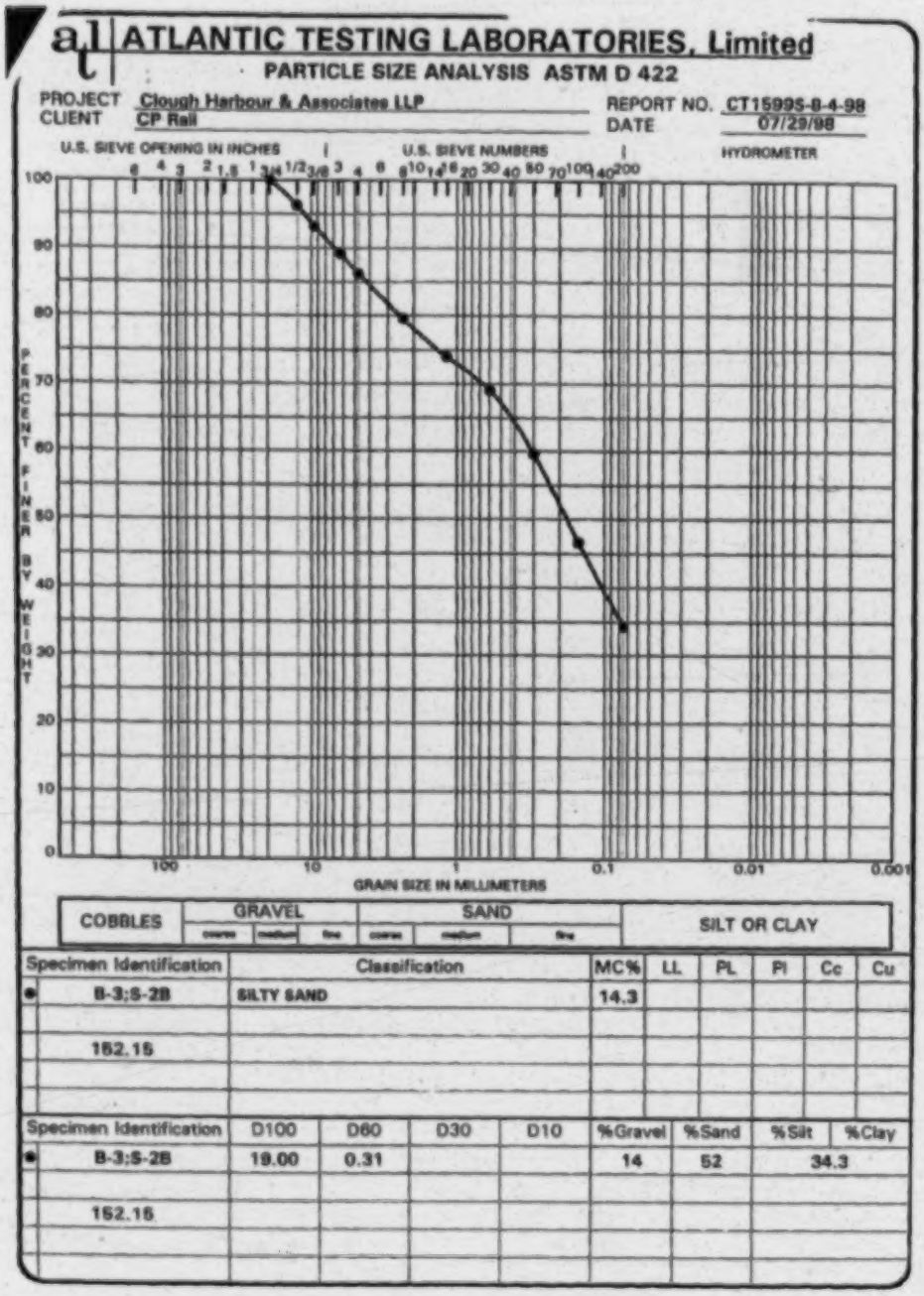

Specimen Identification	Classification	MC%	LL	PL	PI	Cc	Cu
● B-3;S-2B	SILTY SAND	14.3					
152.15							

Specimen Identification	D100	D60	D30	D10	%Gravel	%Sand	%Silt	%Clay
● B-3;S-2B	19.00	0.31			14	52	34.3	
152.15								

Figure B-5 Grain size curve for embankment material at MP 152.15

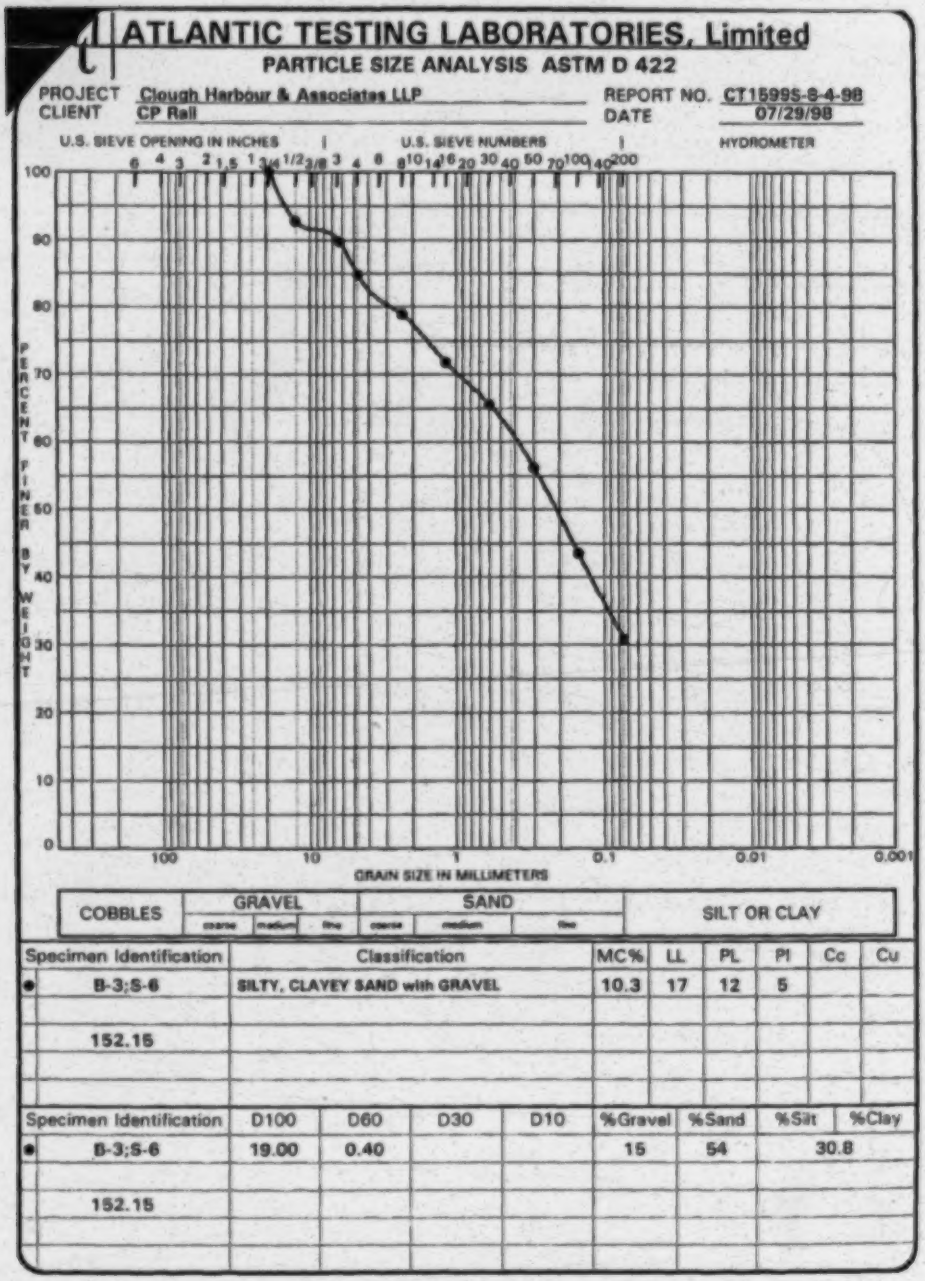
ATLANTIC TESTING LABORATORIES, Limited
PARTICLE SIZE ANALYSIS ASTM D 422
PROJECT Clough Harbour & Associates LLP
CLIENT CP Rail
REPORT NO. CT1599S-S-4-98
DATE 07/29/98
U.S. SIEVE OPENING IN INCHES
U.S. SIEVE NUMBERS
HYDROMETER
6 4 3 2 1.5 1 3/4 1/2 3/8 3 4 6 8 10 14 16 20 30 40 50 70 100 140 200
PERCENT FINER BY WEIGHT
100 90 80 70 60 50 40 30 20 10 0
100 10 1 0.1 0.01 0.001
GRAIN SIZE IN MILLIMETERS
COBBLES
GRAVEL
coarse medium fine
SAND
coarse medium fine
SILT OR CLAY

Specimen Identification	Classification	MC%	LL	PL	PI	Cc	Cu
● B-3;S-6	SILTY, CLAYEY SAND with GRAVEL	10.3	17	12	5		
152.15							

Specimen Identification	D100	D60	D30	D10	%Gravel	%Sand	%Silt	%Clay
● B-3;S-6	19.00	0.40			15	54	30.8	
152.15								

Figure B-5 Grain size curve for embankment material at MP 152.15 (Cont'd)

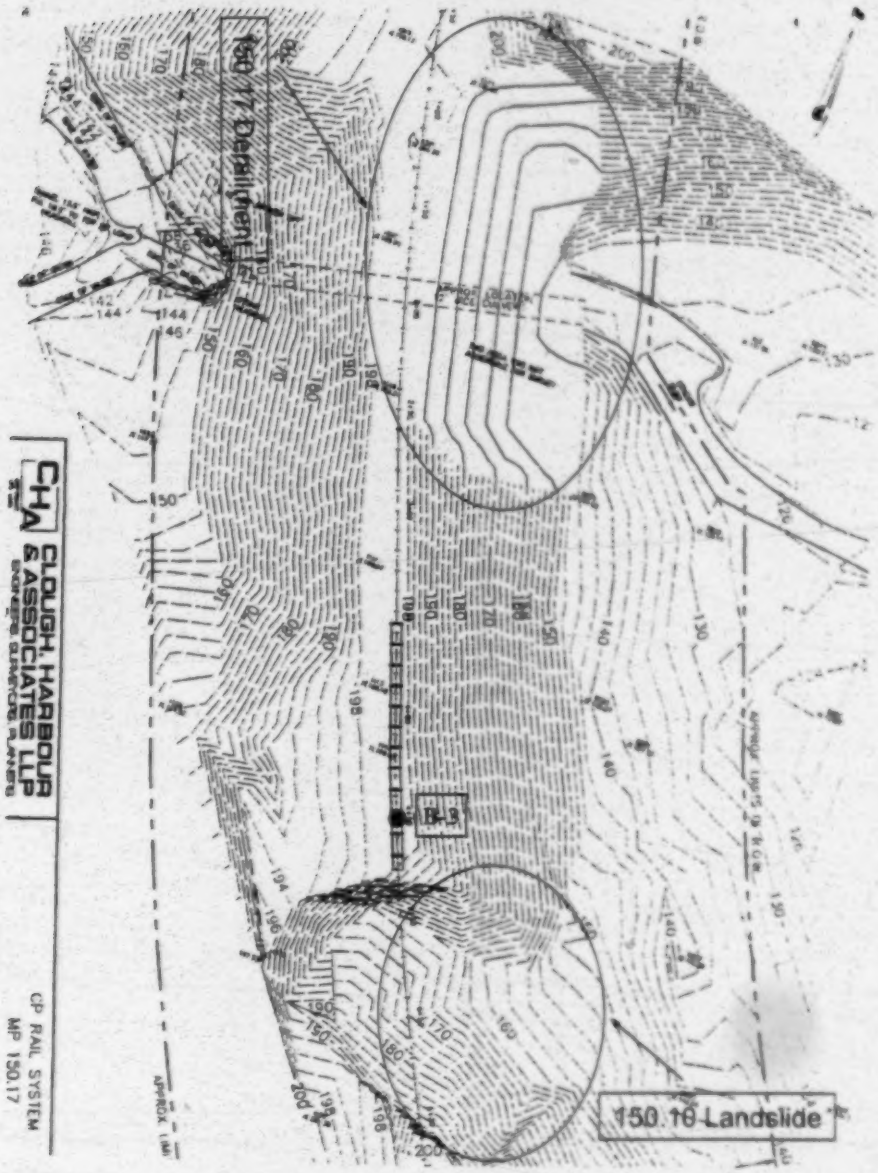

Figure B-6 Site topography for MP 150.17 and 150.10 landslides

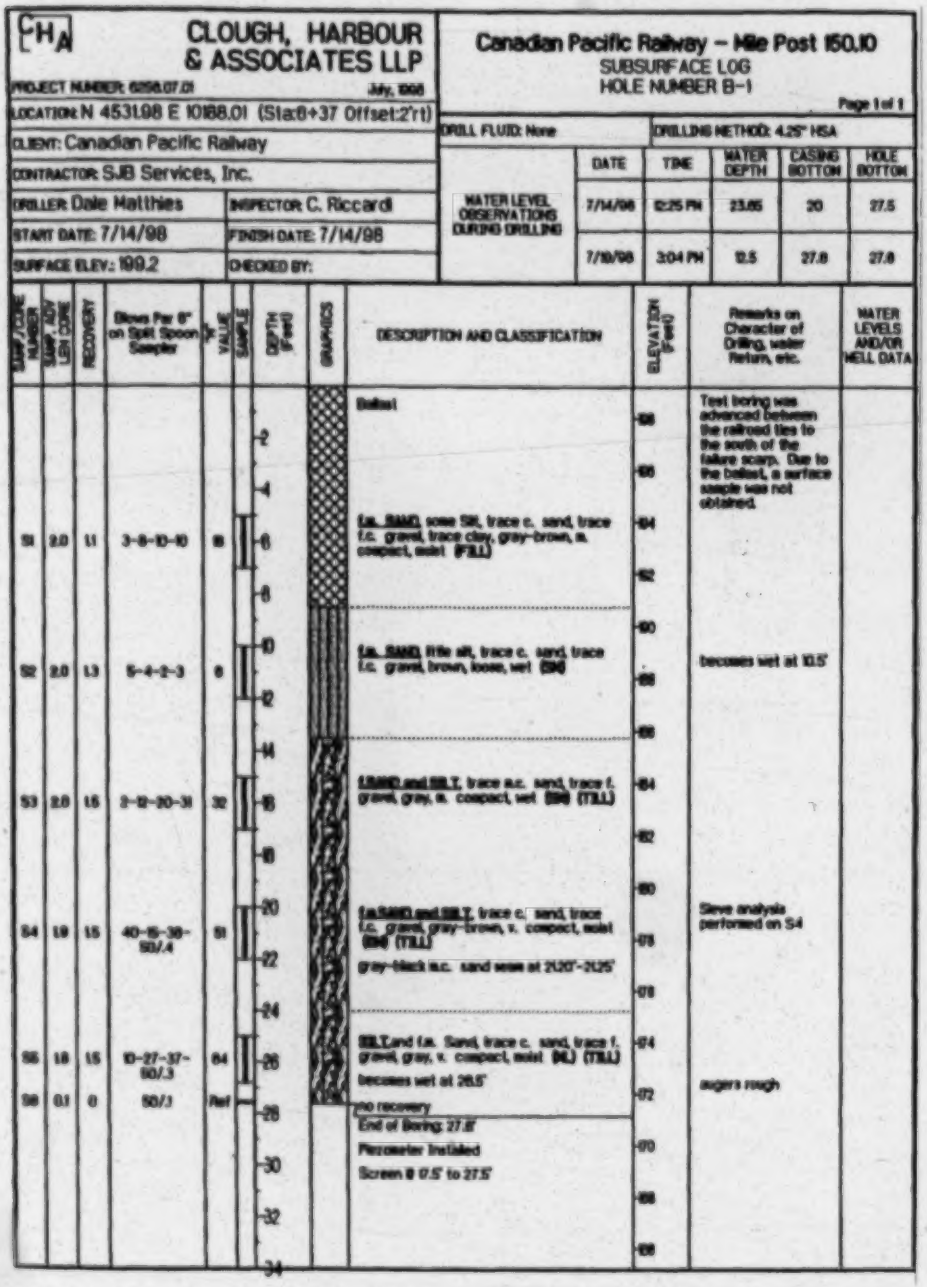

CLOUGH, HARBOUR & ASSOCIATES LLP

Canadian Pacific Railway – Mile Post 150.10

SUBSURFACE LOG

HOLE NUMBER B-1

Page 1 of 1

PROJECT NUMBER: 6258.07.01 — July, 1998

LOCATION: N 4531.98 E 10188.01 (Sta:6+37 Offset:2'rt)

CLIENT: Canadian Pacific Railway

CONTRACTOR: SJB Services, Inc.

DRILLER: Dale Matthies — INSPECTOR: C. Riccardi

START DATE: 7/14/98 — FINISH DATE: 7/14/98

SURFACE ELEV.: 199.2 — CHECKED BY:

DRILL FLUID: None — DRILLING METHOD: 4.25" HSA

WATER LEVEL OBSERVATIONS DURING DRILLING	DATE	TIME	WATER DEPTH	CASING BOTTOM	HOLE BOTTOM
	7/14/98	12:25 PM	23.65	20	27.5
	7/15/98	3:04 PM	12.5	27.8	27.8

SAMPLE/CORE NUMBER	SAMP./ADV. LEN CORE	RECOVERY	Blows Per 6" on Split Spoon Sampler	"N" VALUE	SAMPLE	DEPTH (Feet)	GRAPHICS	DESCRIPTION AND CLASSIFICATION	ELEVATION (Feet)	Remarks on Character of Drilling, water Return, etc.	WATER LEVELS AND/OR WELL DATA
						2		Ballast	198	Test boring was advanced between the railroad ties to the south of the failure scarp. Due to the ballast, a surface sample was not obtained.	
						4			196		
S1	2.0	1.1	3-8-10-10	18		6		f.s. SAND, some Silt, trace c. sand, trace f.c. gravel, trace clay, gray-brown, m. compact, moist (FILL)	194		
						8			192		
						10			190		
S2	2.0	1.3	5-4-2-3	6		12		f.s. SAND, little silt, trace c. sand, trace f.c. gravel, brown, loose, wet (SM)	188	becomes wet at 10.5'	
						14			186		
S3	2.0	1.5	2-12-20-31	32		16		f.SAND and SILT, trace m.c. sand, trace f. gravel, gray, m. compact, wet (SM) (FILL)	184		
						18			182		
						20			180		
S4	1.9	1.5	40-15-38-50/.4	51		22		f.s.SAND and SILT, trace c. sand, trace f.c. gravel, gray-brown, v. compact, moist (SM) (FILL)	178	Sieve analysis performed on S4	
						24		gray-black m.c. sand seam at 21.20'-21.25'	176		
						26		SILT and f.s. Sand, trace c. sand, trace f. gravel, gray, v. compact, moist (ML) (FILL)	174		
S5	1.8	1.5	10-27-37-50/.3	64				becomes wet at 26.5'			
S6	0.1	0	50/.1	Ref				no recovery	172	augers rough	
						28		End of Boring: 27.8'			
								Piezometer Installed	170		
						30		Screen @ 17.5' to 27.5'			
						32			168		
									166		
						34					

Figure B-7 Borehole log B-1 at MP 150.1

CLOUGH, HARBOUR & ASSOCIATES LLP

Canadian Pacific Railway – Mile Post 150.10
SUBSURFACE LOG
HOLE NUMBER B-2
Page 1 of 1

PROJECT NUMBER: 0258.07.01 July, 1998
LOCATION: N4550.99 E10162.26 (Sta:8+07 Offset:15'rt)
CLIENT: Canadian Pacific Railway
CONTRACTOR: SJB Services, Inc.
DRILLER: Dale Matthies INSPECTOR: C. Riccardi
START DATE: 7/14/98 FINISH DATE: 7/14/98
SURFACE ELEV.: 197.6 CHECKED BY:

DRILL FLUID: None DRILLING METHOD: 4.25" HSA

WATER LEVEL OBSERVATIONS DURING DRILLING	DATE	TIME	WATER DEPTH	CASING BOTTOM	HOLE BOTTOM

SAMP./CORE NUMBER	SAMP. ADV LEN CORE	RECOVERY	Blows Per 6" on Split Spoon Sampler	"N" VALUE	SAMPLE	DEPTH (Feet)	GRAPHICS	DESCRIPTION AND CLASSIFICATION	ELEVATION (Feet)	Remarks on Character of Drilling, water Return, etc.	WATER LEVELS AND/OR WELL DATA
S1	2.0	1.4	1-1-2-2	3				f.m.c. SAND, little silt, black, v. loose, moist (FILL)			
						2			198		
S2	2.0	0.5	2-3-2-1	5				f.m. SAND, some SIL, trace c. sand, trace f. gravel, brown, loose, moist (FILL)			
						4			194		
S3	2.0	1.0	5-10-7-10	17				f.m. SAND and SILT, trace roots, dark brown, m. compact, moist (FILL)		Sieve analysis performed on S3	
						6			192		
S4	2.0	1.5	9-10-12-8	22				f.m.c. SAND, some SIL, trace f. gravel, gray/brown, m. compact, moist (SW)			
S5	0.2	0	50/.2	Ref		8		no recovery	190		
S6	2.0	0.8	1-3-1-2	4		10		f.SAND, some Clayey SIL, orange/brown, v.loose, wet (SW)	188	Sieve analysis performed on S6	
						12		f. SAND, some SIL, gray/brown, m. compact, wet (SW)	186		
S7	2.0	2.0	2-5-8-15	14							
						14		becomes compact, moist (SW)	184		
S8	2.0	2.0	4-21-21-30	42							
S9	0.3	0.3	50/.3	Ref		16		becomes very compact (SW)	182		
									180		
S10	1.7	0.8	8-30-29-50/.2	59		18		Similar Soil (SW)			
						20		grades with little m.c. sand (SW)	178		
S11	2.0	0.5	10-29-30-30	59							
S12	0.4	0.2	50/.4	Ref		22		Similar Soil, becomes wet (SW)	176		
S13	0.3	0.1	50/.3	Ref		24		Similar Soil (SW)	174	auger refusal at 24.1	
								End of Boring: 24.1			
						26		Grout to Surface	172		
									170		
						28					
						30			168		
						32			166		
						34			164		

Figure B-7 Borehole log B-2 at MP 150.1 (Cont'd)

CLOUGH, HARBOUR & ASSOCIATES LLP

Canadian Pacific Railway – Mile Post 150.10
SUBSURFACE LOG
HOLE NUMBER B-3
Page 1 of 2

PROJECT NUMBER: 6258.07.01 — July, 1998
LOCATION: N4700.34 E10108.71 (Sta:4+50 Offset:2'rt)
CLIENT: Canadian Pacific Railway
CONTRACTOR: SJB Services, Inc.
DRILLER: Dale Matthies — INSPECTOR: C. Riccardi
START DATE: 7/15/98 — FINISH DATE: 7/15/98
SURFACE ELEV.: 197.9 — CHECKED BY:

DRILL FLUID: None — DRILLING METHOD: 4.25" HSA

WATER LEVEL OBSERVATIONS DURING DRILLING

DATE	TIME	WATER DEPTH	CASING BOTTOM	HOLE BOTTOM
7/15/98	1:00 PM	43.5	53	60.5
7/20/98	2:00 AM	44.95	53	60.5
7/24/98	1:00 AM	45.05	53	60.5

SAMP/CORE NUMBER	SAMP. ADV. LEN. CORE	RECOVERY	Blows Per 6" on Split Spoon Sampler	"N" VALUE	SAMPLE	DEPTH (Feet)	GRAPHICS	DESCRIPTION AND CLASSIFICATION	ELEVATION (Feet)	Remarks on Character of Drilling, water Return, etc.	WATER LEVELS AND/OR WELL DATA
S1	2.0	0.0	5-8-5-5	11		2		no recovery	198		
						4			196		
						6			194		
						8			192		
S2	2.0	0.5	1-2-3-3	5		10		f.w. SAND, little silt, little c. sand, trace f. gravel, brown, loose, moist (SW)	190		
						12			188		
						14			186		
S3	2.0	0.8	2-2-2-2	4		16		f.w. SAND, and Silt, little c. sand, trace f. gravel, grey/ brown, loose, wet (SW)	184	Sieve analysis performed on S3	
						18			182		
S4	2.0	1.5	1-1-2-2	3		20		f.w.SAND, some Clayey Silt, little c. sand, trace f. gravel, brown, v. loose, wet (SW)	180	Sieve analysis performed on S4	
						22			178		
						24			176		
S5	2.0	0.2	1-2-2-1	4		26		f.w. SAND,and Silt,trace c. sand, trace f.gravel, grey/brown, v. loose, wet (SW)	174		
						28			172		
S6	2.0	0.4	1-1-1-1	2		30		grades with some Silt, little c. sand, trace f. gravel (SW)	170		
						32			168		
						34			166		

Figure B-7 Borehole log B-3 at MP 150.1 (Cont'd)

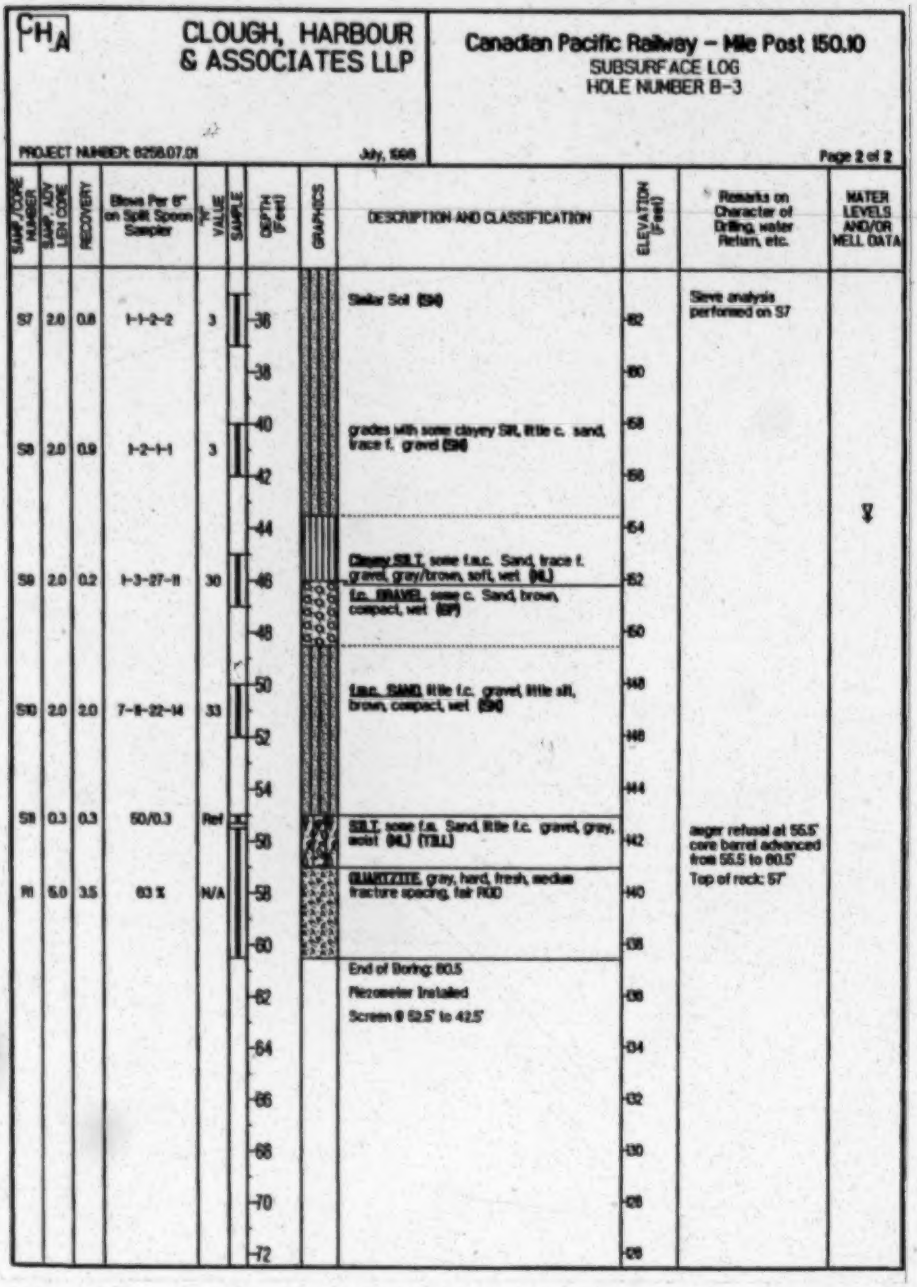
CLOUGH, HARBOUR & ASSOCIATES LLP
Canadian Pacific Railway – Mile Post 150.10
SUBSURFACE LOG
HOLE NUMBER B-3
PROJECT NUMBER: 6258.07.01
July, 1998
Page 2 of 2
SAMP./CORE NUMBER
SAMP./UNDISTURBED CORE
RECOVERY
Blows Per 6" on Split Spoon Sampler
"N" VALUE
SAMPLE
DEPTH (Feet)
GRAPHICS
DESCRIPTION AND CLASSIFICATION
ELEVATION (Feet)
Remarks on Character of Drilling, water Return, etc.
WATER LEVELS AND/OR WELL DATA
S7 2.0 0.8 1-1-2-2 3
S8 2.0 0.9 1-2-1-1 3
S9 2.0 0.2 1-3-27-11 30
S10 2.0 2.0 7-8-22-14 33
S11 0.3 0.3 50/0.3 Ref
R1 5.0 3.5 63 % N/A
Sieve analysis performed on S7
auger refusal at 55.5' core barrel advanced from 55.5 to 60.5'
Top of rock: 57'
End of Boring: 60.5
Piezometer Installed
Screen @ 52.5' to 42.5'

Figure B-7 Borehole log B-3 at MP 150.1 (Cont'd)

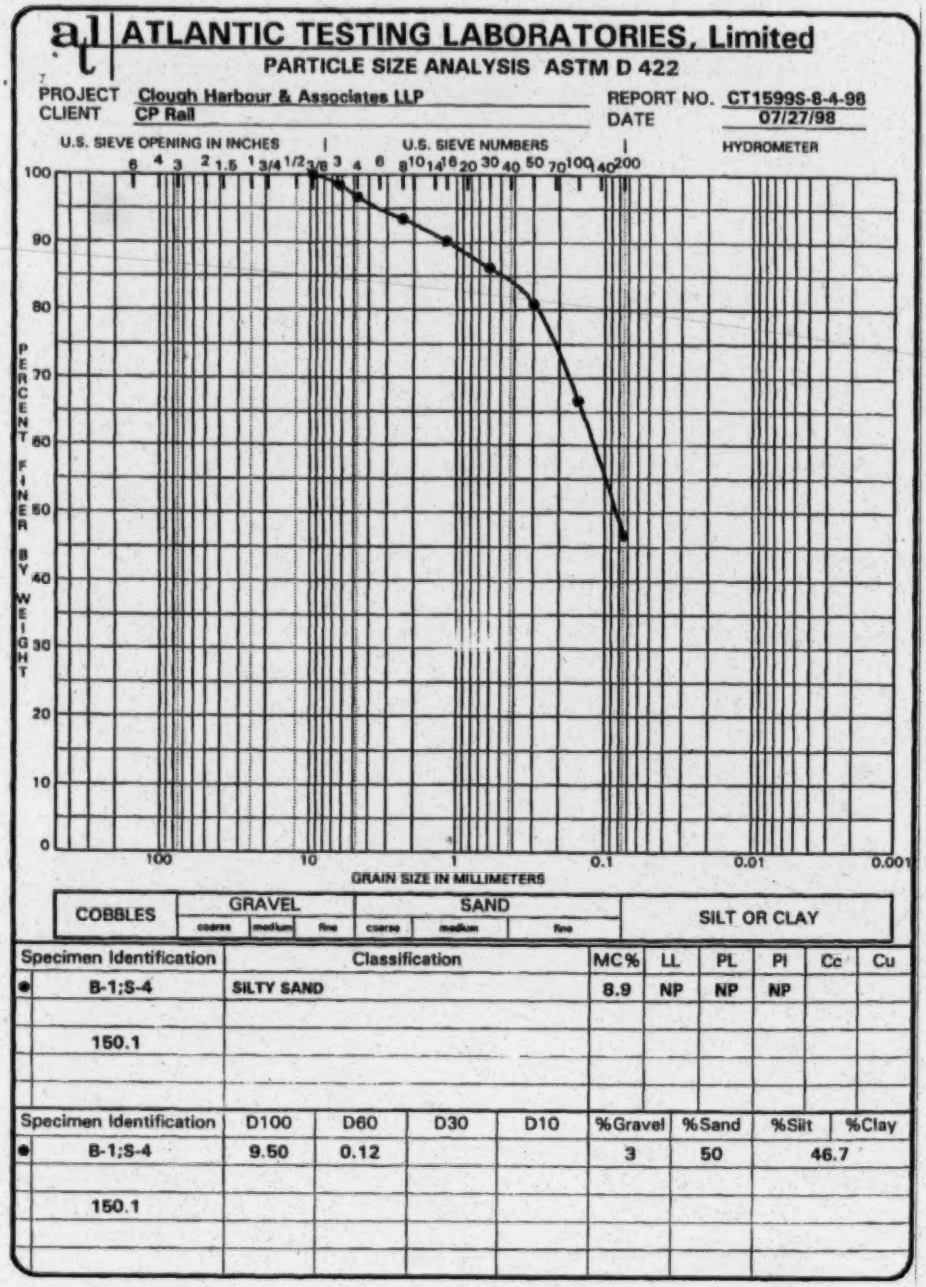

Specimen Identification	Classification	MC%	LL	PL	PI	Cc	Cu
● B-1;S-4	SILTY SAND	8.9	NP	NP	NP		
150.1							

Specimen Identification	D100	D60	D30	D10	%Gravel	%Sand	%Silt	%Clay
● B-1;S-4	9.50	0.12			3	50	46.7	
150.1								

Figure B-8 Grain size curve for embankment material at MP 150.1

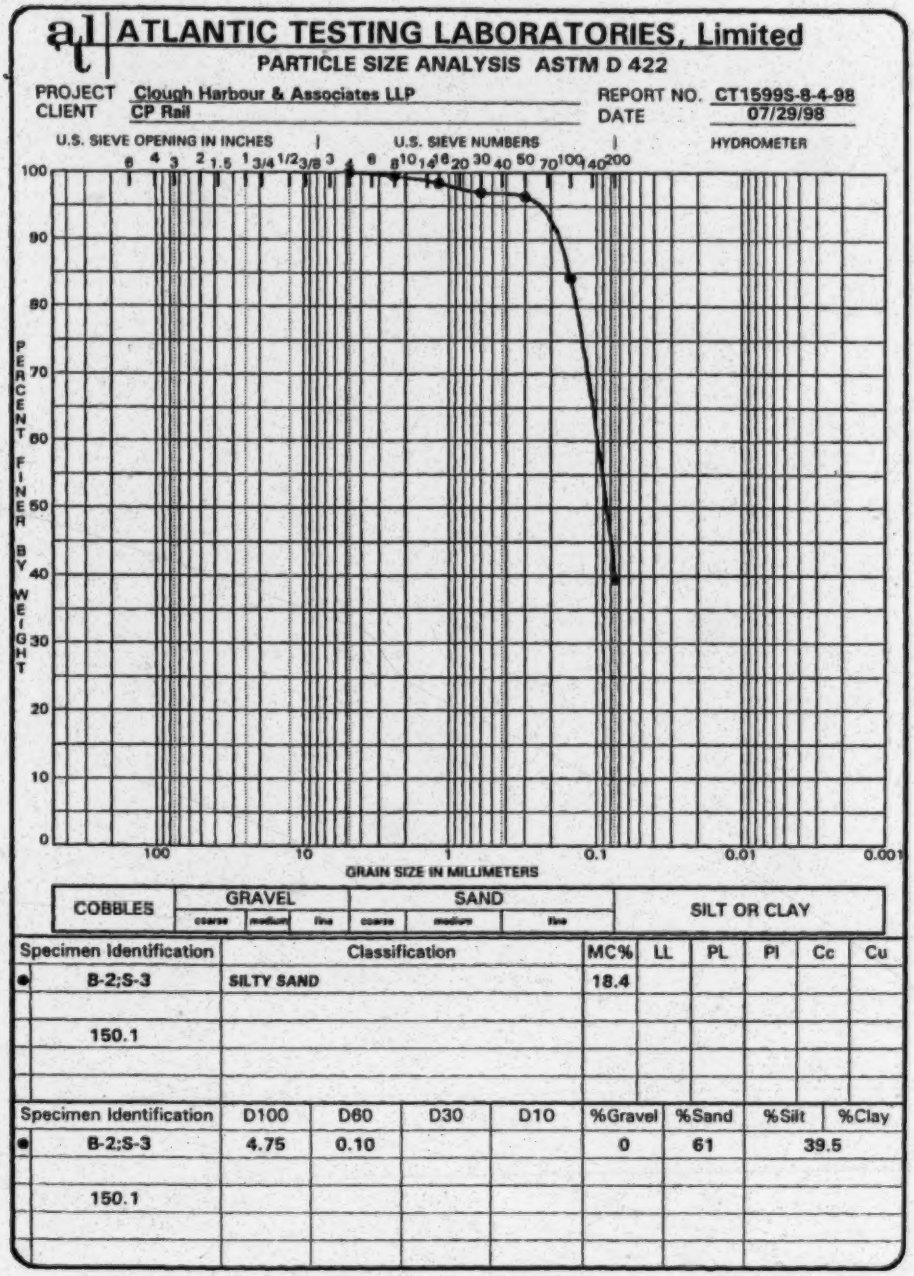

Figure B-8 Grain size curve for embankment material at MP 150.1 (cont'd)

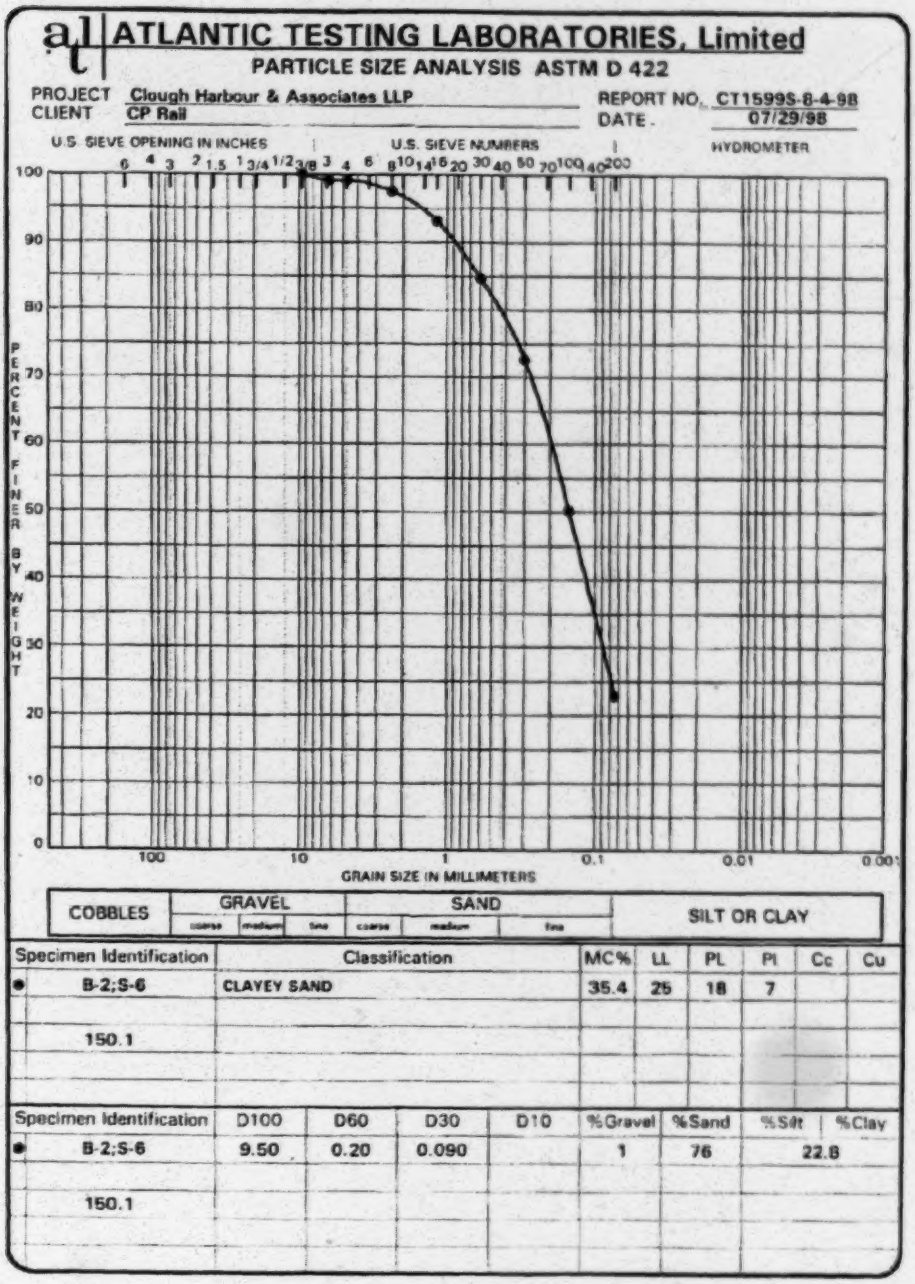

Specimen Identification	Classification	MC%	LL	PL	PI	Cc	Cu
● B-2;S-6	CLAYEY SAND	35.4	25	18	7		
150.1							

Specimen Identification	D100	D60	D30	D10	%Gravel	%Sand	%Silt	%Clay
● B-2;S-6	9.50	0.20	0.090		1	76	22.8	
150.1								

Figure B-8 Grain size curve for embankment material at MP 150.1 (cont'd)

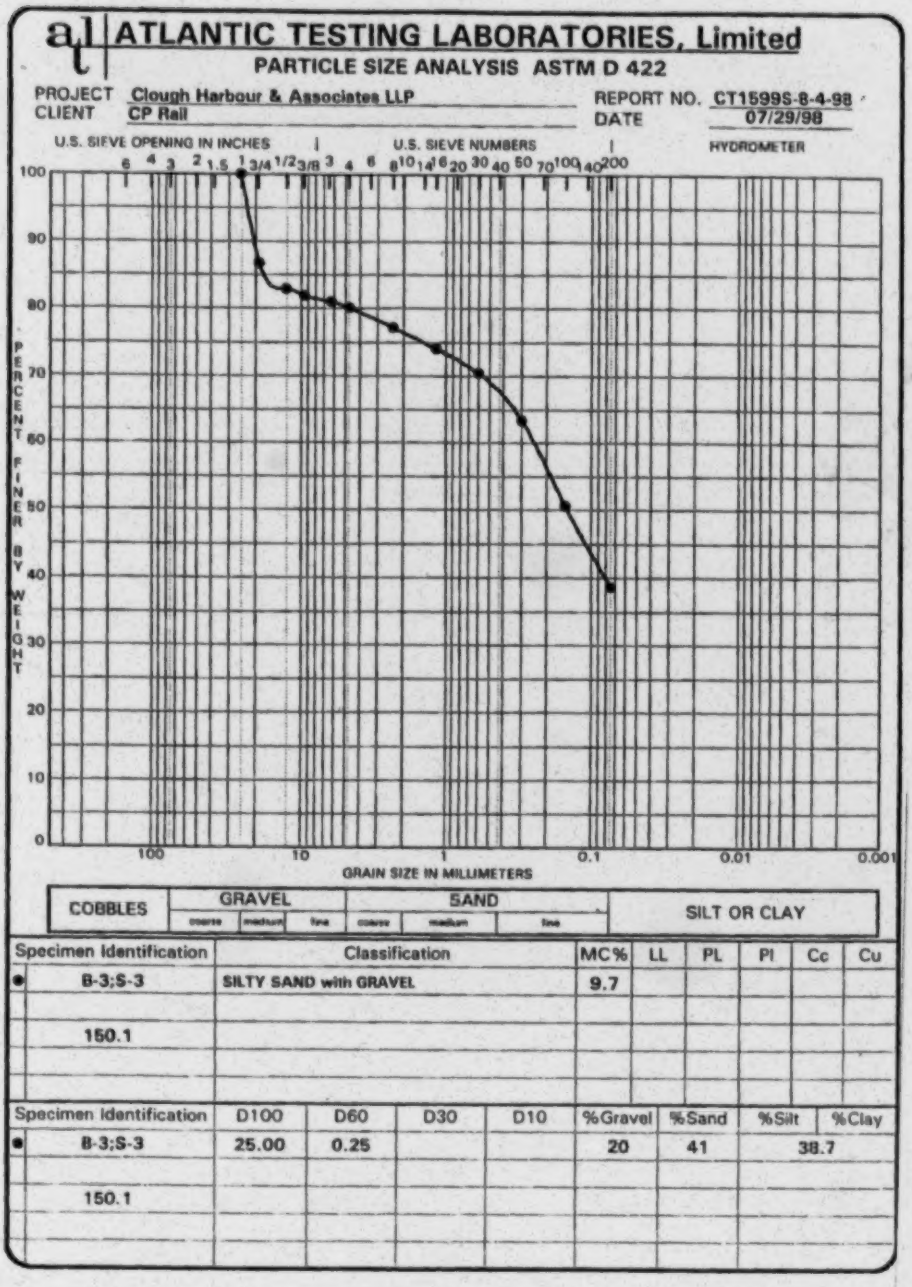

Specimen Identification	Classification	MC%	LL	PL	PI	Cc	Cu
● B-3;S-3	SILTY SAND with GRAVEL	9.7					
150.1							

Specimen Identification	D100	D60	D30	D10	%Gravel	%Sand	%Silt	%Clay
● B-3;S-3	25.00	0.25			20	41	38.7	
150.1								

Figure B-8 Grain size curve for embankment material at MP 150.1 (cont'd)

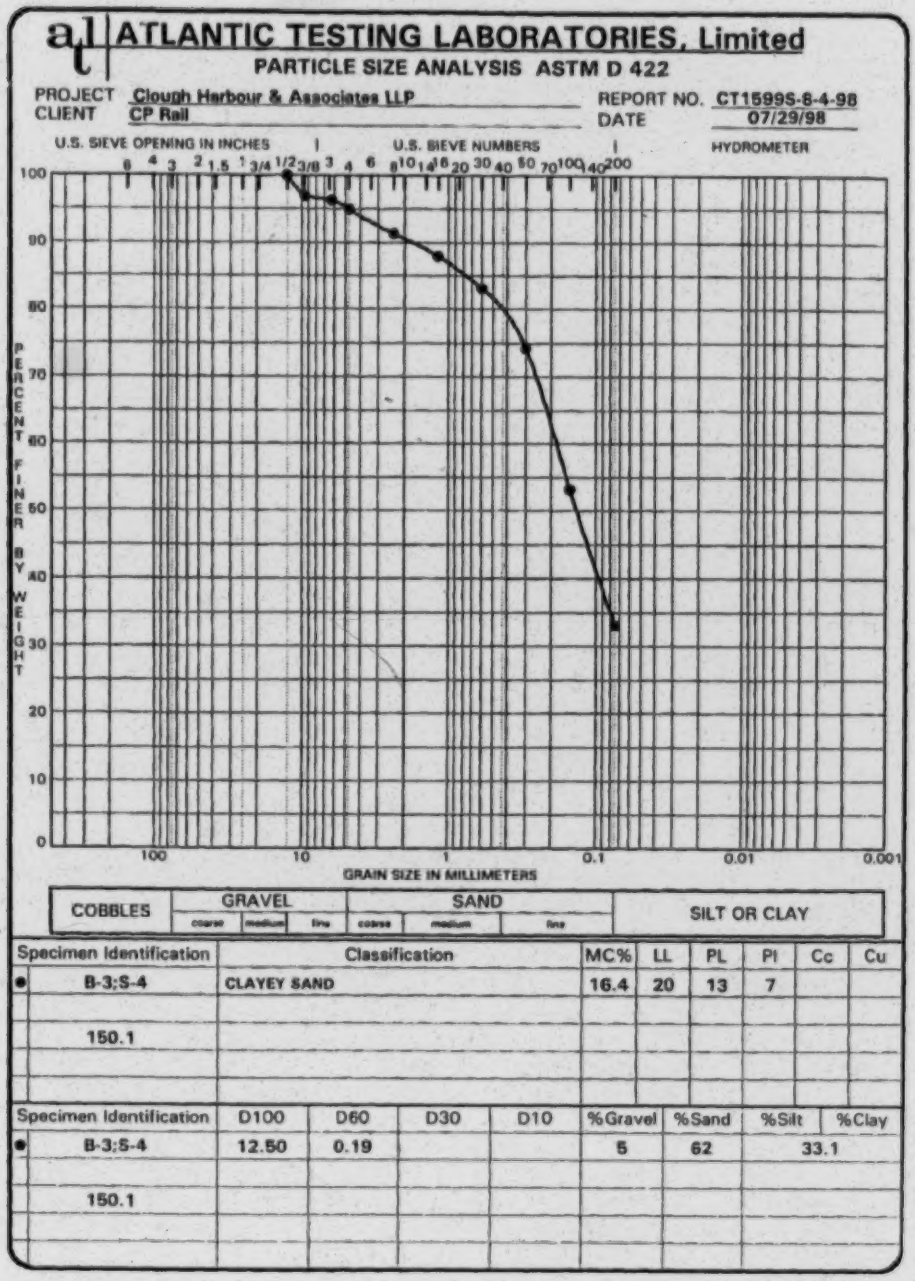

Specimen Identification	Classification	MC%	LL	PL	PI	Cc	Cu
● B-3;S-4	CLAYEY SAND	16.4	20	13	7		
150.1							

Specimen Identification	D100	D60	D30	D10	%Gravel	%Sand	%Silt	%Clay
● B-3;S-4	12.50	0.19			5	62	33.1	
150.1								

Figure B-8 Grain size curve for embankment material at MP 150.1 (cont'd)

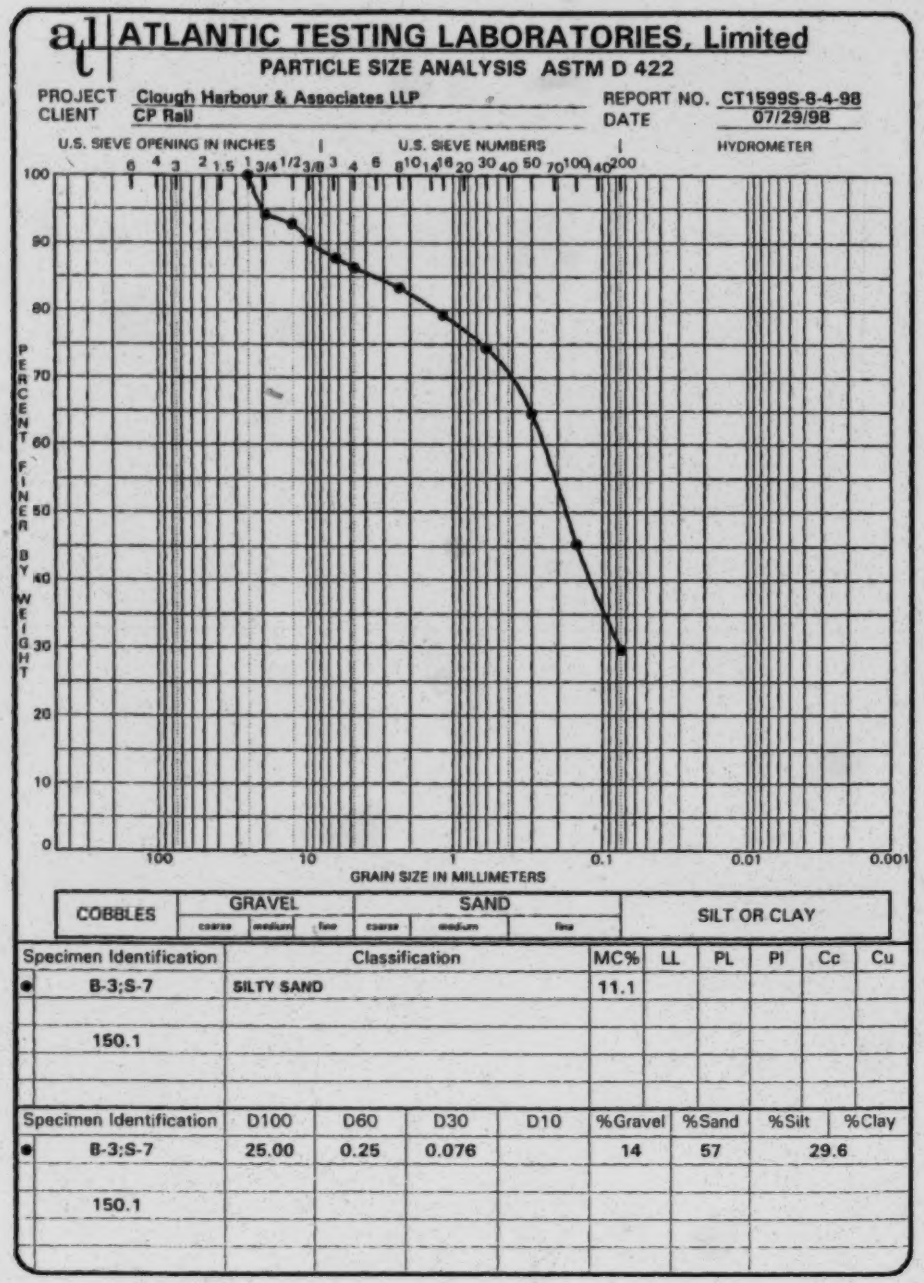
ATLANTIC TESTING LABORATORIES, Limited
PARTICLE SIZE ANALYSIS ASTM D 422
PROJECT Clough Harbour & Associates LLP
CLIENT CP Rail
REPORT NO. CT1599S-8-4-98
DATE 07/29/98
U.S. SIEVE OPENING IN INCHES
U.S. SIEVE NUMBERS
HYDROMETER
6 4 3 2 1.5 1 3/4 1/2 3/8 3 4 6 8 10 14 16 20 30 40 50 70 100 140 200
PERCENT FINER BY WEIGHT
100 90 80 70 60 50 40 30 20 10 0
100 10 1 0.1 0.01 0.001
GRAIN SIZE IN MILLIMETERS
COBBLES
GRAVEL
coarse medium fine
SAND
coarse medium fine
SILT OR CLAY

Specimen Identification	Classification	MC%	LL	PL	PI	Cc	Cu
● B-3;S-7	SILTY SAND	11.1					
150.1							

Specimen Identification	D100	D60	D30	D10	%Gravel	%Sand	%Silt	%Clay
● B-3;S-7	25.00	0.25	0.076		14	57	29.6	
150.1								

Figure B-8 Grain size curve for embankment material at MP 150.1 (Cont'd)

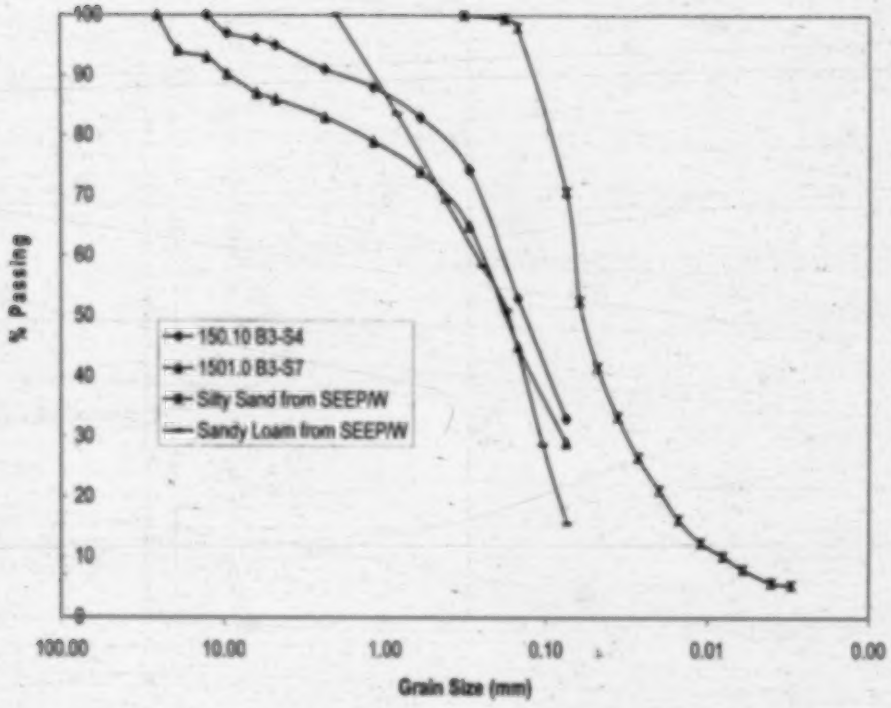

Figure B-9 Grain size curves for embankment material and samples from SEEP/W

Table B-2 Properties of silty sand material from SEEP/W database

Silty Sand	K_{sat} (m/s)	θ_s	AEV (kPa)	D10 (mm)	D60 (mm)
#6	5e-7	0.51	12	0.008	0.07

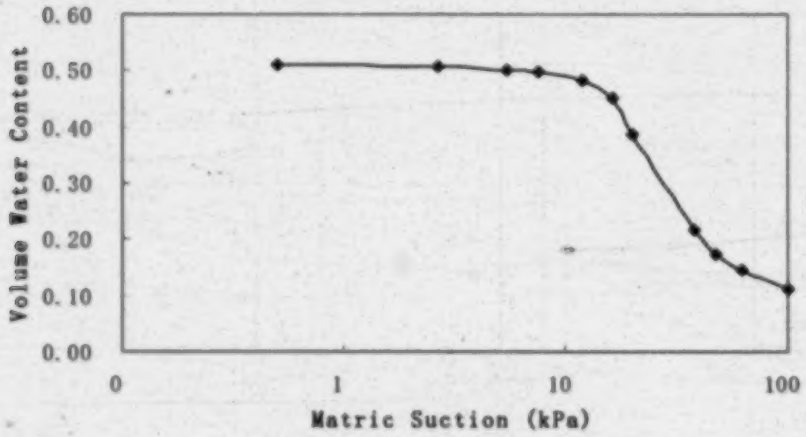

(a) volume water content function

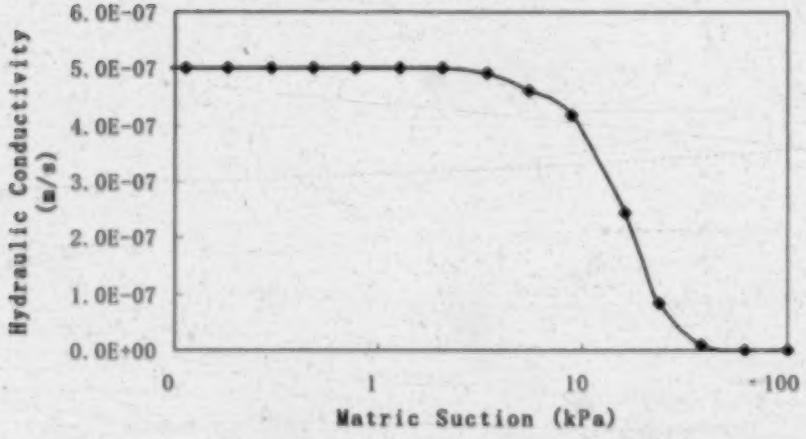

(b) hydraulic conductivity function

Figure B-10 Volume water content and hydraulic conductivity functions for silty sand material from SEEP/W database

Table B-3 Properties of sandy loam material from SEEP/W database

Sandy Loam	Ksat (m/s)	θs	AEV (kPa)	D10 (mm)	D60 (mm)
#3	5.83e-6	0.38	6	0.06	0.3

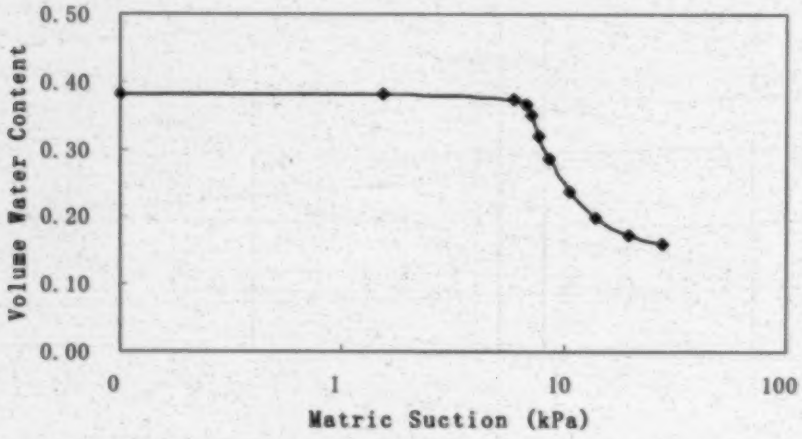

(a) volume water content function

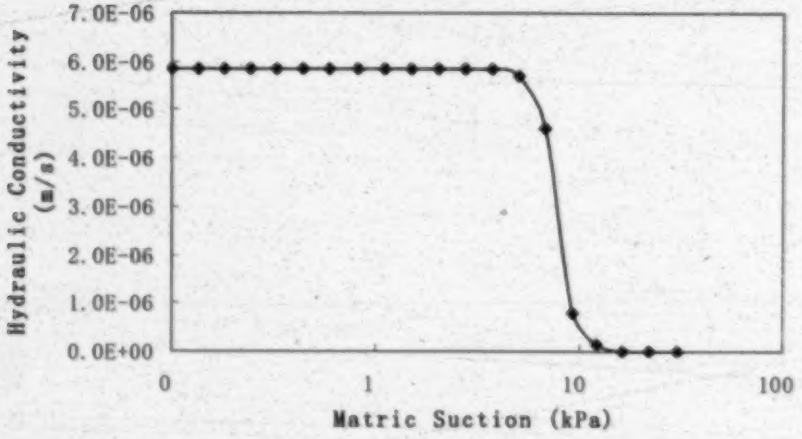

(b) hydraulic conductivity function

Figure B-11 Volume water content and hydraulic conductivity functions for sandy loam material from SEEP/W database

Appendix C Seepage Modeling Results

1. Seepage Modeling Results for Embankment at MP 154.47

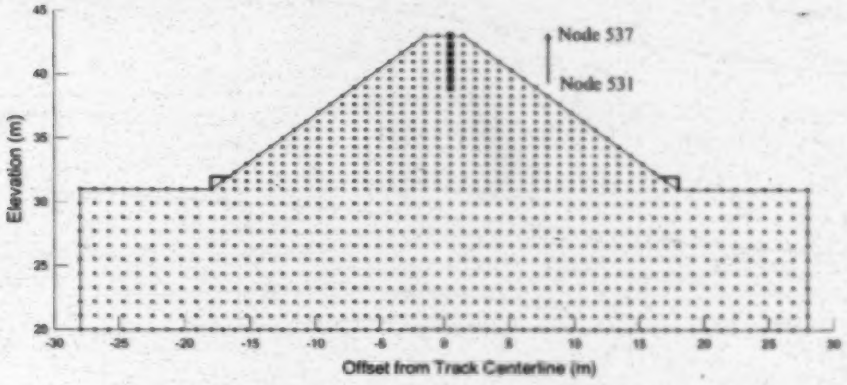

(a) location of the nodes selected

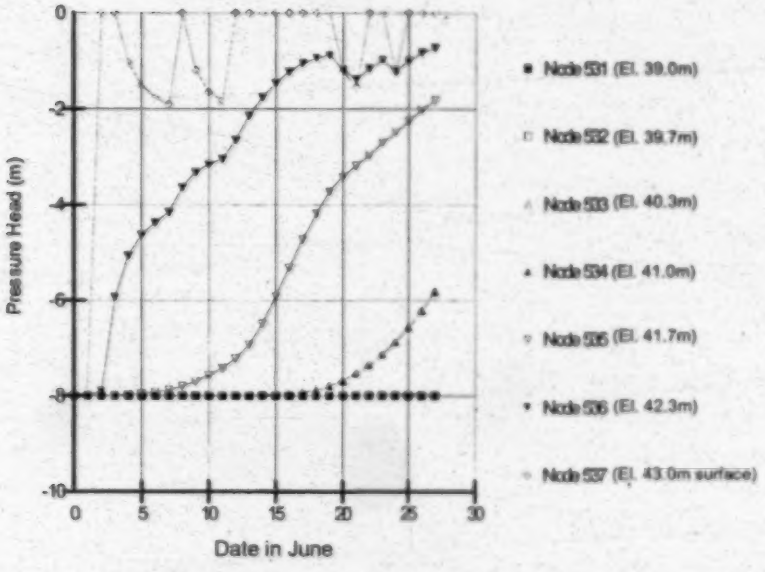

(b) for Ksat = 5E-8m/s

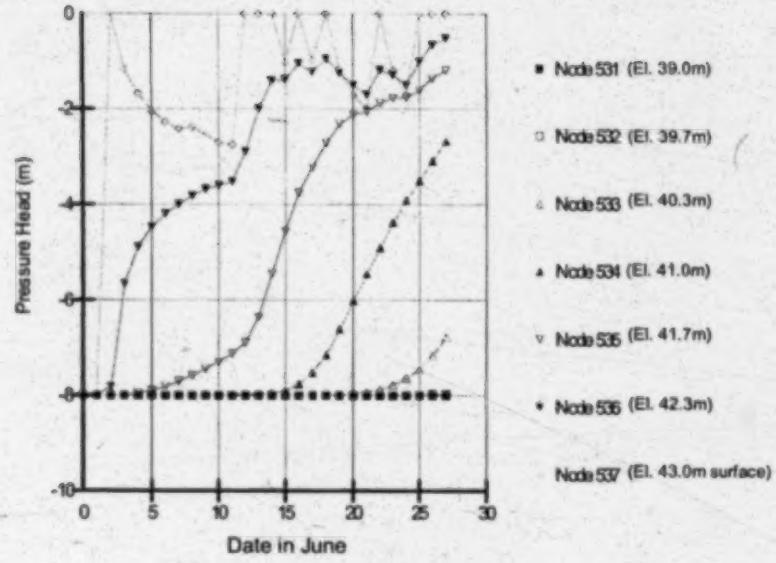

(c) for Ksat = 1E-7m/s

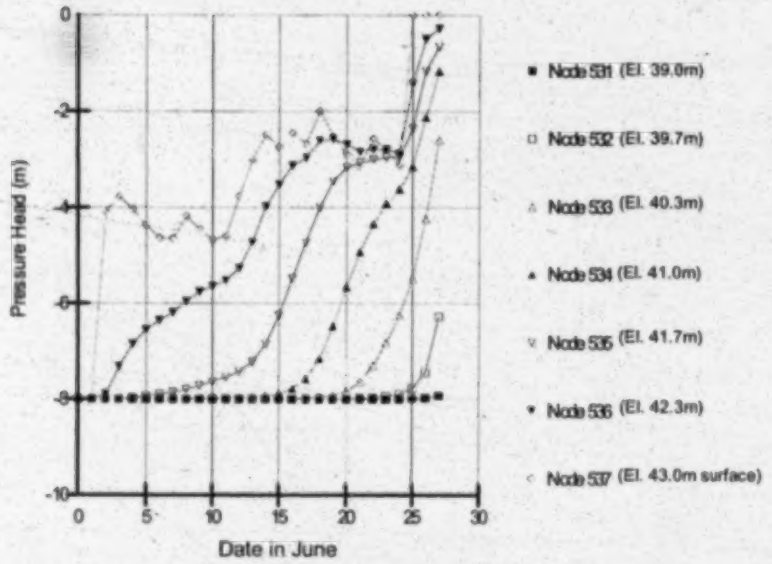

(d) for Ksat = 5E-7m/s

Figure C-1 Evolution of pore-water pressure change
at the crest for initially dry embankment at MP 154.47

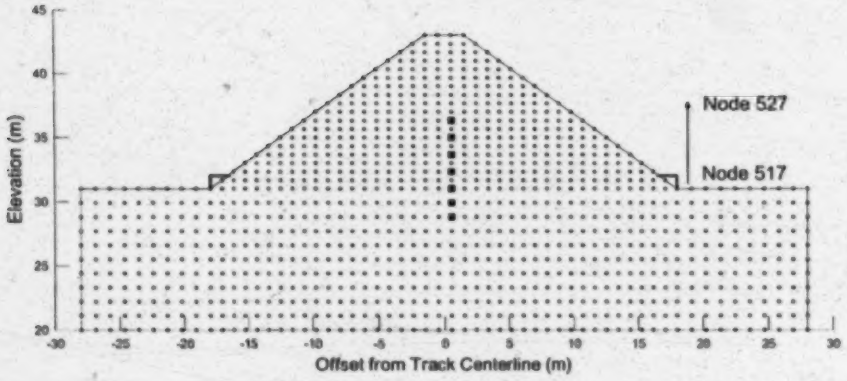

(a) location of the nodes selected

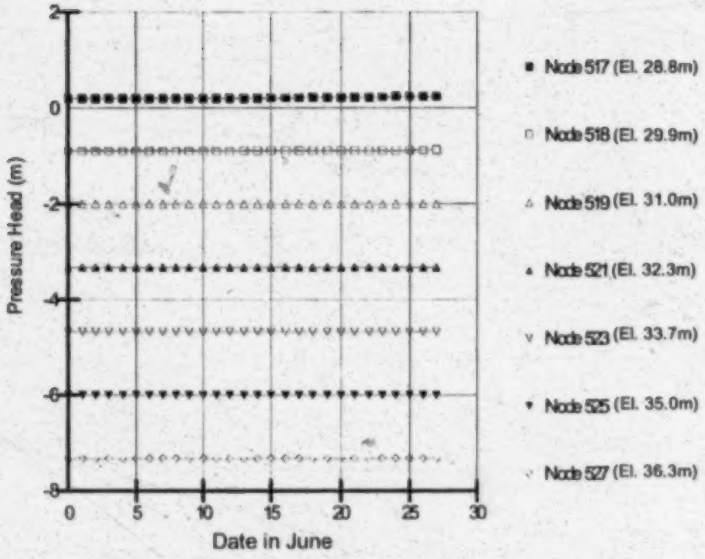

(b) for Ksat = 5E-8m/s

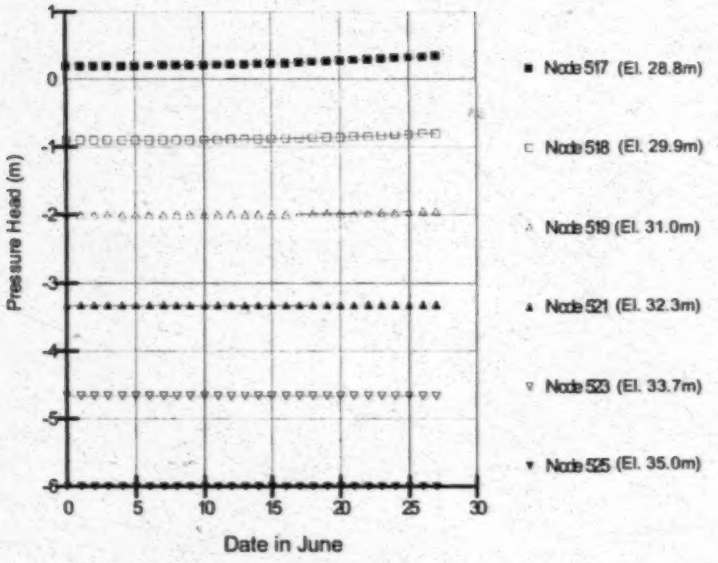

(c) for Ksat = 1E-7m/s

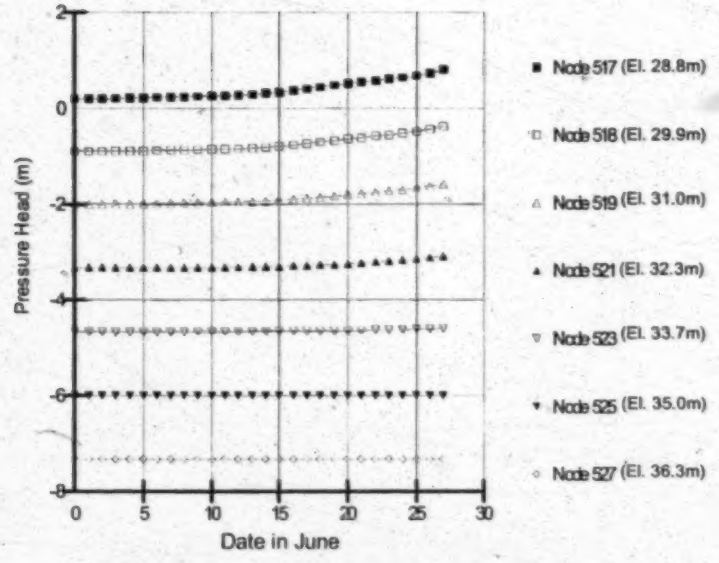

(d) for Ksat = 5E-7m/s

Figure C-2 Evolution of pore-water pressure
at the bottom for initially dry embankment at MP 154.47

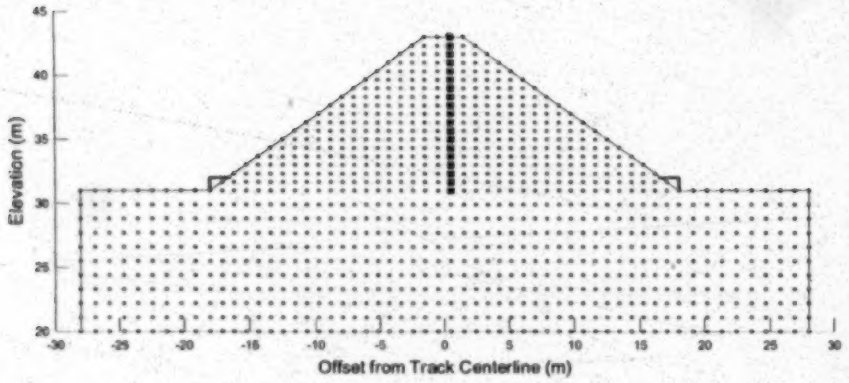

(a) location of the nodes selected

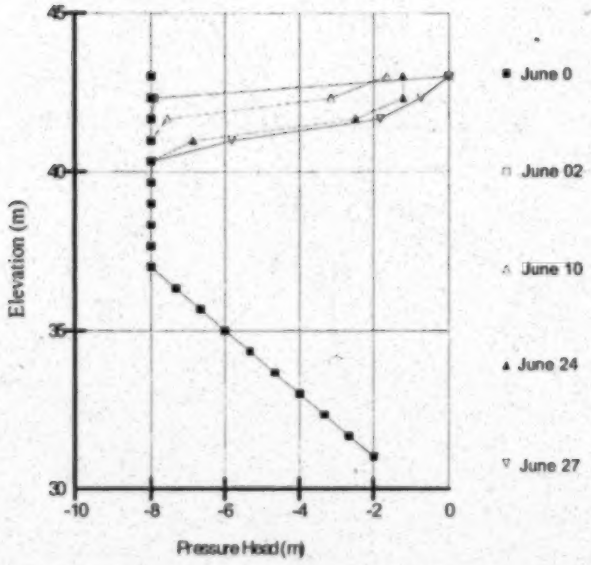

(b) for Ksat = 5E-8m/s

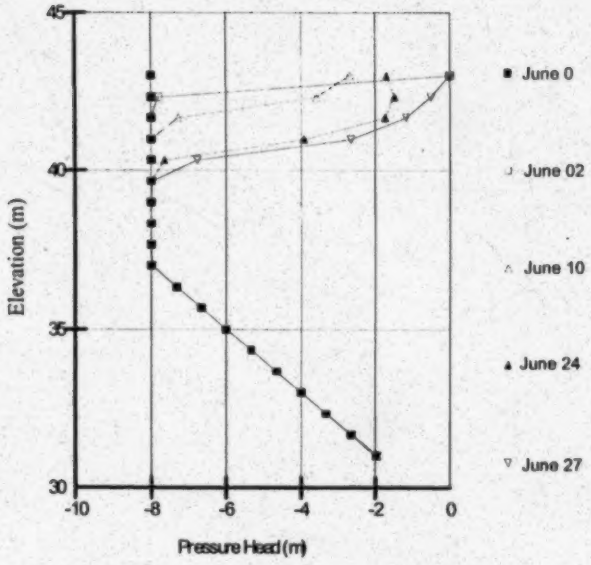

(c) for Ksat = 1E-7m/s

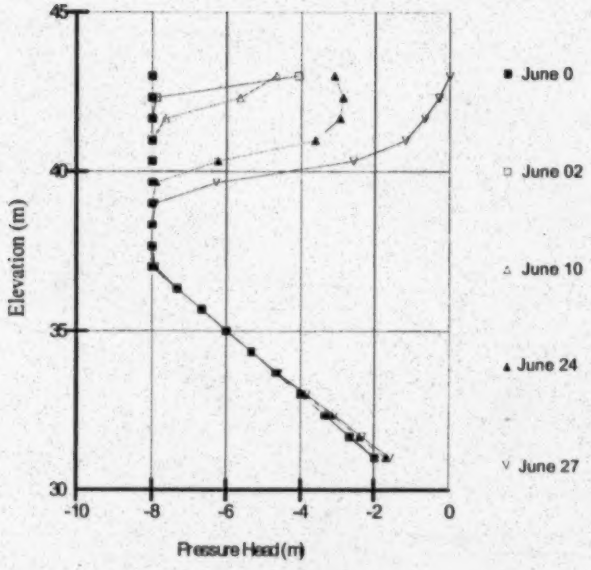

(d) for Ksat = 5E-7m/s

Figure C-3 Pore-water pressure profile along a vertical line for initially dry embankment at MP 154.47

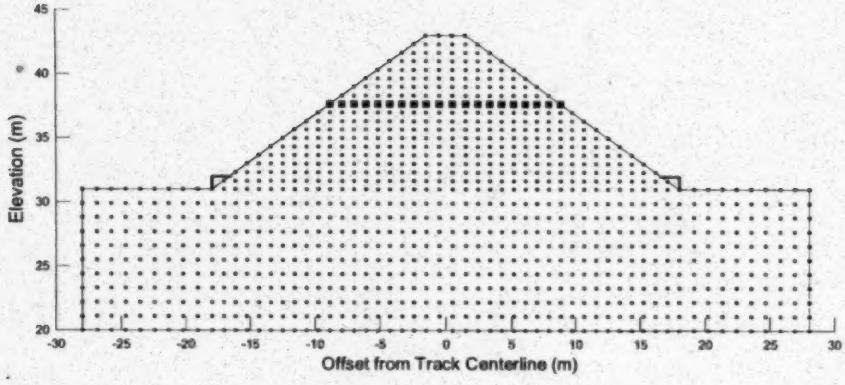

(a) location of the nodes selected

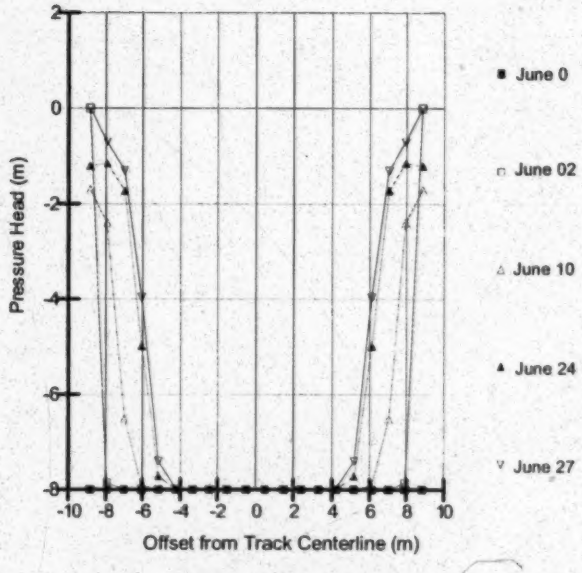

(b) for Ksat = 5E-8m/s

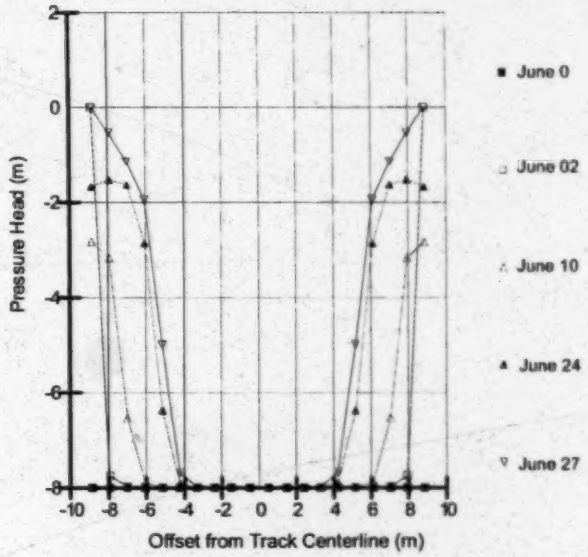

(c) for Ksat = 1E-7m/s

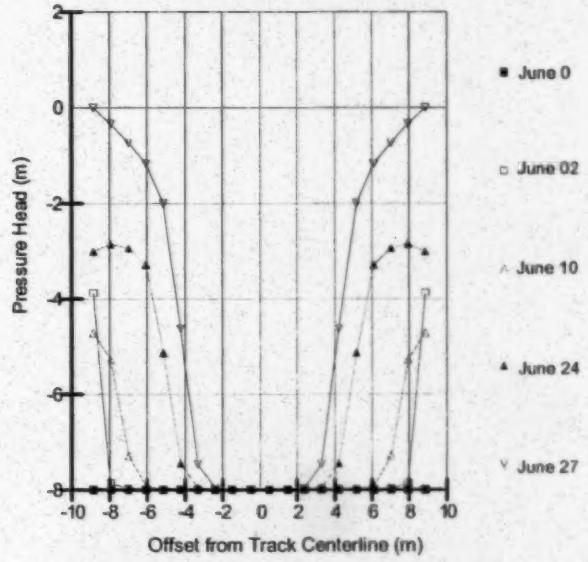

(d) for Ksat = 5E-7m/s

Figure C-4 Pore-water pressure profile along a horizontal line for initially dry embankment at MP 154.47

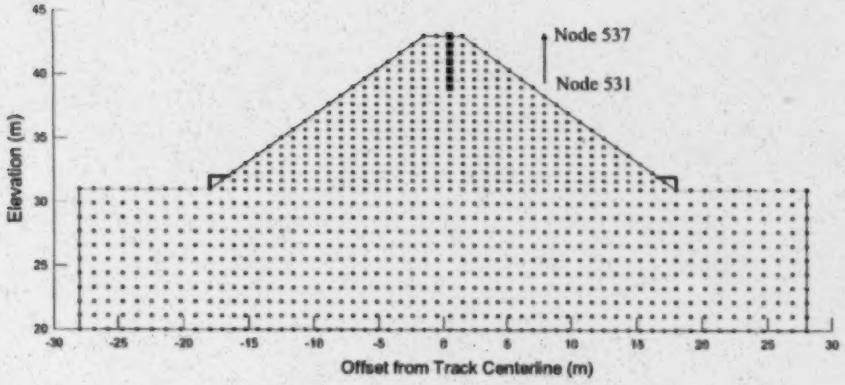

(a) location of the nodes selected

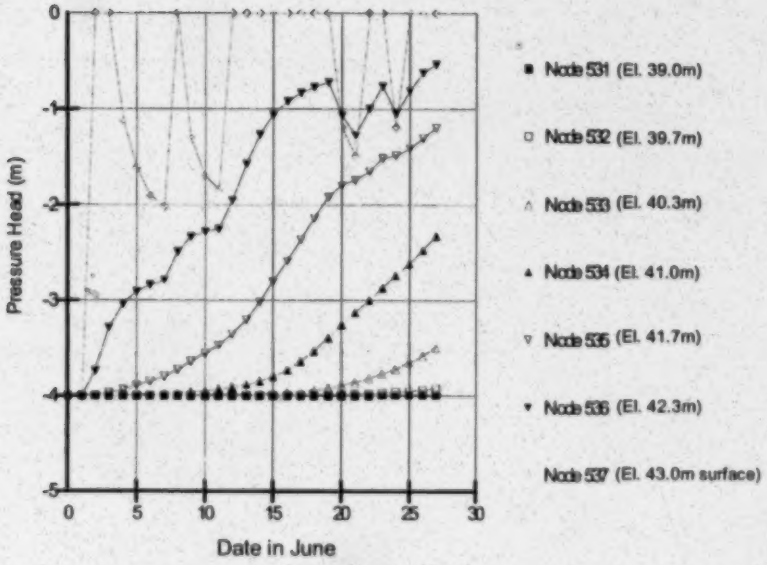

(b) for Ksat = 5E-8m/s

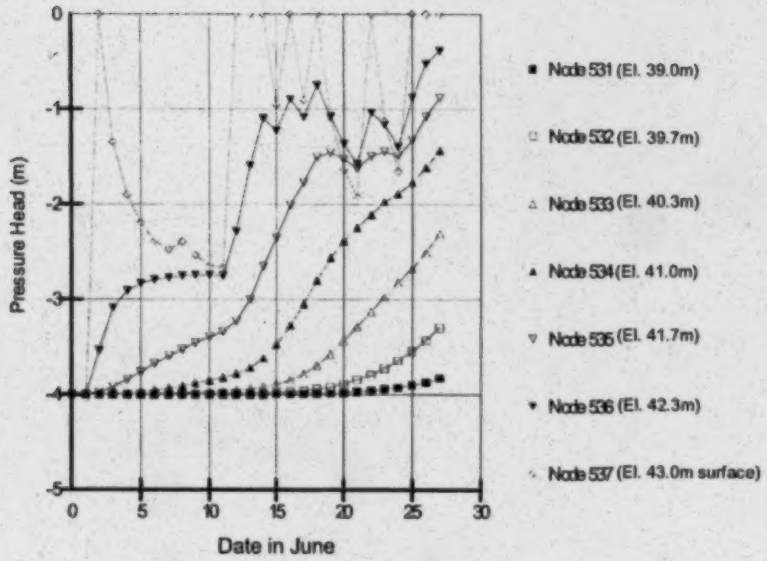

(c) for Ksat = 1E-7m/s

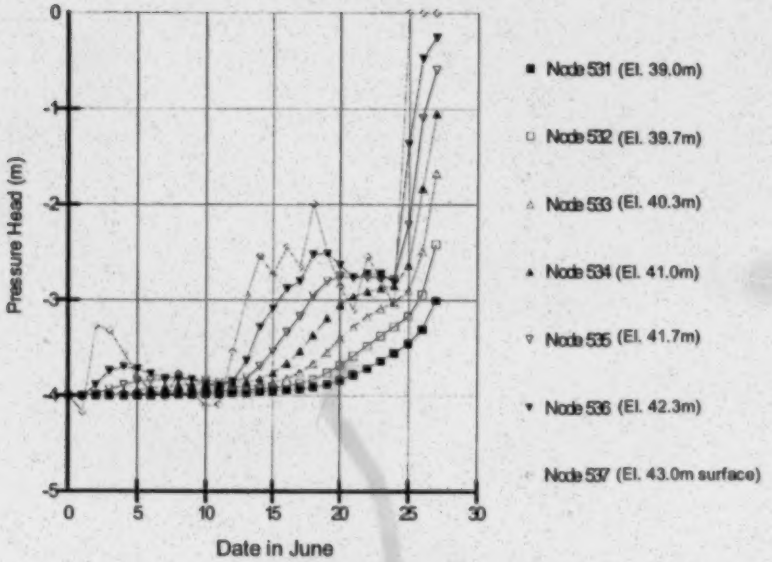

(d) for Ksat = 5E-7m/s

Figure C-5 Evolution of pore-water pressure
at the crest for initially wet embankment at MP 154.47

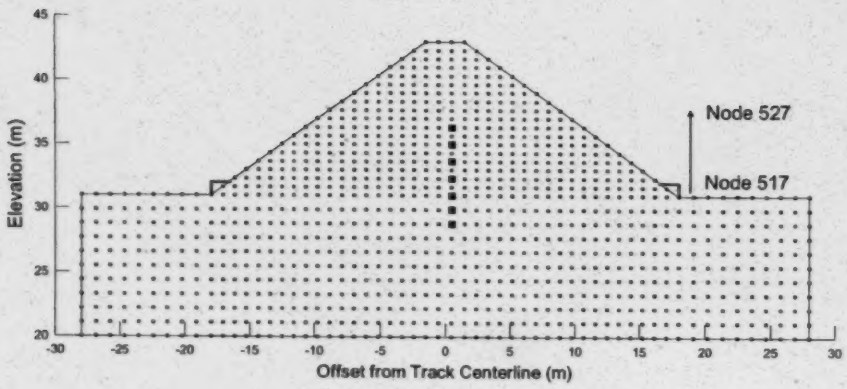

(a) location of the nodes selected

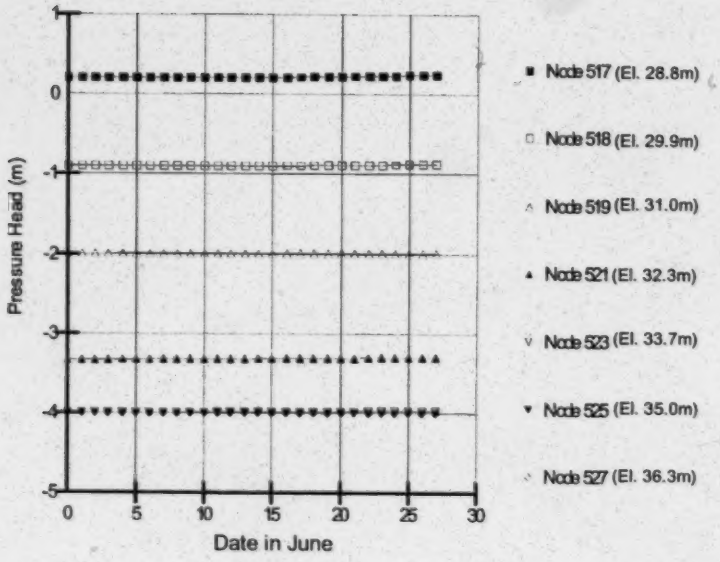

(b) for Ksat = 5E-8m/s

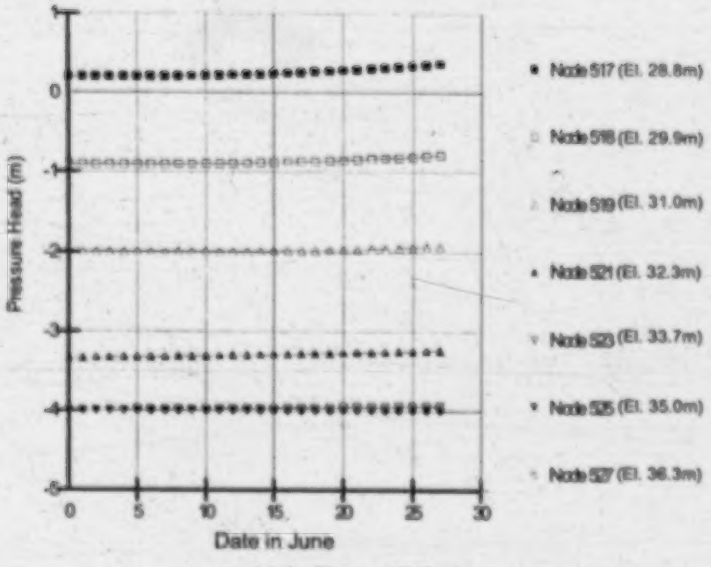

(c) for Ksat = 1E-7m/s

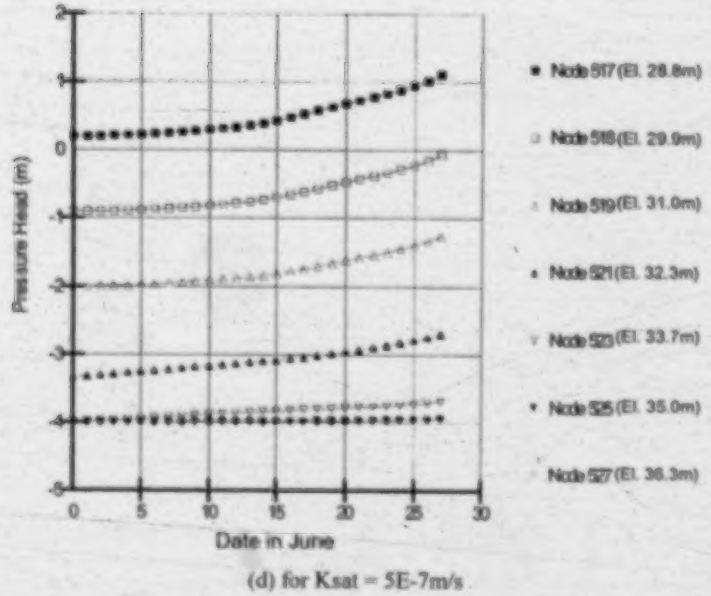

(d) for Ksat = 5E-7m/s

Figure C-6 Evolution of pore-water pressure
at the bottom for initially wet embankment at MP 154.47

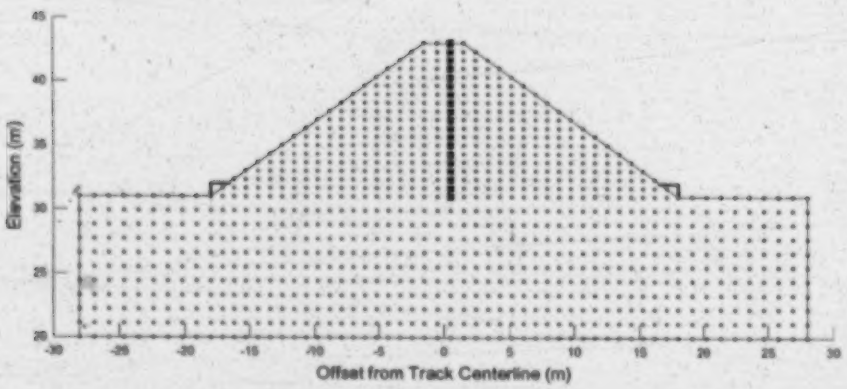

(a) location of the nodes selected

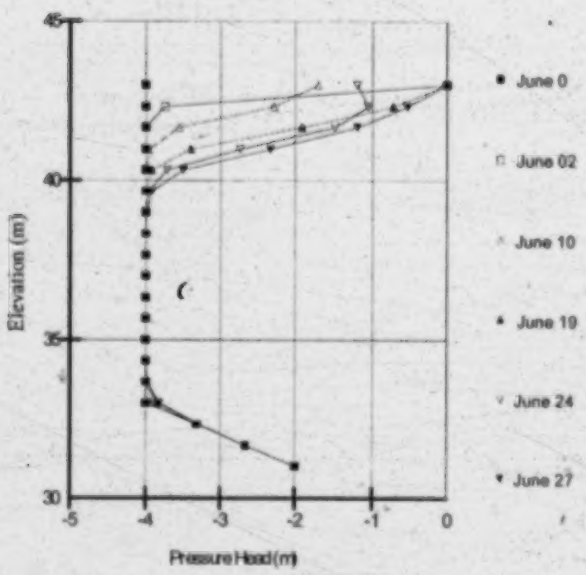

(b) for Ksat = 5E-8m/s

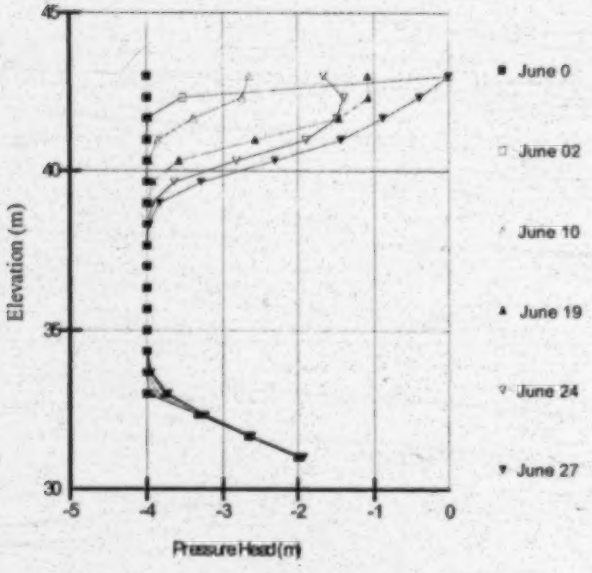

(c) for Ksat = 1E-7m/s

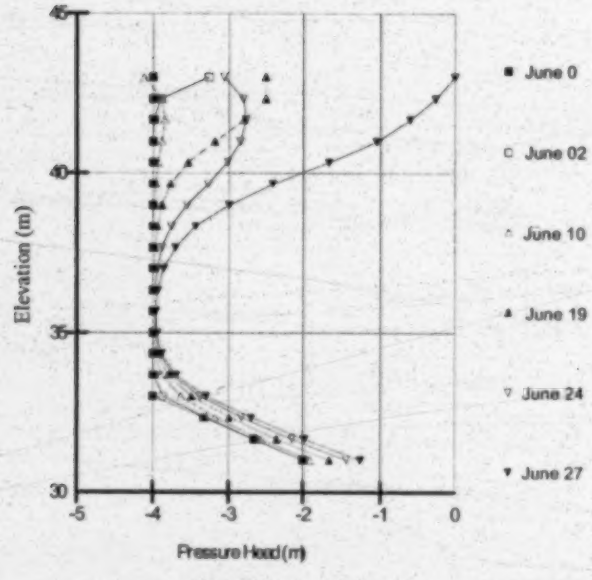

(d) for Ksat = 5E-7m/s

Figure C-7 Pore-water Pressure Profile along a Vertical Line for Initially Wet Embankment at MP 154.47

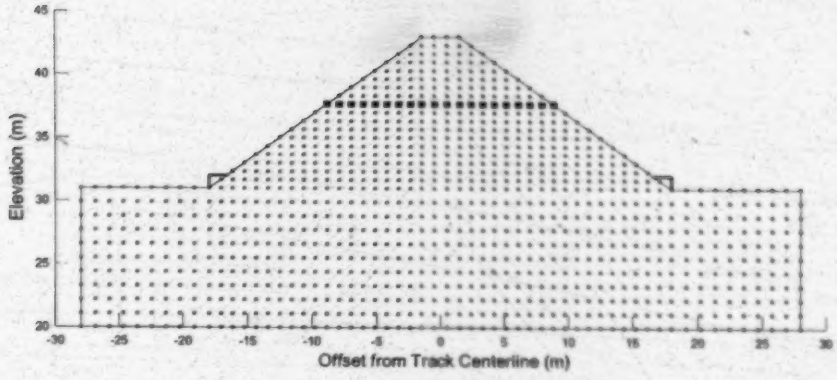

(a) location of the nodes selected

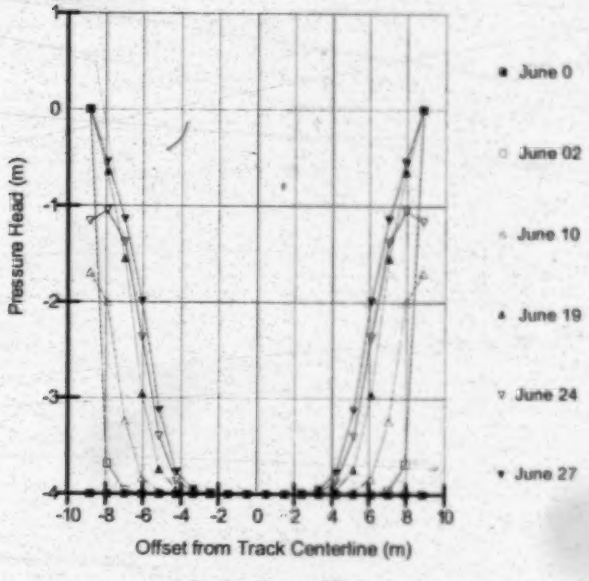

(b) for Ksat = 5E-8m/s

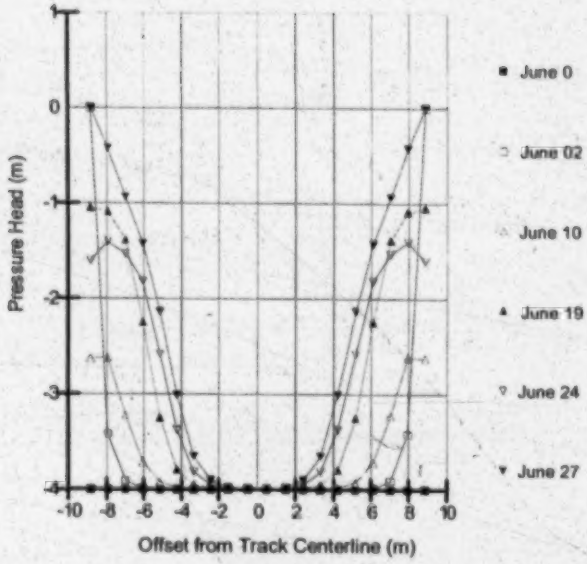

(c) for Ksat = 1E-7m/s

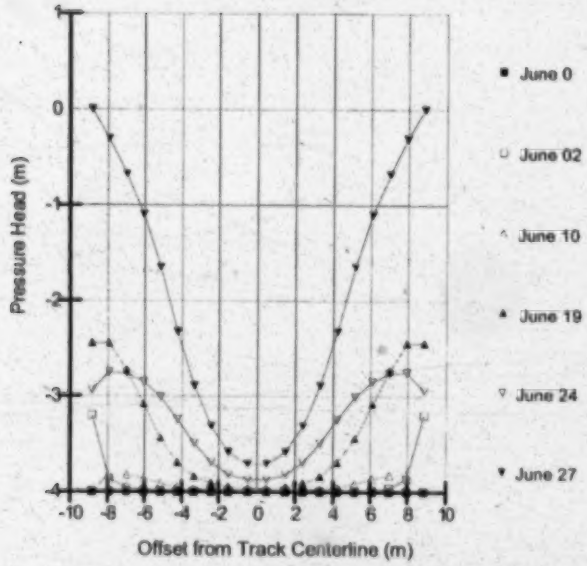

(d) for Ksat = 5E-7m/s

Figure C-8 Pore-water pressure profile along a horizontal line for initially wet embankment at MP 154.47

2. Seepage Modeling Results for Embankment at MP 150.17

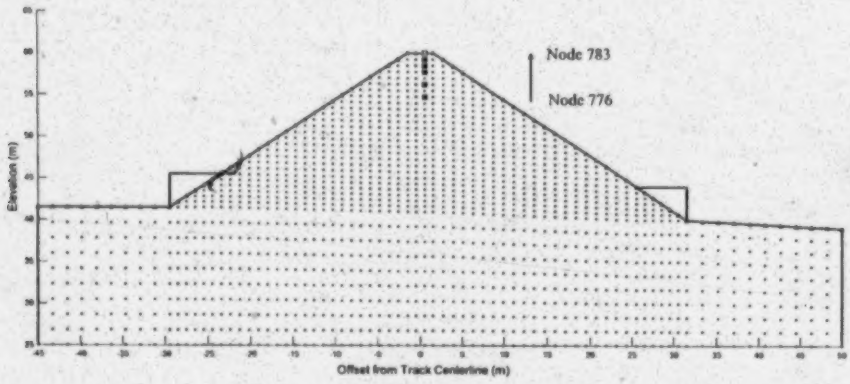

(a) location of nodes selected

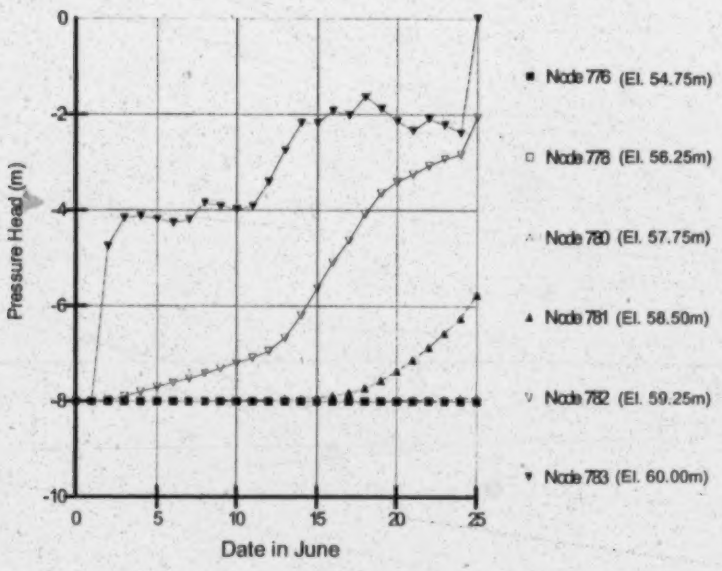

(b) for Ksat = 5E-7m/s

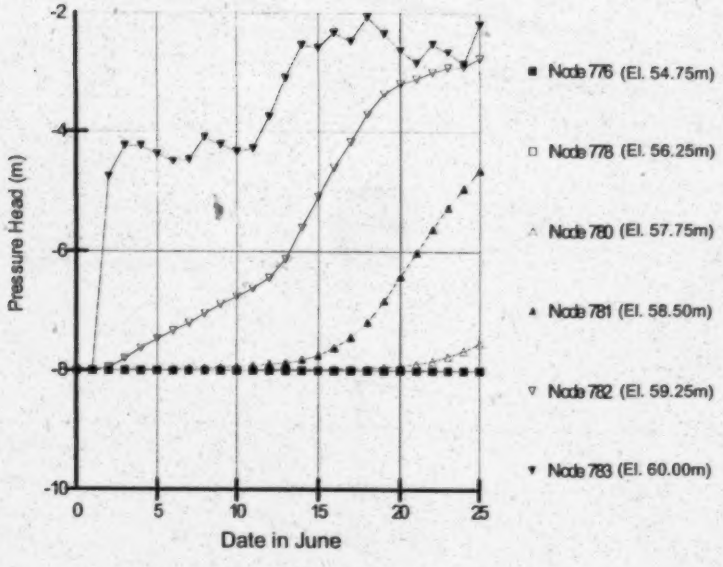

(c) for Ksat = 1E-6m/s

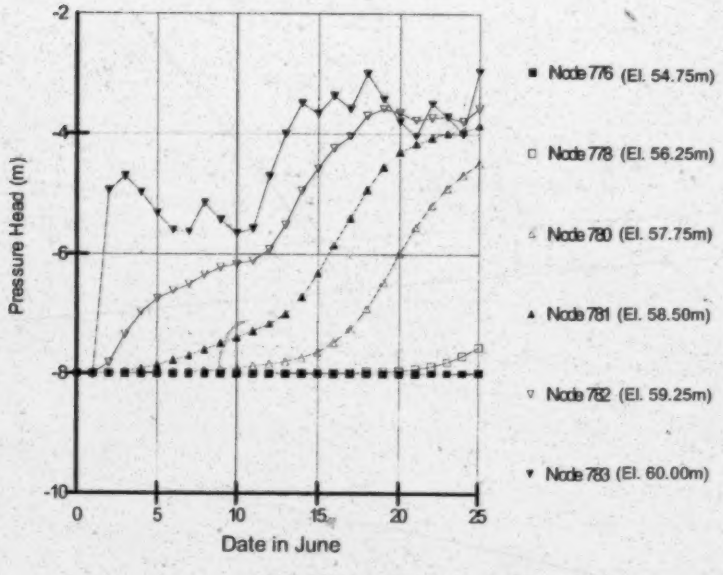

(d) for Ksat = 5E-6m/s

Figure C-9 Evolution of pore-water pressure
at the crest for initially dry embankment at MP 150.17

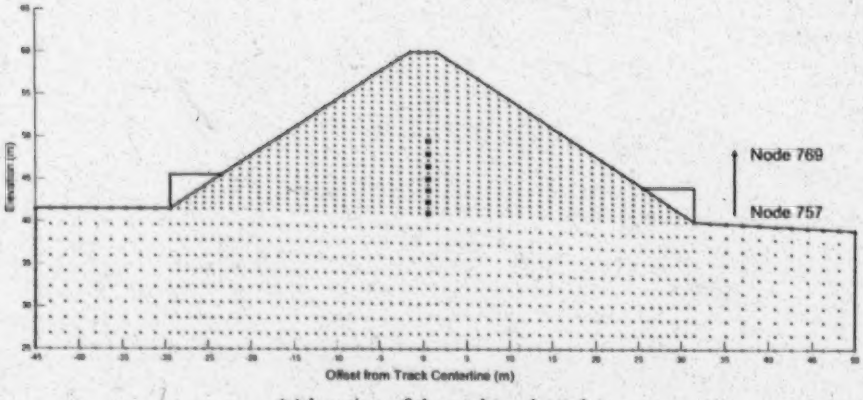

(a) location of the nodes selected

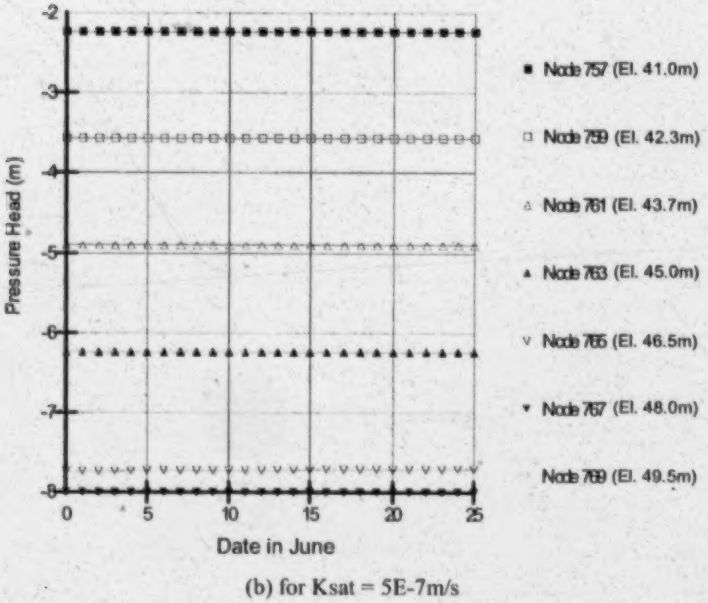

(b) for Ksat = 5E-7m/s

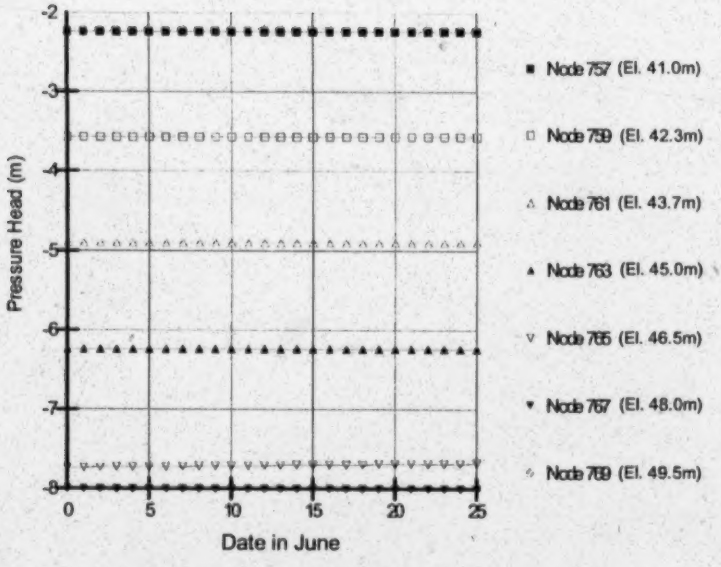

(c) for Ksat = 1E-6m/s

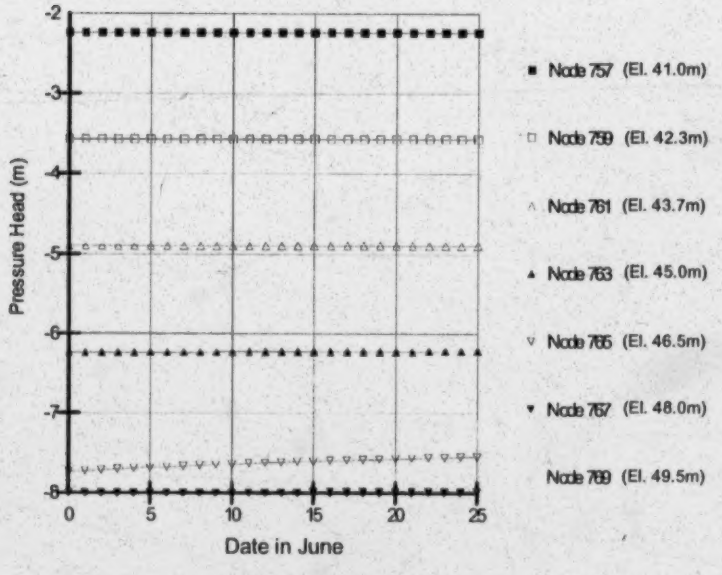

(d) for Ksat = 5E-6m/s

Figure C-10 Evolution of pore-water pressure
at the bottom for initially dry embankment at MP 150.17

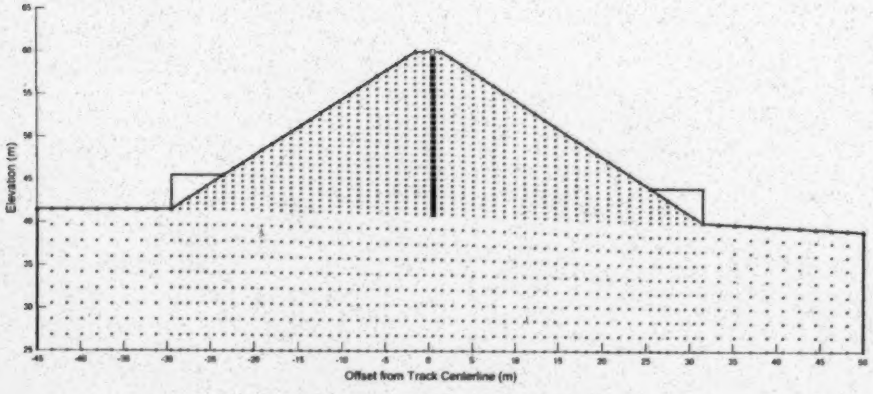

(a) location of the nodes selected

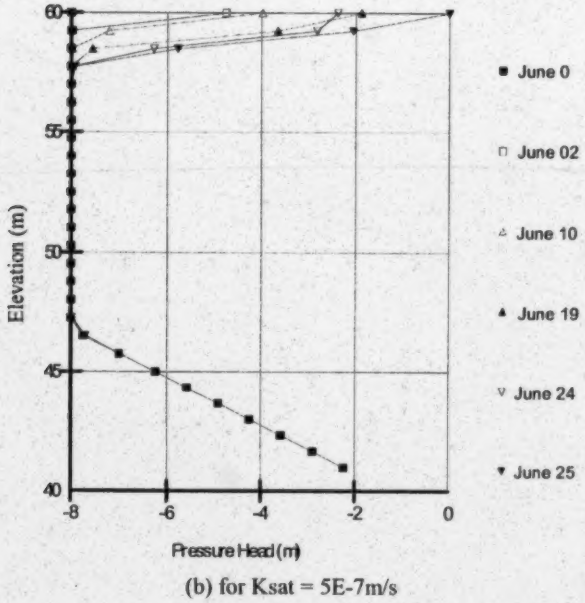

(b) for Ksat = 5E-7m/s

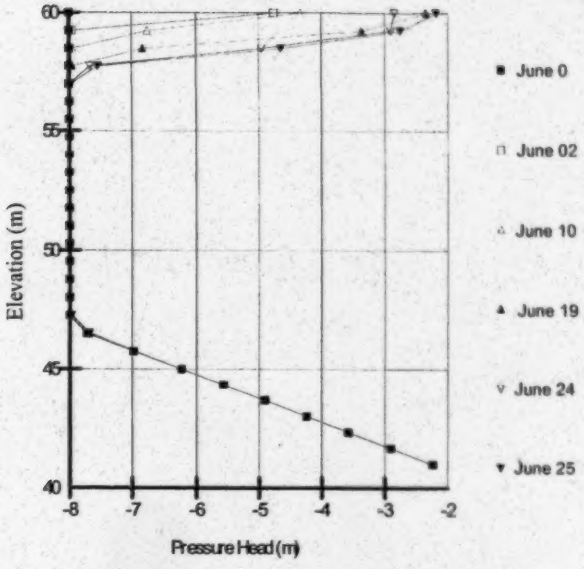

(c) for Ksat = 1E-6m/s

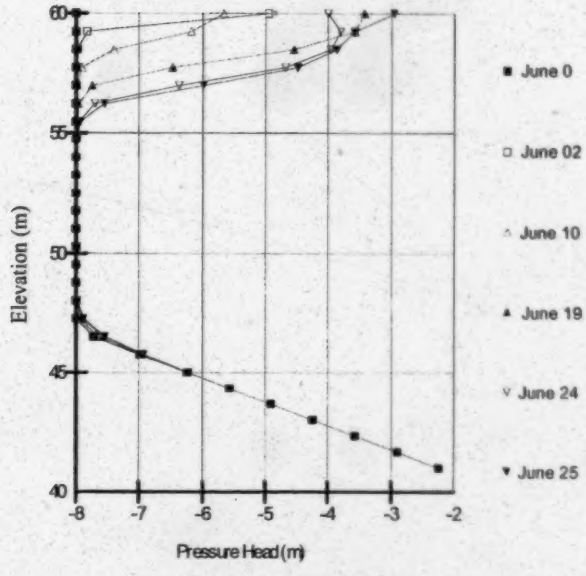

(d) for Ksat = 5E-6m/s

Figure C-11 Pore-water pressure profile along a vertical line for initially dry embankment at MP 150.17

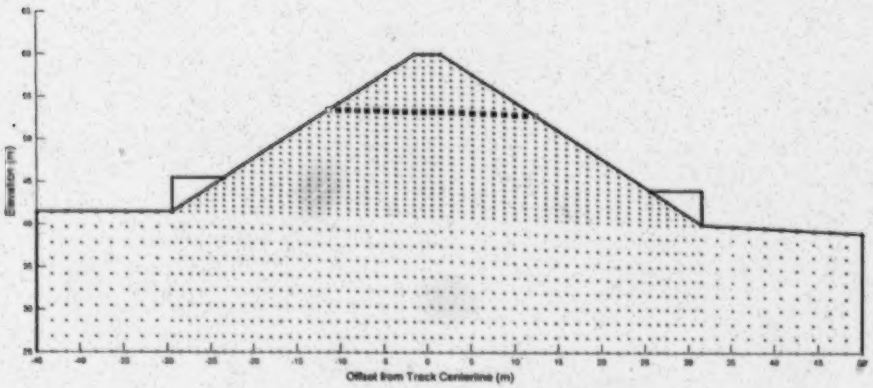

(a) location of the nodes selected

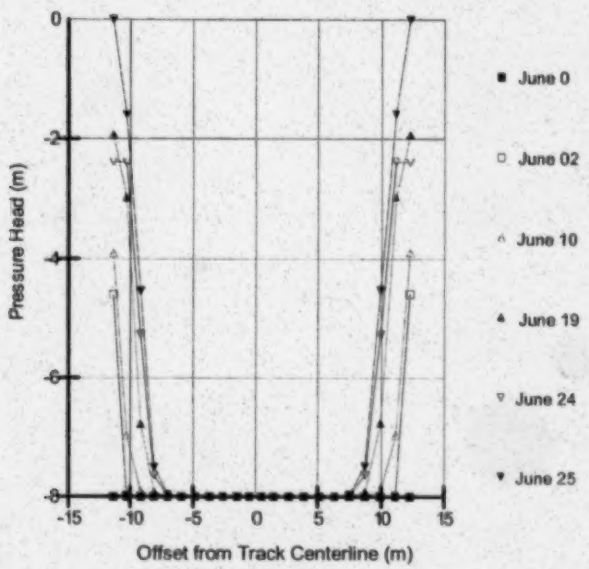

(b) for Ksat = 5E-7m/s

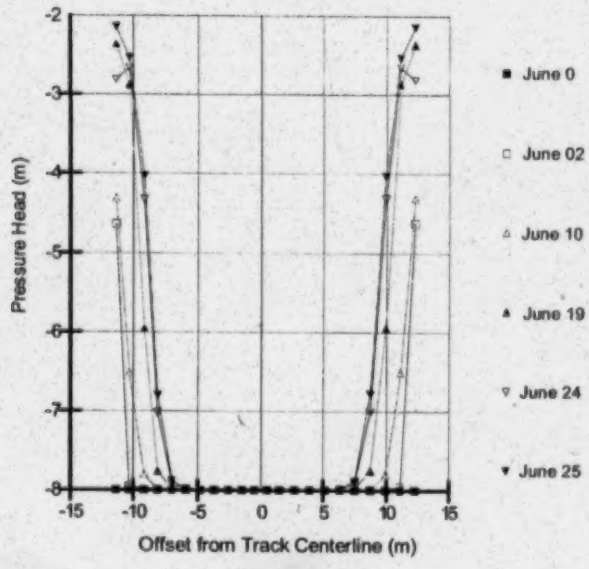

(c) for Ksat = 1E-6m/s

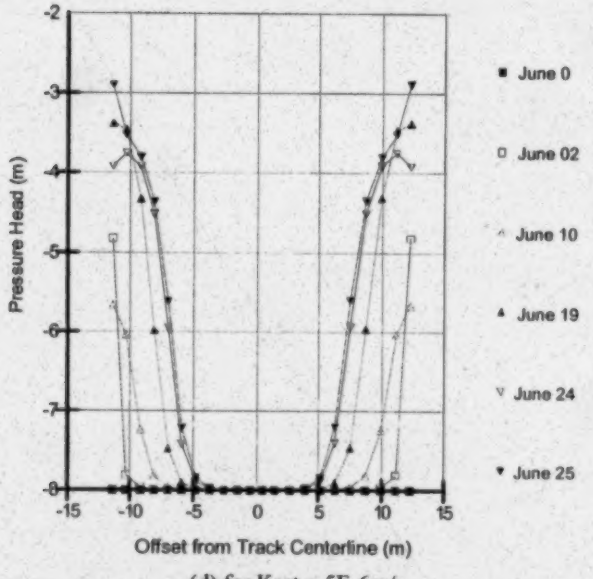

(d) for Ksat = 5E-6m/s

Figure C-12 Pore-water pressure profile along a horizontal line for initially dry embankment at MP 150.17

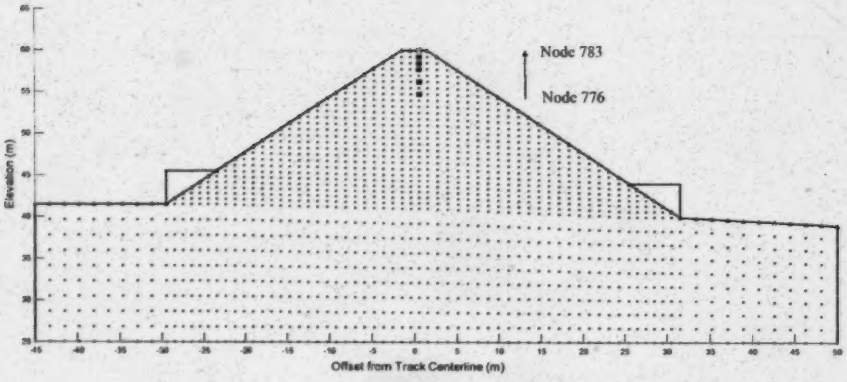

(a) location of the nodes selected

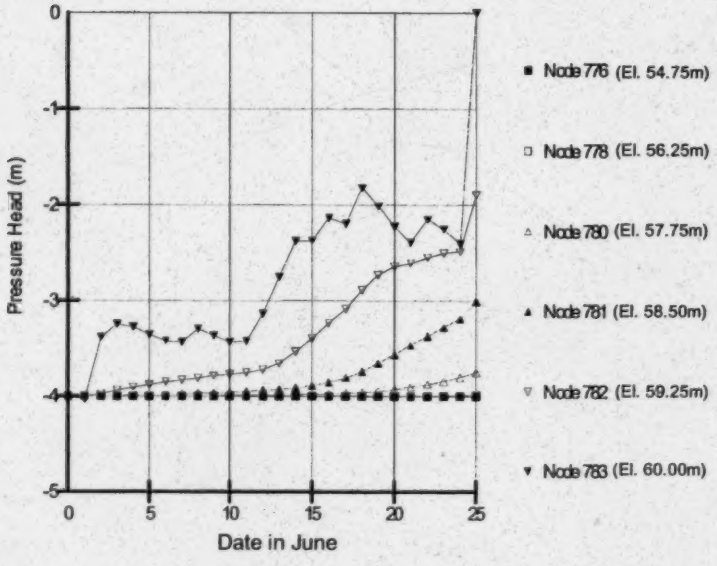

(b) for Ksat = 5E-7m/s

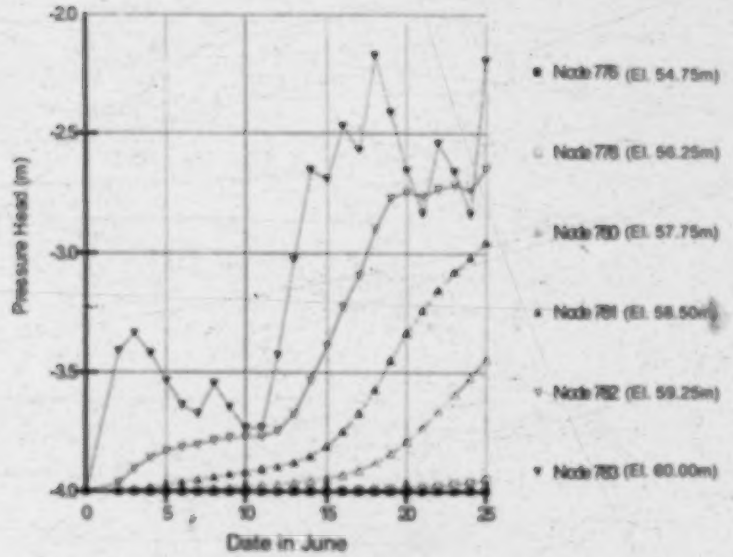

(c) for Ksat = 1E-6m/s

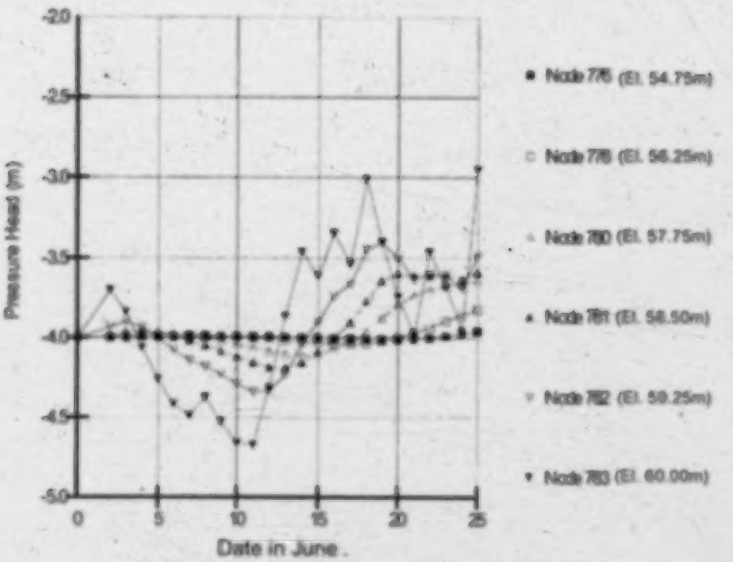

(d) for Ksat = 5E-6m/s

Figure C-13 Evolution of pore-water pressure
at the crest for initially wet embankment at MP 150.17

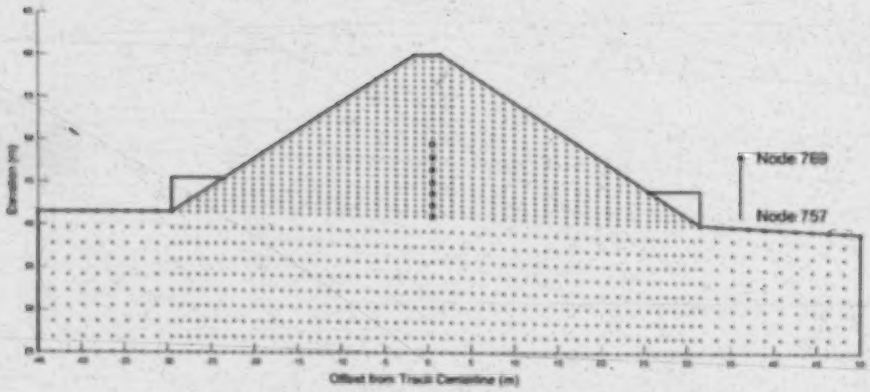

(a) location of the nodes selected

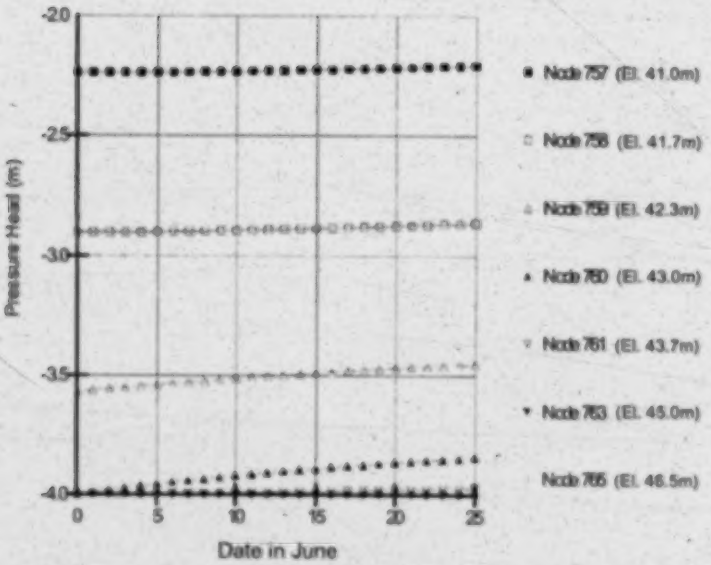

(b) for Ksat = 5E-7m/s

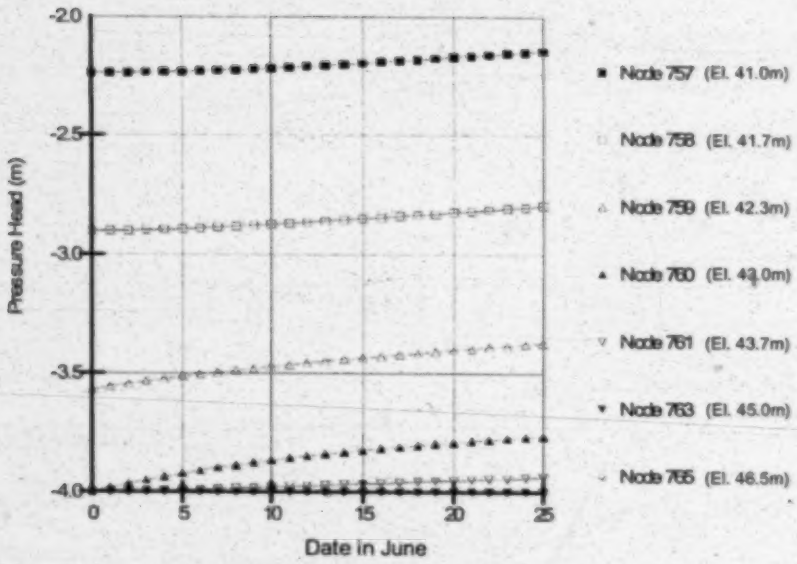

(c) for Ksat = 1E-6m/s

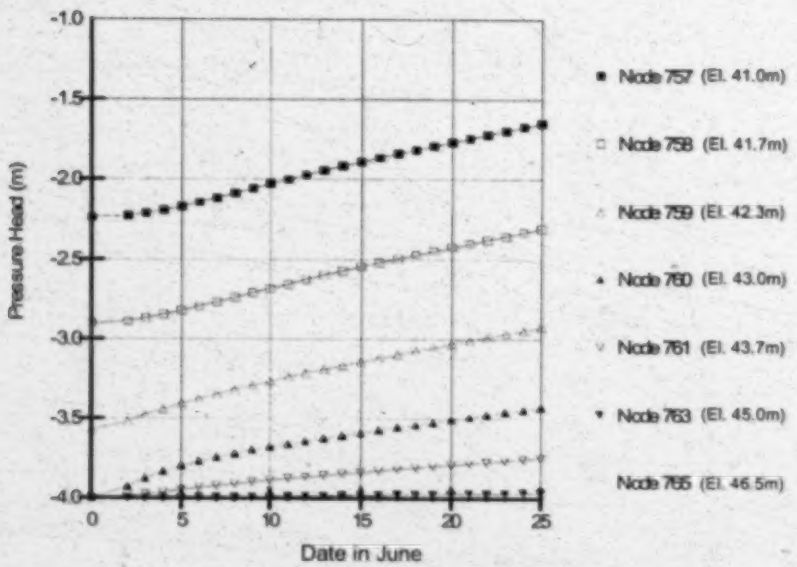

(d) for Ksat = 5E-6m/s

Figure C-14 Evolution of pore-water pressure
at the bottom for initially wet embankment at MP 150.17

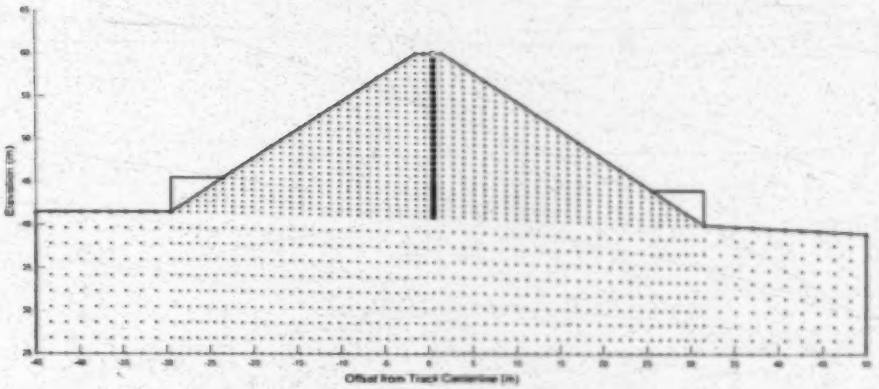

(a) location of the nodes selected

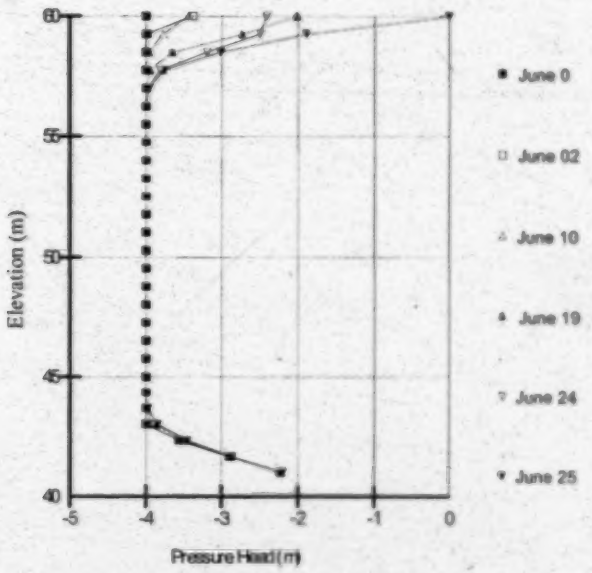

(b) for Ksat = 5E-7m/s

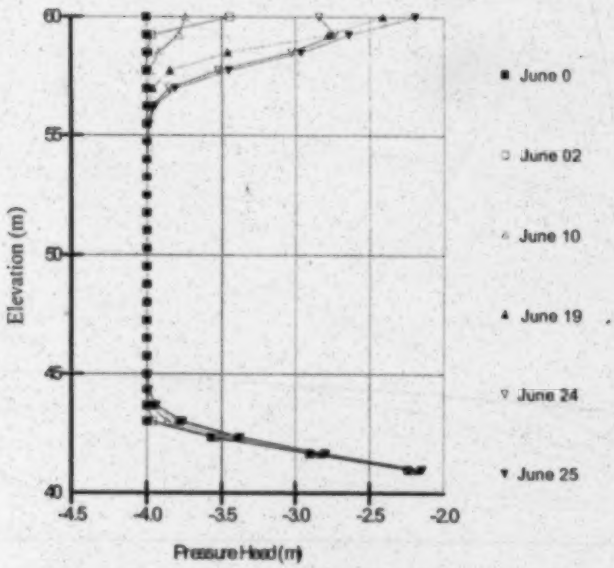

(c) for Ksat = 1E-6m/s

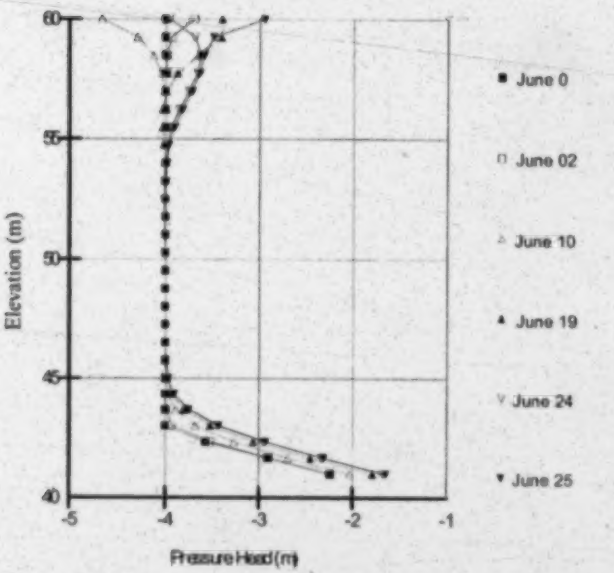

(d) for Ksat = 5E-6m/s

Figure C-15 Pore-water pressure profile along a vertical line for initially wet embankment at Mp 150.17

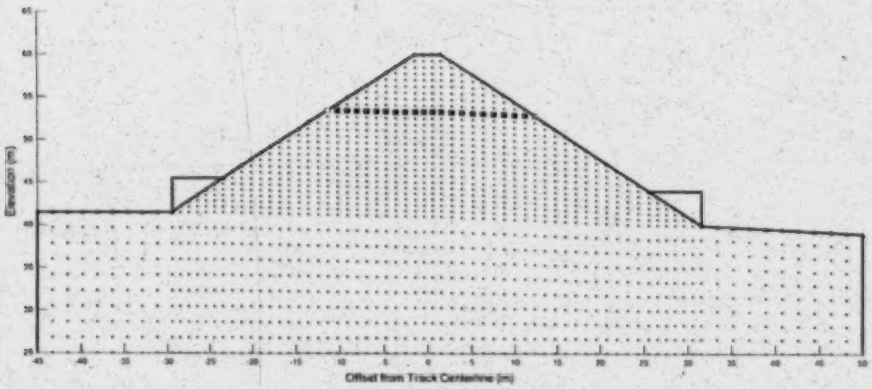

(a) location of the nodes selected

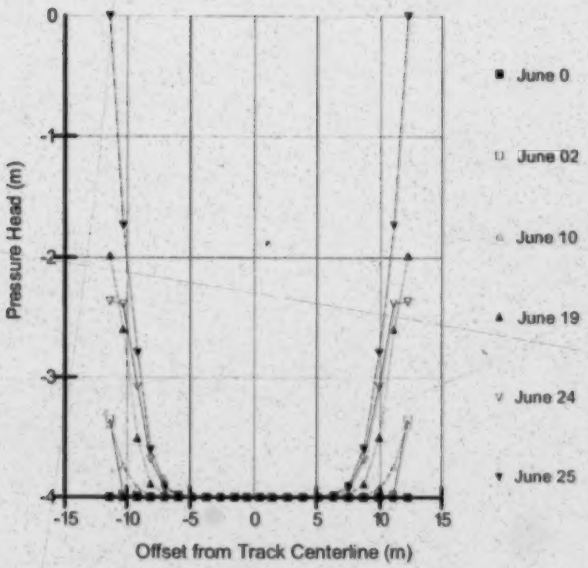

(b) for Ksat = 5E-7m/s

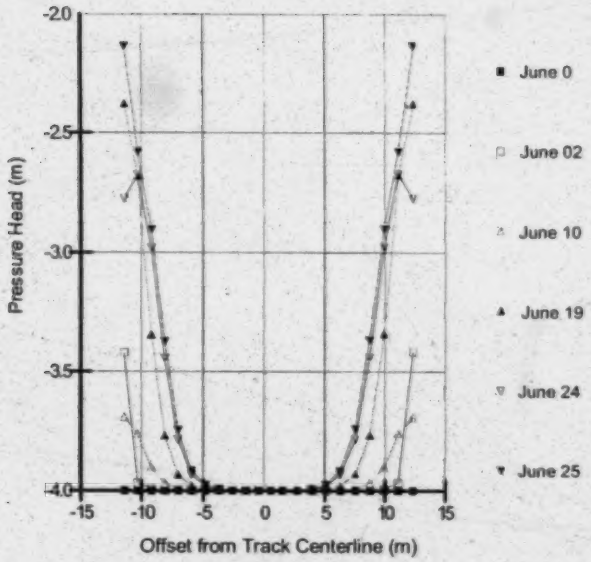

(c) for Ksat = 1E-6m/s

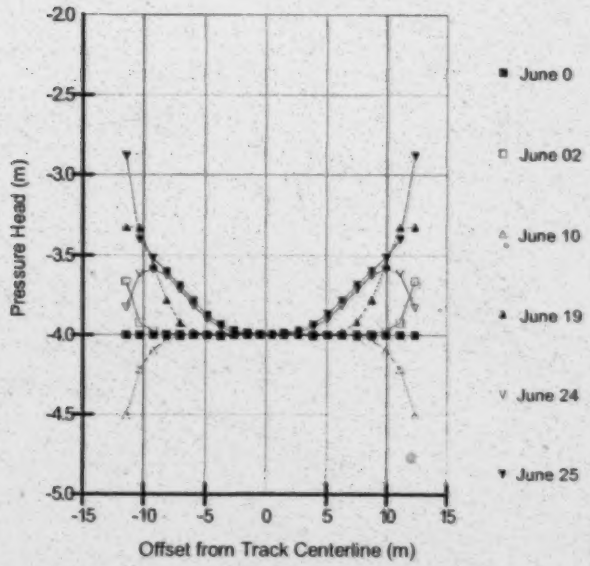

(d) for Ksat = 5E-6m/s

Figure C-16 Pore-water pressure profile along a horizontal line for initially wet embankment at MP 150.17

Appendix D Hydrology and Hydraulic Results

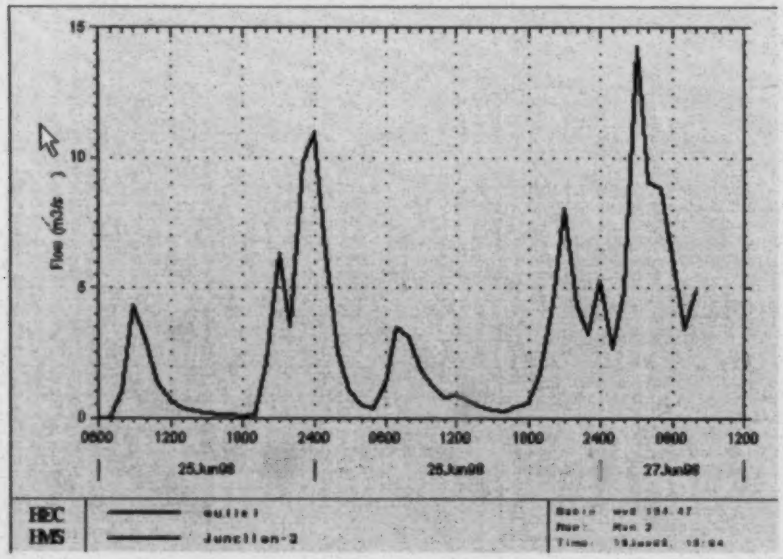

Figure D-1 Modelled hydrograph at outlet of watershed 154.47

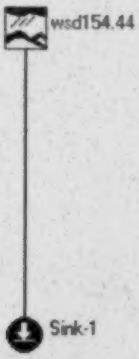

Figure D-2 Hydrologic model for watershed 154.44

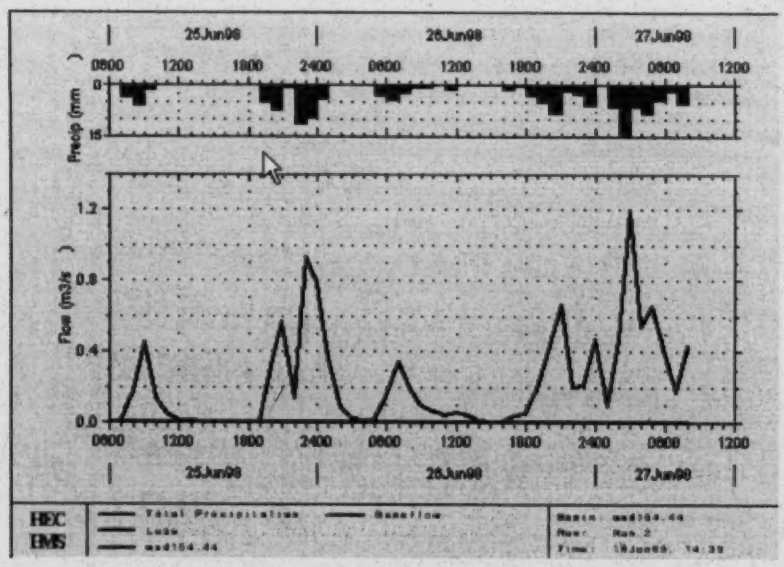

Figure D-2 Modelled hydrograph at outlet of watershed 154.44 (cont'd)

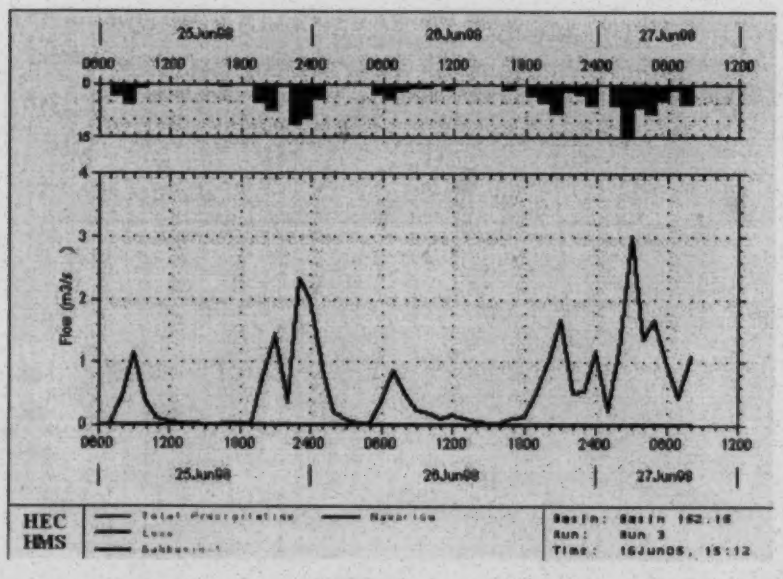

Figure D-3 Modelled hydrograph at outlet of watershed 152.15

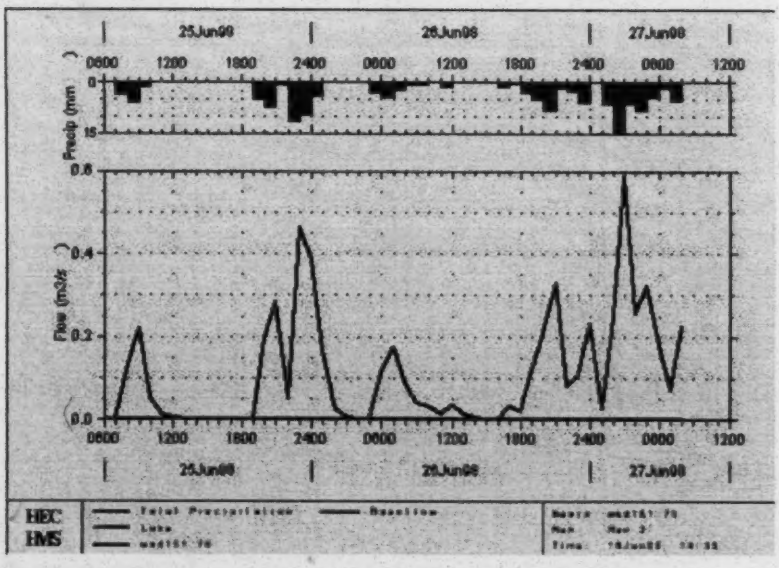

Figure D-4 Modelled hydrograph at outlet of watershed 151.70

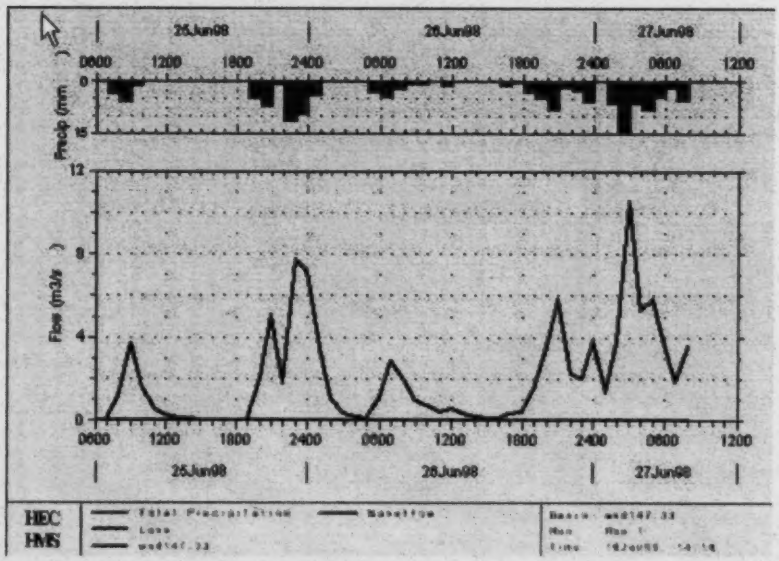

Figure D-5 Modelled hydrograph at outlet of watershed 147.33

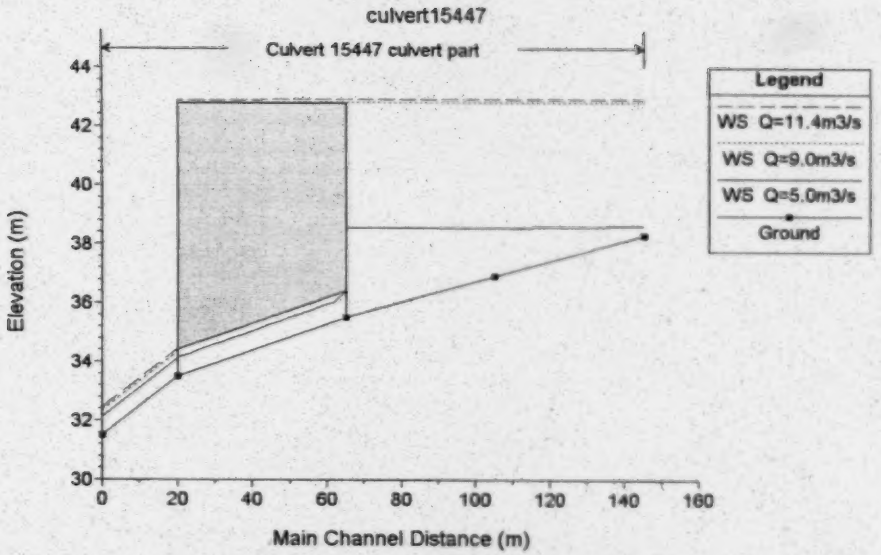

Figure D-6 Modelled water surface profiles for culvert at MP 154.47

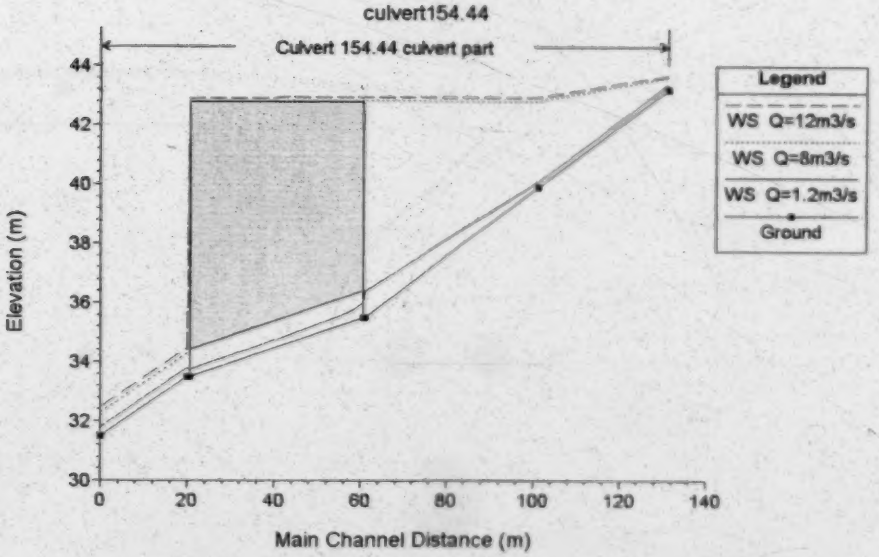

Figure D-7 Modelled water surface profiles for culvert at MP 154.44

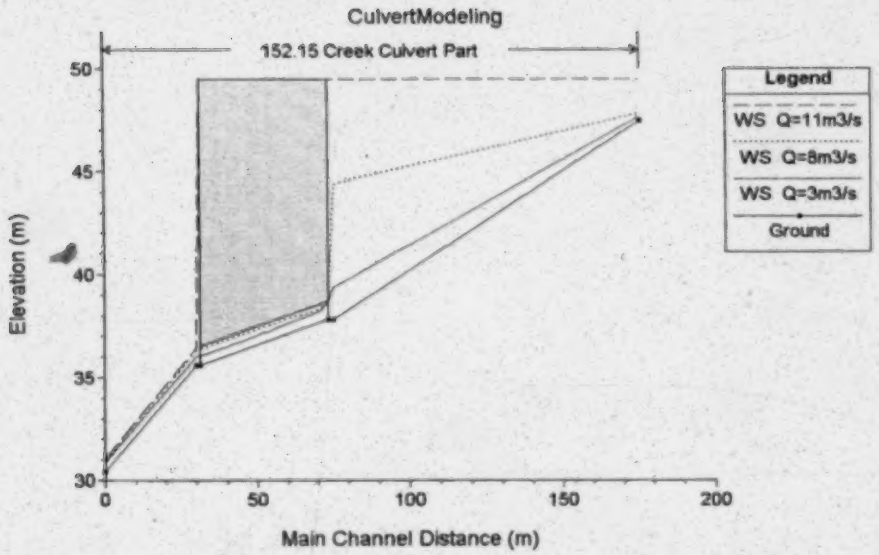

Figure D-8 Modelled water surface profiles for culvert at MP 152.15

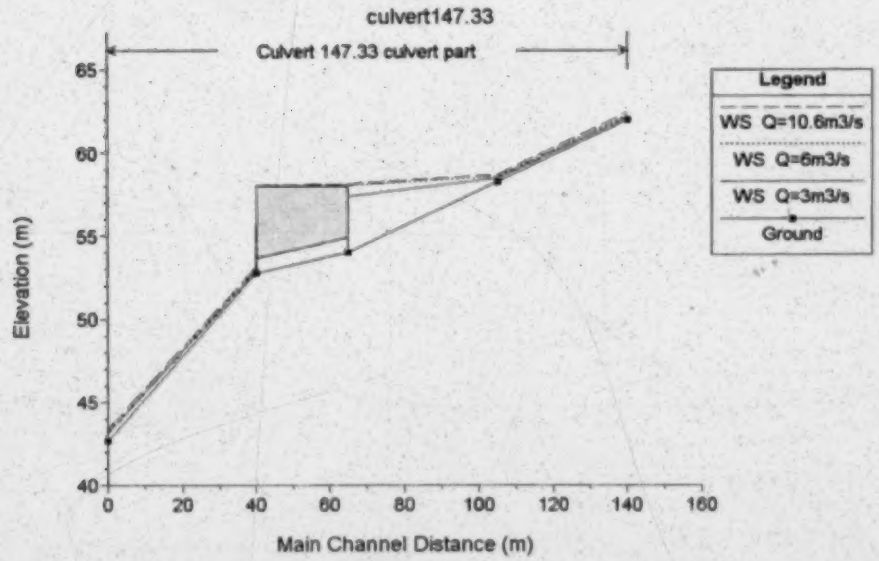

Figure D-9 Modelled water surface profiles for culvert at MP 147.33